CTAO School Lectures

Astrophysical non-jetted outflows in gamma-rays

Pol Bordas, CTAO School
Bertinoro, June 2024

CTAO

ICCUB Institut de Ciències del Cosmos

EXCELENCIA MARÍA DE MAEZTU

UNIVERSITAT DE BARCELONA

IEEC Institut d'Estudis Espacials de Catalunya

NOTES ON THIS LECTURE

- Since this School is devoted to the Science with CTAO, we will restrict to the **gamma-ray energy domain**, focusing on the **VHE range** (info in the UHE, GeV or lower-energy ranges is provided when necessary)

- The **variety of sources** featuring non-jetted outflows and emitting gamma-rays is large. Prominent examples will be discussed for a selection of these (non-exhaustive review)

- The material used for these Lectures comes mainly from published **papers** in specialised journals, and books and **PhD Thesis** in the field of high-energy gamma-ray astrophysics. References are provided at the end of these notes.

- CTAO perspectives are given qualitatively from previous studies using instrument capabilities based on numerical simulations for the different sub-arrays on (possibly) different configurations

OUTLINE

- Intro to non-jetted gamma-ray sources
- Source catalogs @ VHEs
- Sources of VHE gamma-rays:

The Galactic Center region, SNRs, PSRs and PWNe, TeV halos, Binary systems, Fermi bubbles, Globular clusters, Star Forming Regions, Radio Galaxies

intro: **non-jetted** sources

Gamma-rays have been detected from a large variety of astrophysical sources which **don't display relativistic collimated outflows** (jets).

This immediately translates into some general/common properties of these sources based solely on their **detection with current facilities**:

- **Energy reservoir:** the kinetic power of the outflows needs to be relatively large, since no strong flux enhancement due to relativistic effects are expected (i.e. Doppler boosting)
- **Distance:** the large majority of gamma-ray sources which do not account for relativistic boosting are Galactic systems. Some EGAL exceptions exist, however, e.g. galaxy clusters, starburst galaxies
- **Distance:** closer sources and no strong beaming can lead to the possibility of morphological studies to be conducted in a number of cases. Extended sources can be used to constrain particle acceleration and propagation scenarios

a very rough sketch

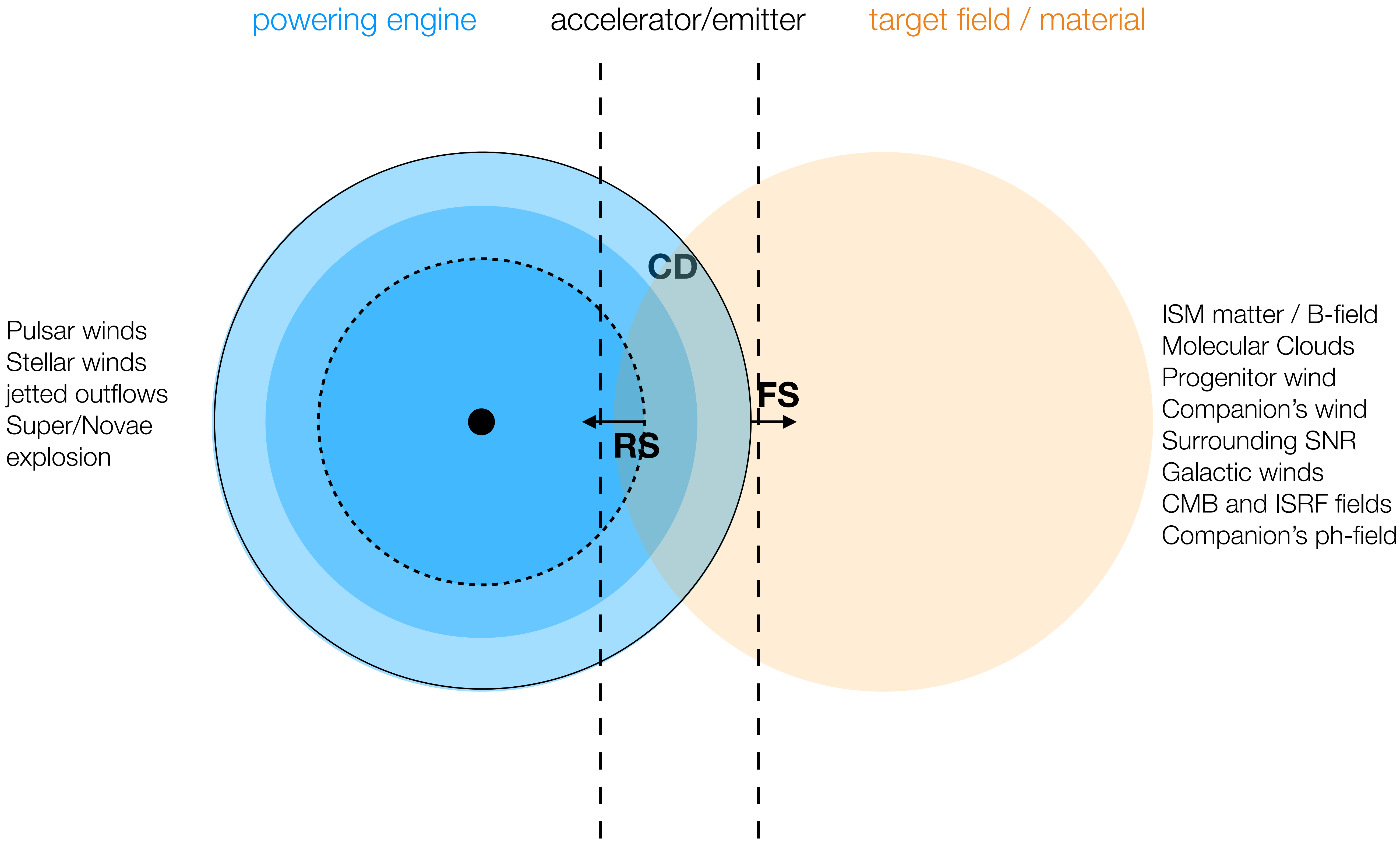

intro: **non-jetted** sources

GALACTIC

HE gamma-ray sources

- Pulsars (>230)
- Supernova Remnants (~24)
- Globular clusters (~30 ?)
- Pulsar Wind Nebulae (11)
- Colliding wind binaries: (2)
- Novae or WD binaries (19)
- X-ray binaries: SS433
- Gamma-ray binaries (9)
- Fermi Bubbles (1+1)

VHE gamma-ray sources

- Galactic Center and Galactic ridge
- Supernova Remnants and SNR/MC (>20)
- Open clusters and stellar assoc. (3)
- Pulsars: Crab, Vela, Geminga (3)
- Globular clusters: Terzan 5
- Pulsar Wind Nebulae (>30)
- Colliding wind binaries: η-Carinae
- Novae or WD binaries: RS Oph
- X-ray binaries: SS 433, V4641 Sgr (?)
- Gamma-ray binaries (9)

EGAL

HE gamma-ray sources

- Radio galaxies
- Starburst galaxies
- Galaxy clusters
- Fermi bubbles

VHE gamma-ray sources

- Radio galaxies
- Starburst galaxies
- Galaxy clusters

intro: **non-jetted** variable sources

GALACTIC

HE gamma-ray sources

- Pulsars (>230)
- Supernova Remnants (~24)
- Globular clusters (~30 ?)
- Pulsar Wind Nebulae: Crab N.
- Colliding wind binaries: (2)
- Novae or WD binaries (19)
- X-ray binaries: SS433 (?)
- Gamma-ray binaries (9)
- Fermi Bubbles

VHE gamma-ray sources

- Galactic Center and Galactic ridge
- Supernova Remnants and SNR/MC (>20)
- Open clusters and stellar assoc. (3)
- Pulsars: Crab, Vela, Geminga
- Globular clusters: Terzan 5
- Pulsar Wind Nebulae (>30)
- Colliding wind binaries: η-Carinae
- Novae or WD binaries: RS Oph
- X-ray binaries: SS 433, V4641 Sgr (?)
- Gamma-ray binaries (9)

EGAL

HE gamma-ray sources

- Radio galaxies
- Starburst galaxies
- Galaxy clusters
- Fermi bubbles

VHE gamma-ray sources

- Radio galaxies
- Starburst galaxies
- Galaxy clusters

Source catalogs @ VHEs

A large number of gamma-ray sources have been discovered thanks to **deep surveys of the Galactic disk** (at VHEs/UHEs; all-sky survey mode by default in HE gamma-ray satellites)

H.E.S.S. GPS

- **2700h** of observation time, taken in about 10 yrs (2004 to 2013)
- -110º<l<+65º, -3.5º<b<+3.5º
- Energy range: 0.2 - 100 TeV
- **~1.5% Crab N. sensitivity**
- resolution ~ 0.08º (5 arcmin)
- **78 VHE sources**, out of which 31 are firmly identified, and **16 are new sources**

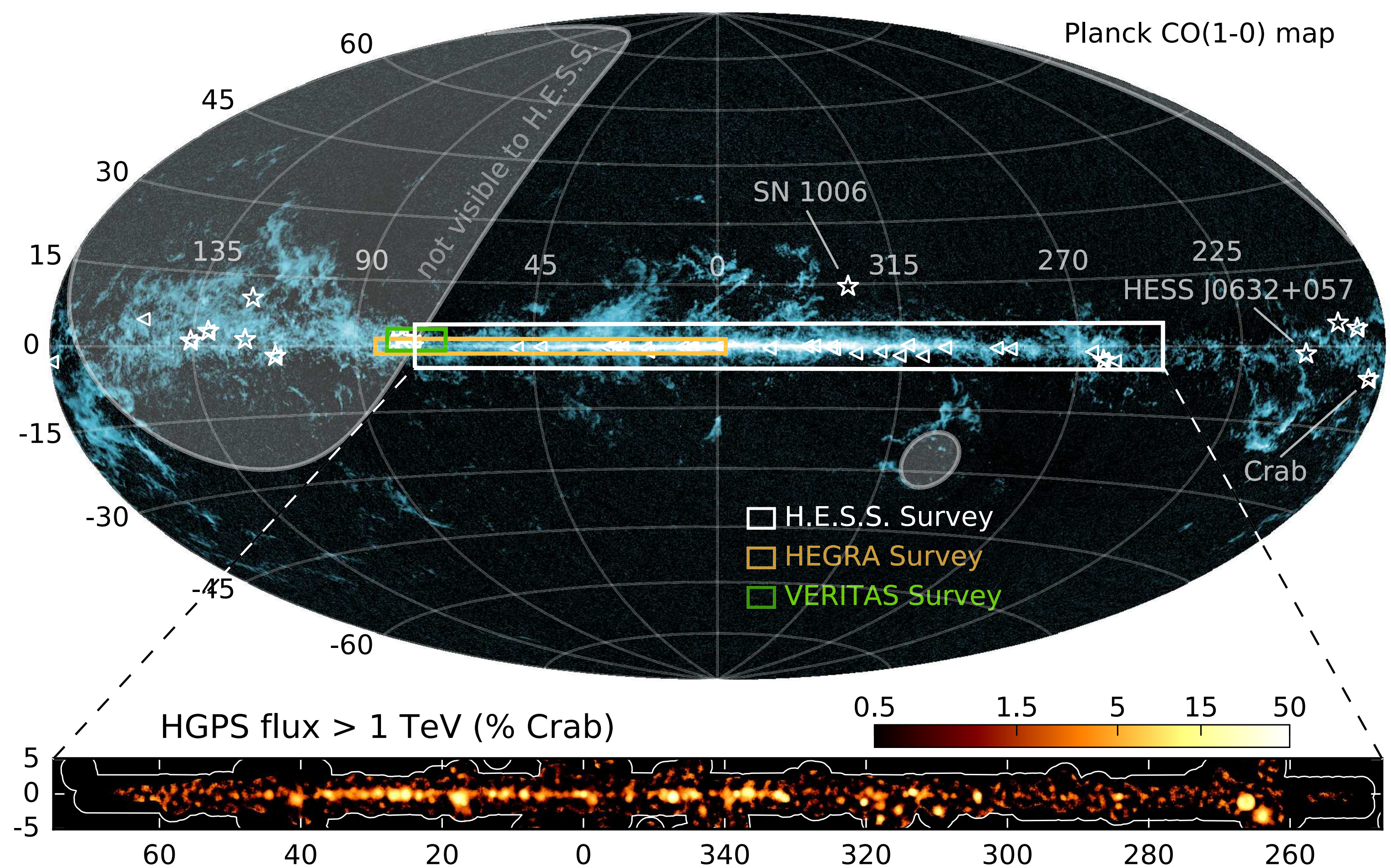

HESS Collaboration 2018

Source catalogs @ VHEs

A large number of gamma-ray sources have been discovered thanks to **deep surveys of the Galactic disk** (at VHEs/UHEs; all-sky survey mode by default in HE gamma-ray satellites)

H.E.S.S. GPS

- **2700h** of observation time, taken in about 10 yrs (2004 to 2013)
- -110°<l<+65°, -3.5°<b<+3.5°
- Energy range: 0.2 - 100 TeV
- **~1.5% Crab N. sensitivity**
- resolution ~ 0.08° (5 arcmin)
- **78 VHE sources**, out of which 31 are firmly identified, and **16 are new sources**

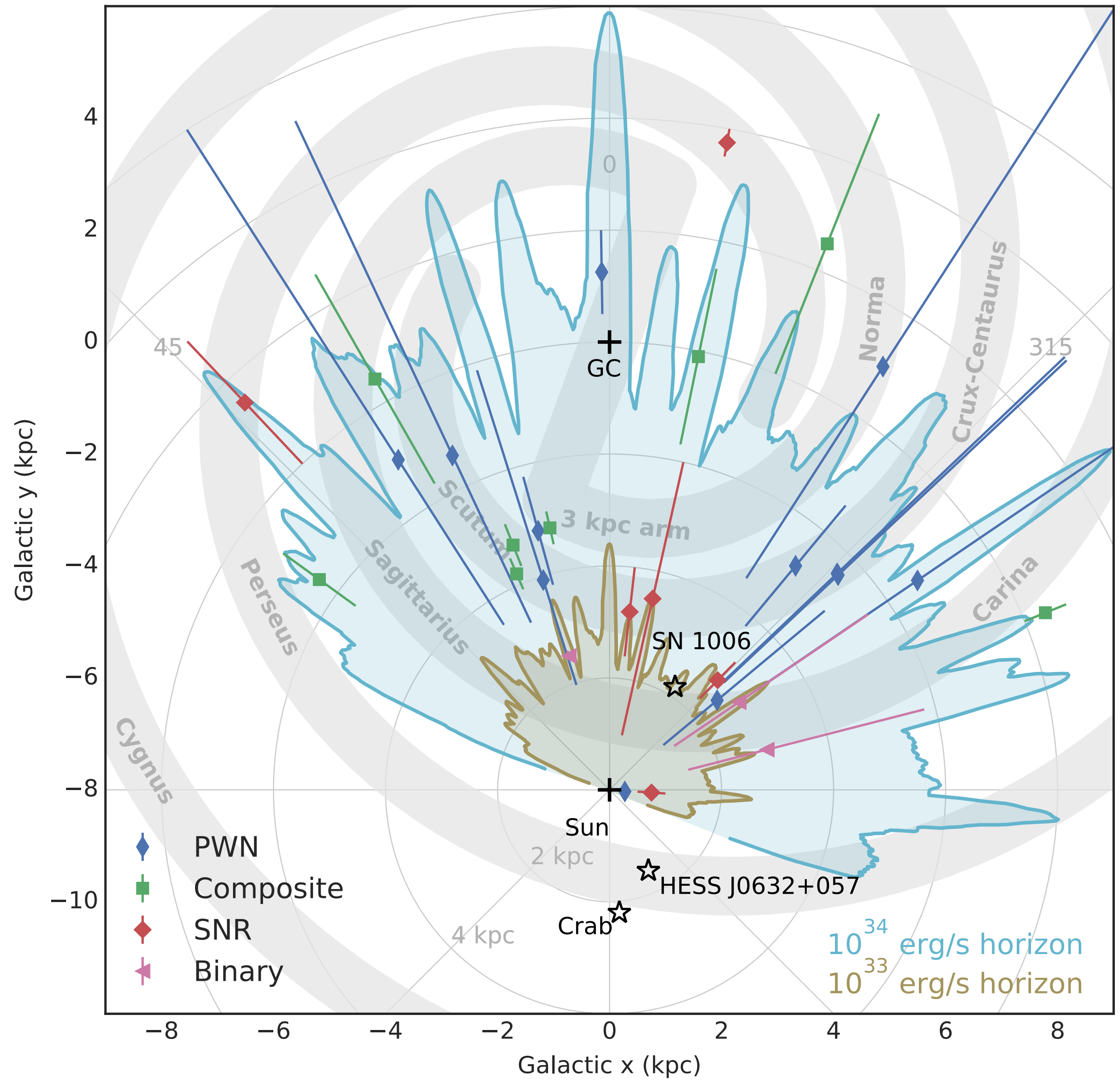

HESS Collaboration 2018

Source catalogs @ VHEs

The HGPS catalog includes 78 sources (64 were detected with the HGPS pipeline analysis + 14 complex regions, e.g. the GC or SNR shells)

Most HGPS sources, ~86%, are associated with at least one object that could potentially power the TeV emission. Is unclear whether unassociated sources (14%) are truly “dark" (emitting exclusively at VHEs)

The largest source class are **PWNe** (12 sources), followed by **shell-type SNRs** (8 sources); **composite SNRs** (PWN and SNR shell, 8) and gamma-ray **binary systems** (3).

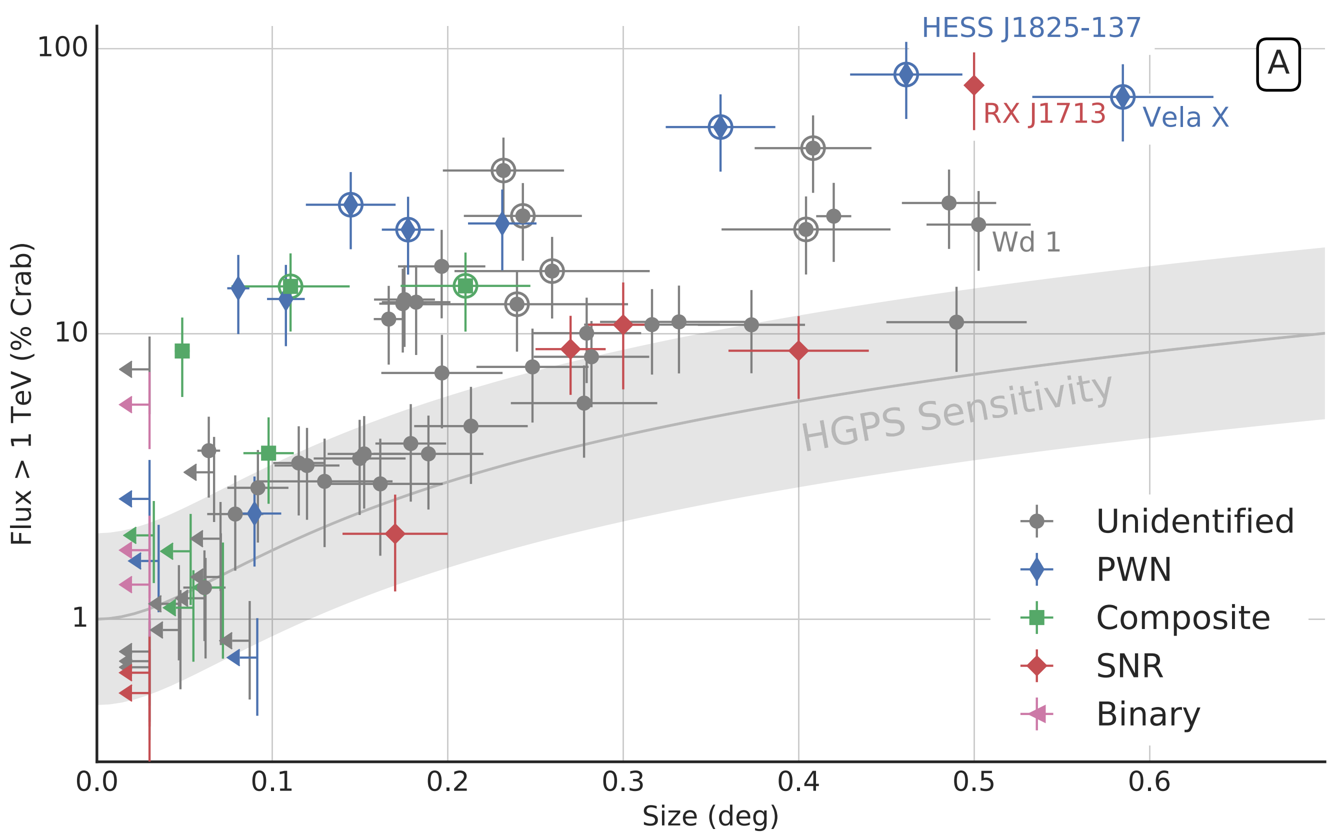

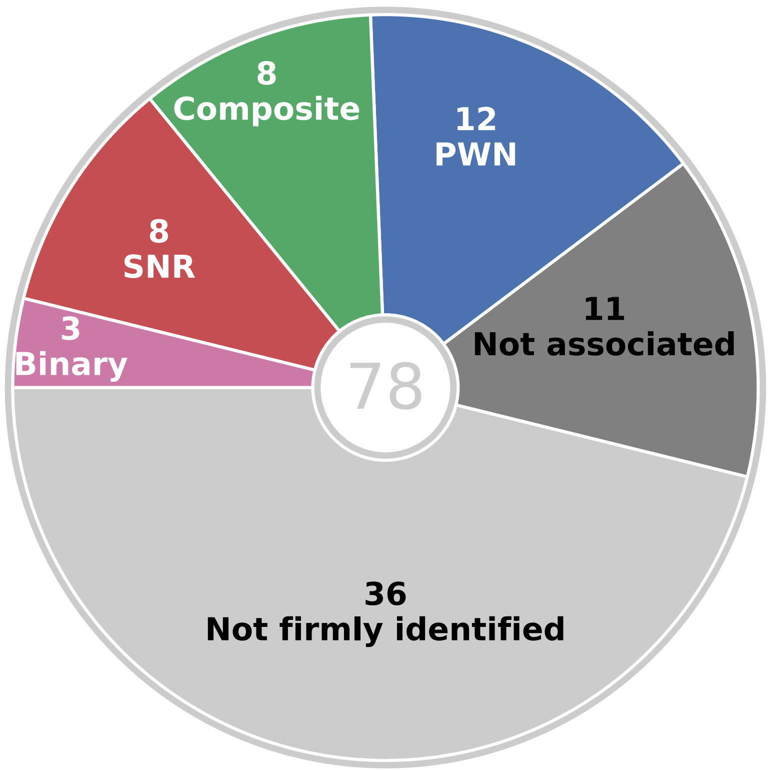

Source catalogs @ VHEs

The H.E.S.S. Collaboration is delivering **all products of its HGPS online**, including sensitivity, significance and flux maps as well the HGPS catalog sources (CAVEAT: non-dedicated single-source analysis)

Survey Maps (FITS)

Survey sky maps are released in FITS format. They are described in the paper in Appendix A.1. Each file is ~ 11 MB.

- **hgps_map_significance_0.1deg_v1.fits.gz**
- **hgps_map_significance_0.2deg_v1.fits.gz**
- **hgps_map_flux_0.1deg_v1.fits.gz**
- **hgps_map_flux_0.2deg_v1.fits.gz**
- **hgps_map_flux_err_0.1deg_v1.fits.gz**
- **hgps_map_flux_err_0.2deg_v1.fits.gz**
- **hgps_map_flux_ul_0.1deg_v1.fits.gz**
- **hgps_map_flux_ul_0.2deg_v1.fits.gz**
- **hgps_map_sensitivity_0.1deg_v1.fits.gz**
- **hgps_map_sensitivity_0.2deg_v1.fits.gz**

The "Extras" section below contains some information how to view and work with the maps.

Source catalog (FITS)

The source catalog and other tables are released in FITS format. They are described in Appendix A.2 and Tables A.1 - A.9 at the end of the paper. This file is small (~ 50 kB).

- **hgps_catalog_v1.fits.gz**

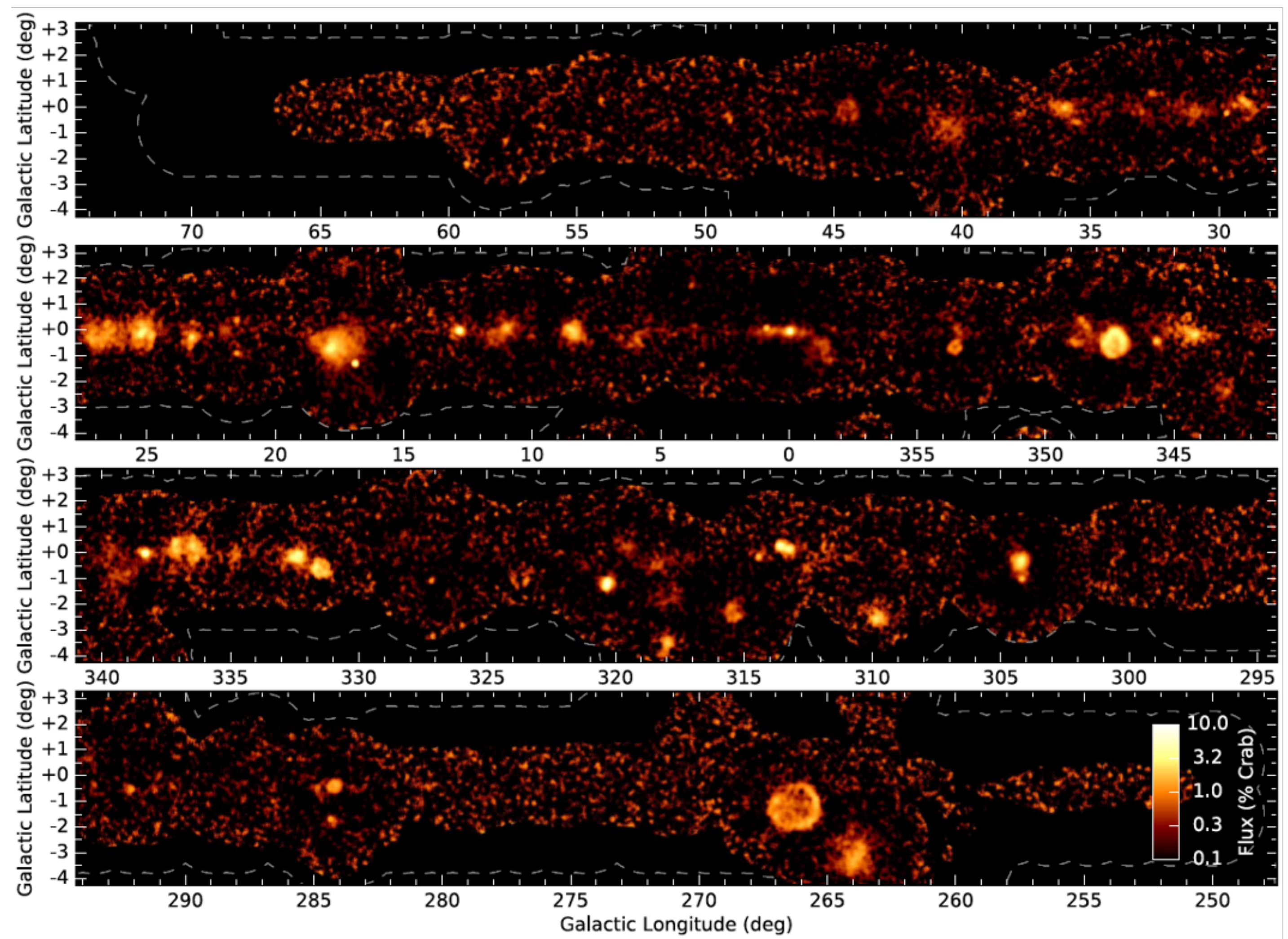

www.mpi-hd.mpg.de/hfm/HESS/hgps/

HESS Collaboration 2018

Source catalogs @ VHEs

3HWC catalog

4.2 yr (1523 days) of data, E-range ~ [0.5 - 200] TeV; HAWC sensitivity ~ **few % Crab flux in 5 years**. About **2/3 of the northern sky are surveyed every night** (from –26° to +64° in declination), with its huge FoV >2.0 sr. Angular resolution (68% containment radius) ~ **0°.1 to 1°.0** depending on the energy range and source zenith angle

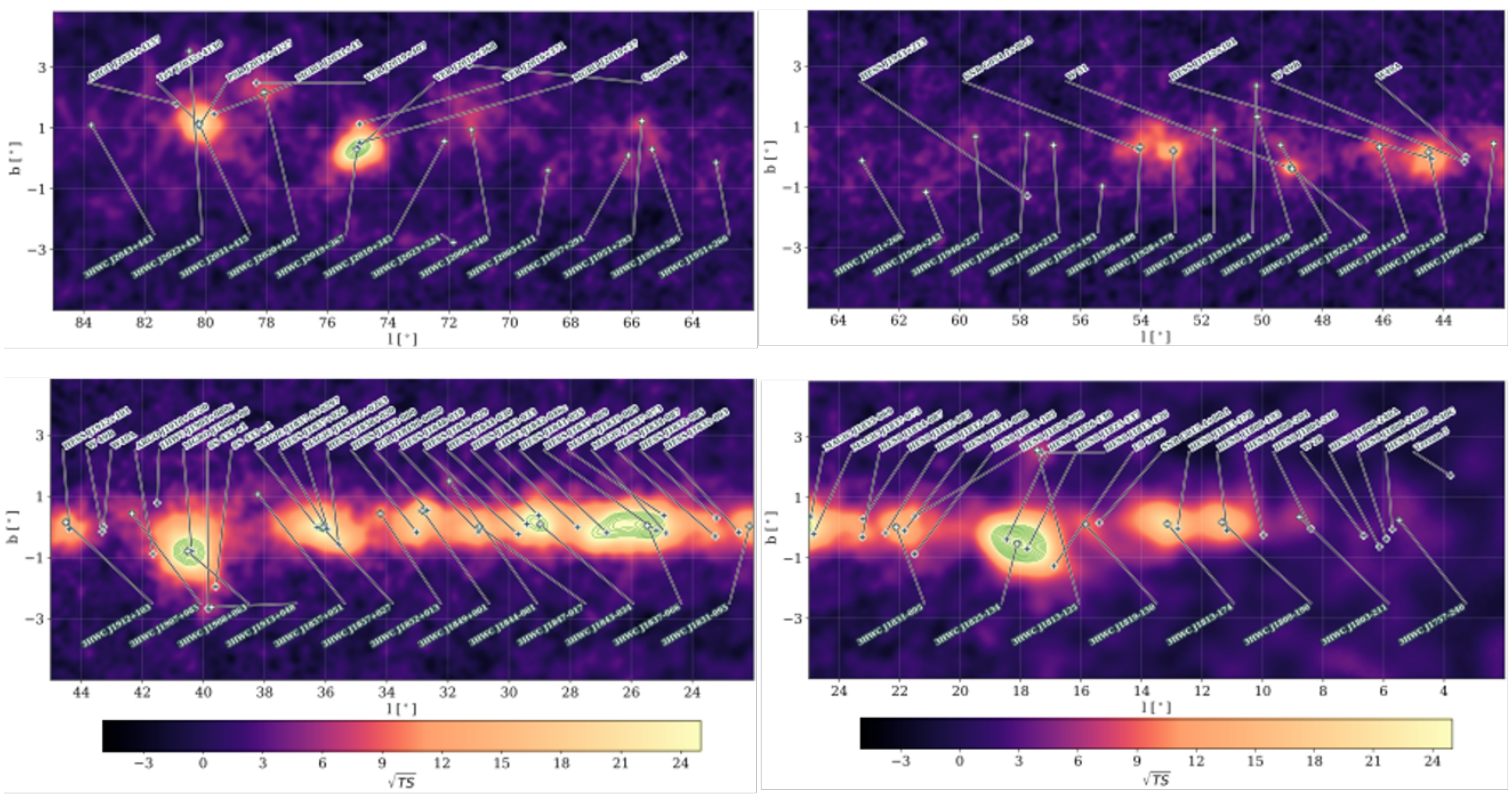

Albert et al. 2020

Source catalogs @ VHEs

The 3HWC catalog contains **65 sources at > 5σ significance**, **8 of which have no 2HWC catalog counterpart**, but are within 1° of previously detected TeV emitters.

From these 65, **20 are new VHE sources**, lying more than 1° away from known TeV sources. Of these, 14 have a potential counterpart in the 4FGL catalog, mostly **associated with pulsars. TeV halos** are revealed as a new source category (discussed later in this Lecture)

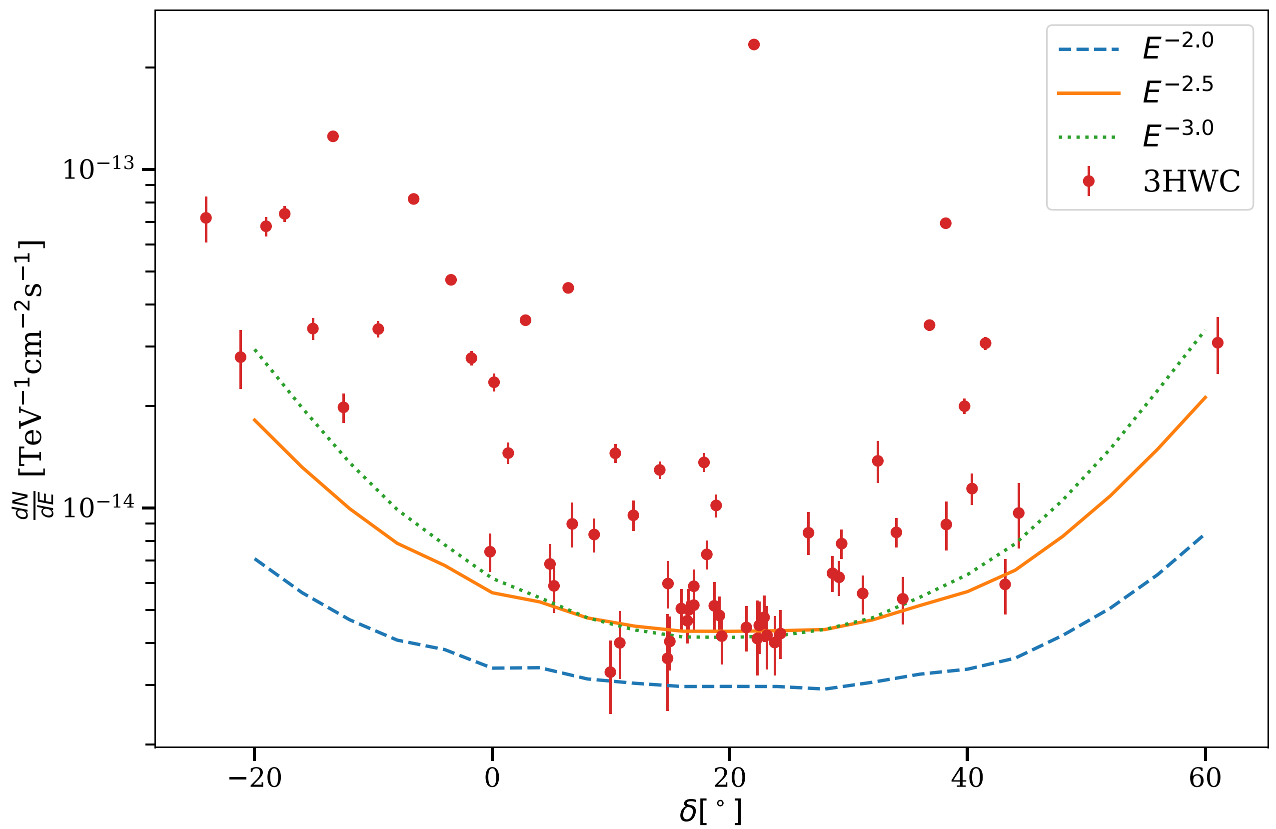

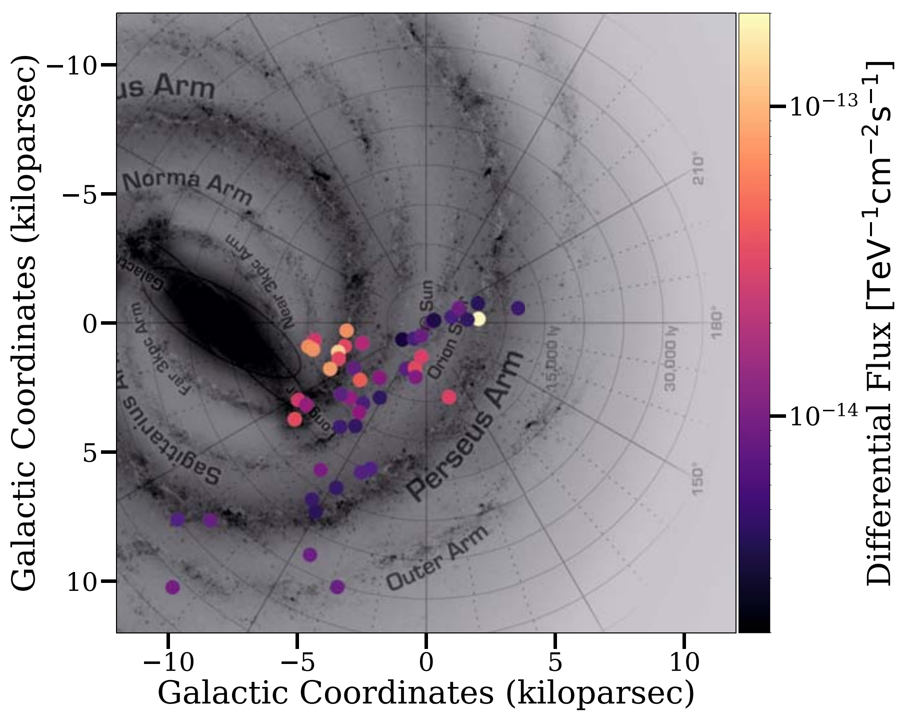

Albert et al. 2020

1LHAASO catalog

508 days with WCDA, 933 days with KM2A, **90 sources smaller than 2º**, **32 new TeV sources**, 43 UHE (E>100 TeV) sources (Cao et al. 2024)

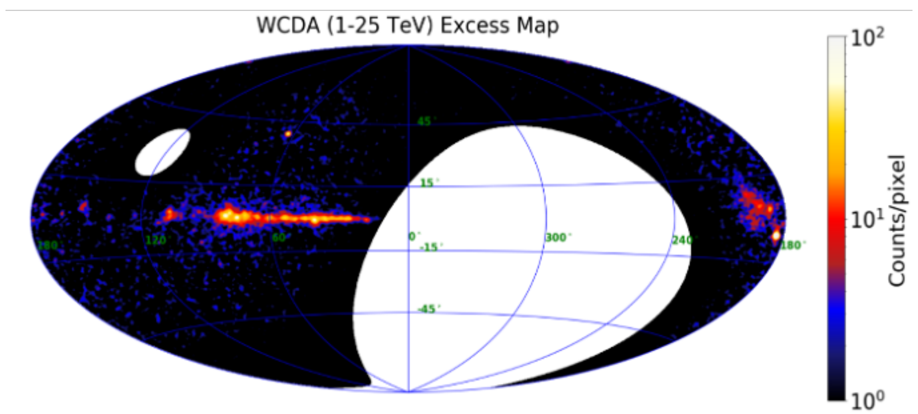

1—25 TeV (WCDA)

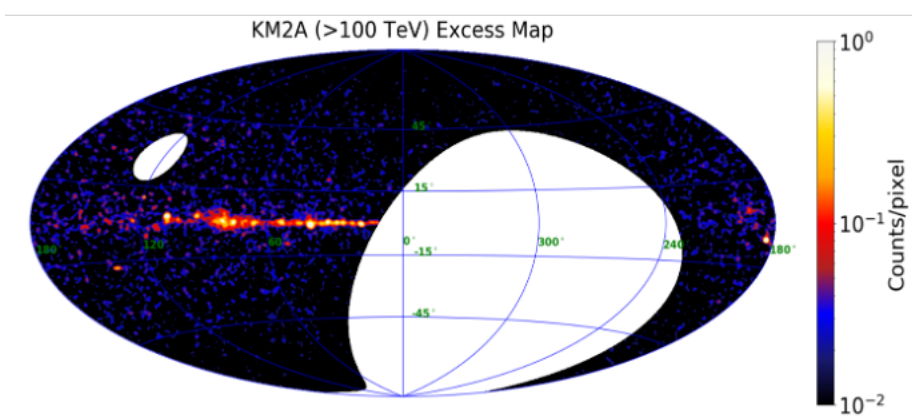

> 100 TeV (KM2A)

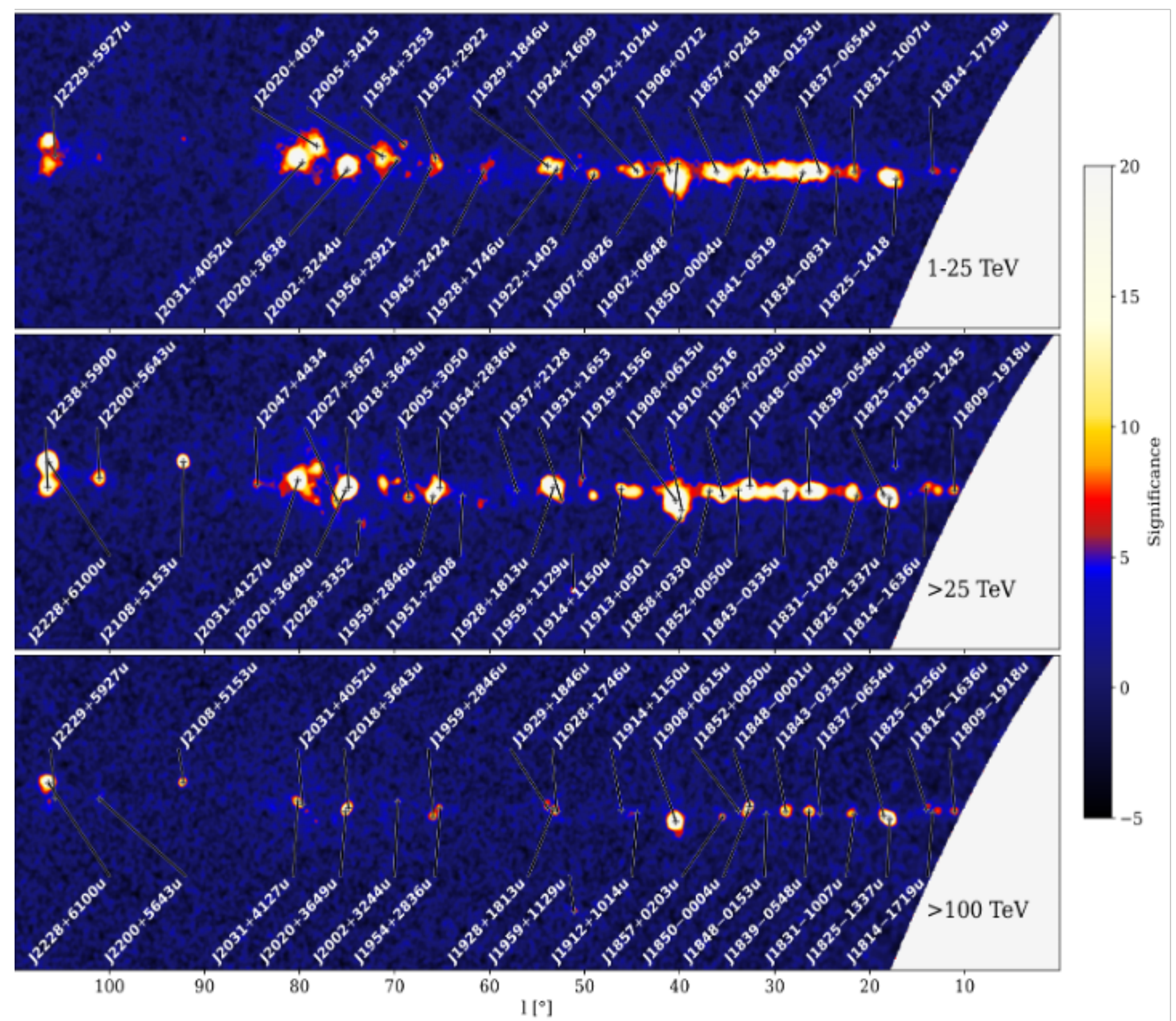

Source catalogs @ VHEs

1LHAASO catalog

Among the 90 sources with extension <2°, 65 sources exhibit extended morphology with a confidence level greater than 3σ. A total of **54 sources have been simultaneously detected by both WCDA and KM2A**.

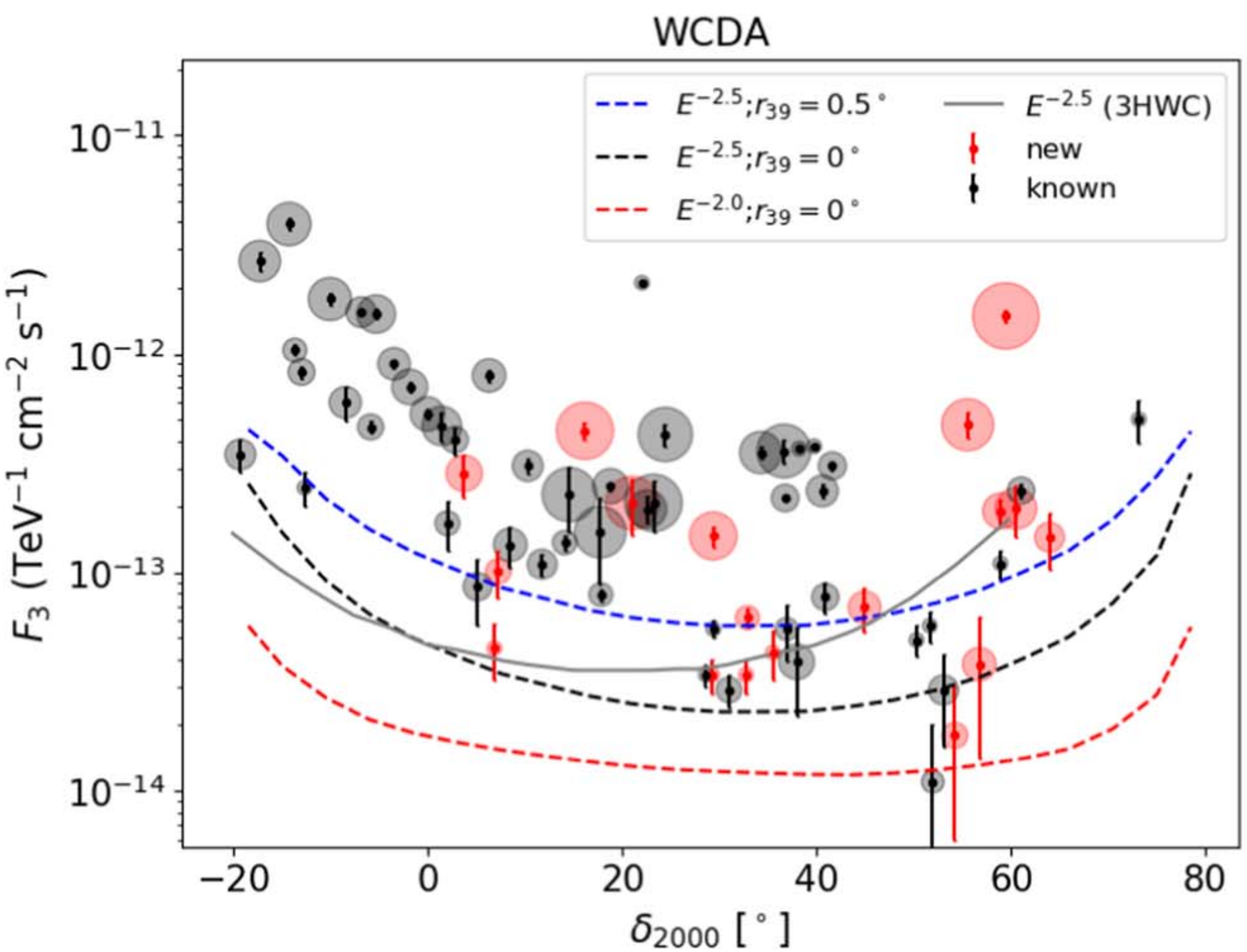

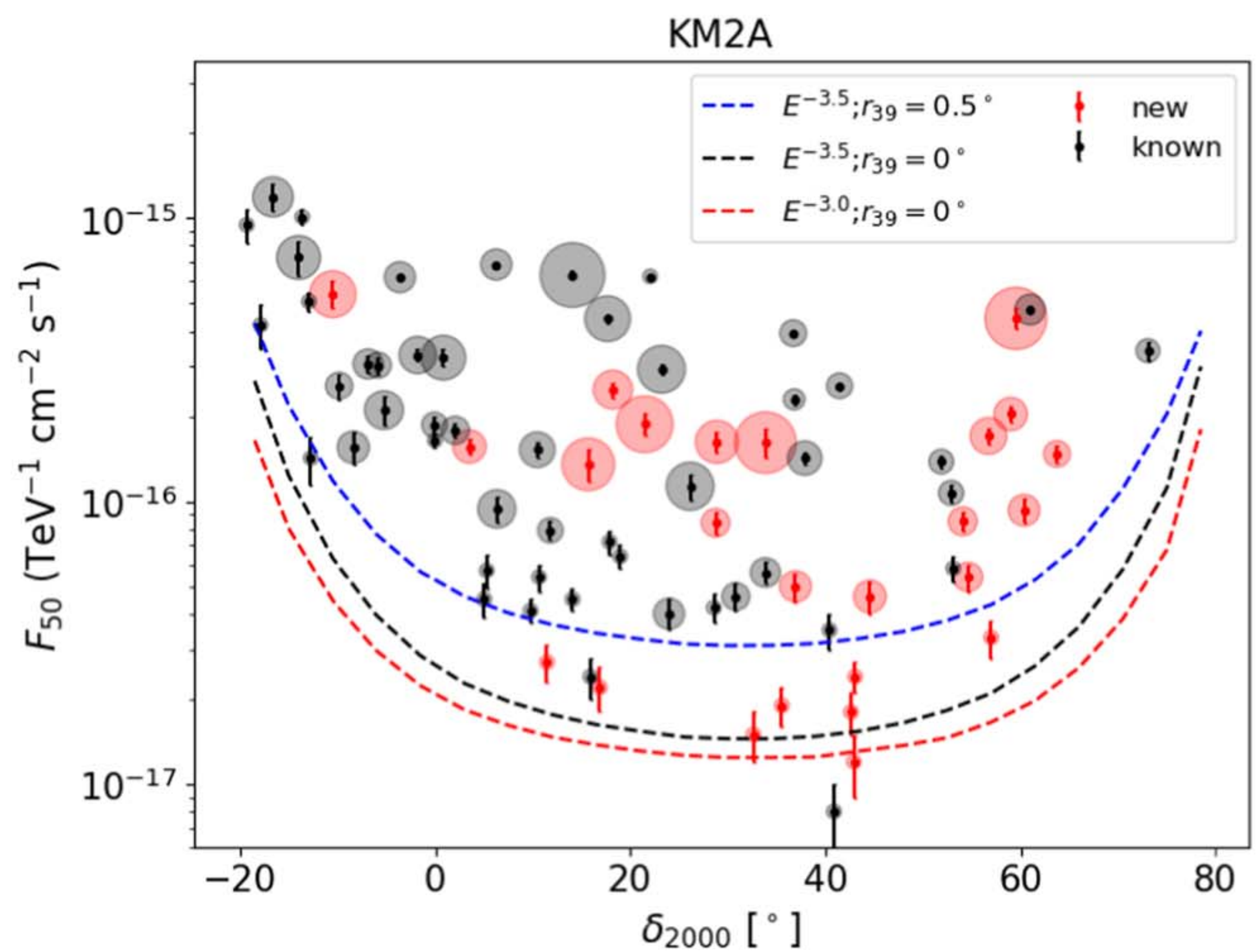

Source catalogs @ VHEs

1LHAASO catalog

About 57% of sources detected at E>25TeV sources are also UHE sources. **Most of these UHE sources have higher significance or harder spectral index than the other E > 25 TeV sources not detected at UHEs**. This could indicate that the remaining E > 25 TeV sources may also be detected as UHE sources by LHAASO in the future with further accumulation of data.

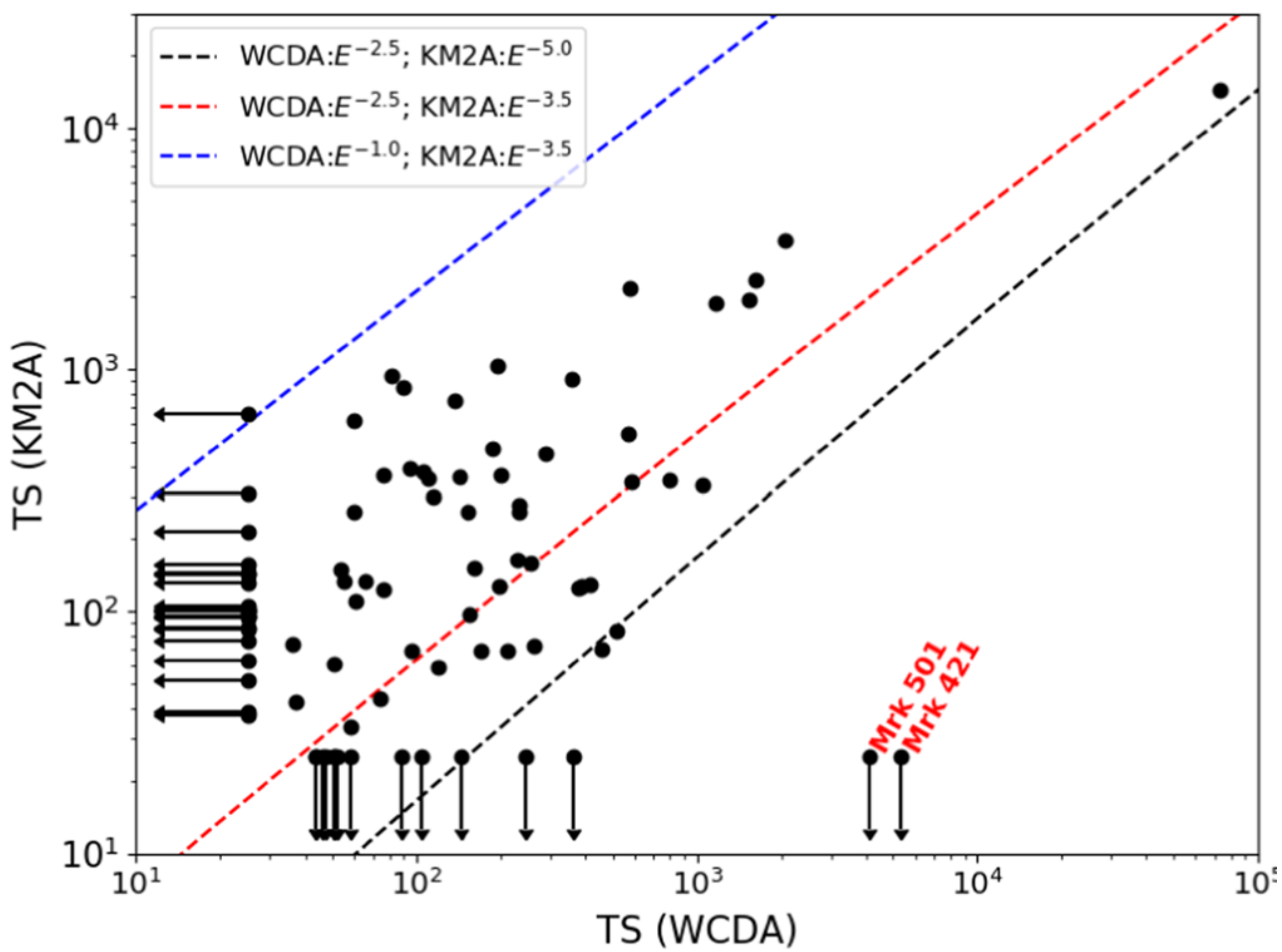

Source catalogs @ VHEs

1LHAASO catalog

35 associations of LHAASO sources with high spin-down power PSRs within a distance of 0.5 deg with a chance probability < 1%. Amongst them, PSR J0218+4232 is the first millisecond PSR reported at VHEs. The confidence level for its spatial association is 2.9 sigma.

LHAASO TeV-associated PSRs display $L_{sd} > 10^{34}$ erg/s. From the total of 35 PSR associations, 24 have $t_{age} < 10^5$ yrs, and 11 $t_{age} > 10^5$ yrs, these latter prompting for the possibility to be TeV Halos.

Most of the $L_{sd} > 10^{36}$ erg/s PSRs are associated with 1LHAASO sources., (on the contrary, no VHE or UHE emission is found for two PSRs with $L_{sd} > 10^{37}$ erg/s), and **22 out of the 35 PSR associations are UHE sources**

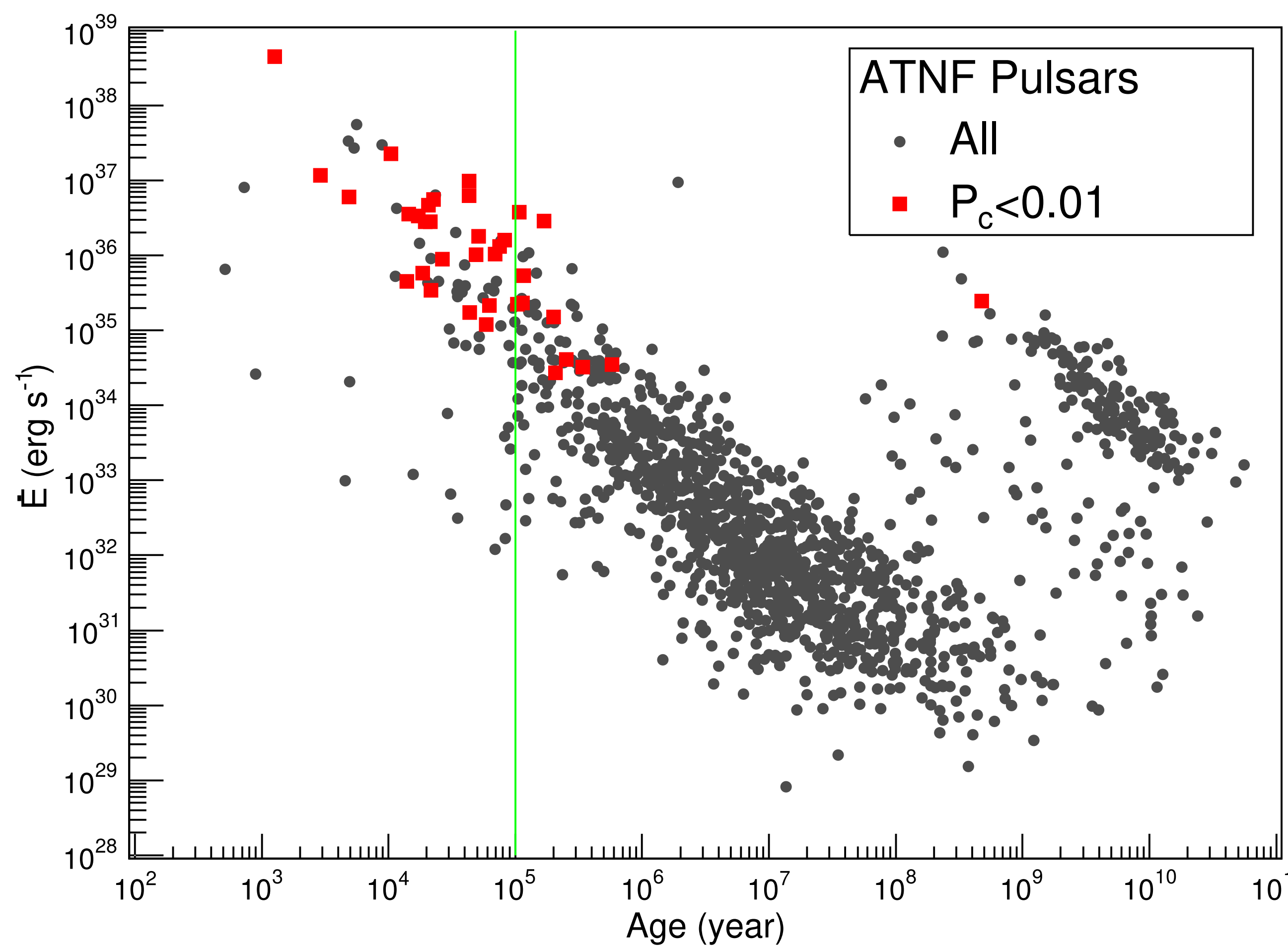

1 - The Galactic Center

The Galactic Center

The GC is a region of high astrophysical interest and has been studied extensively by many observatories at essentially all wavelengths.

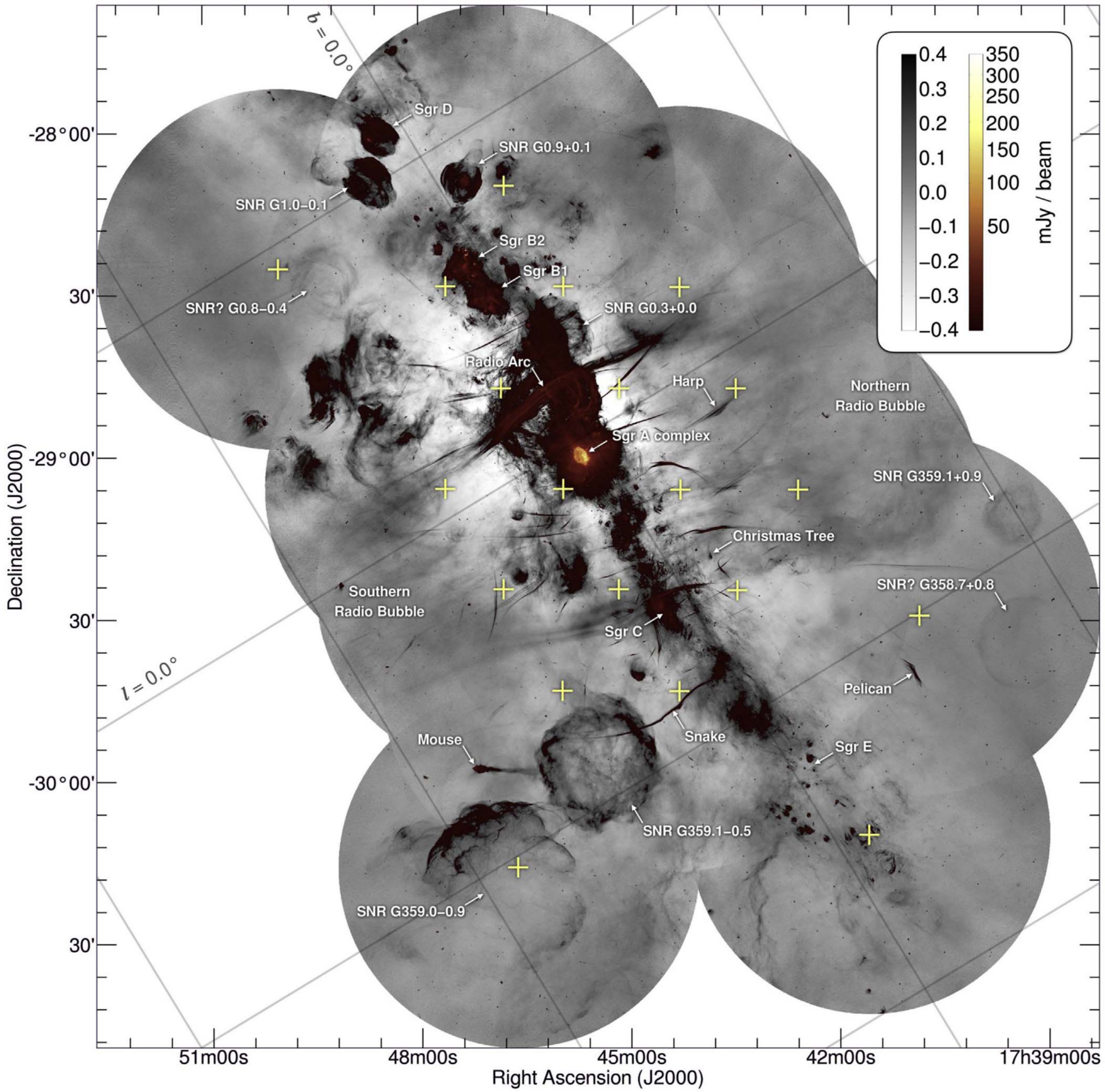

1.28 GHz MeerKAT Galactic Center Mosaic

Heywood et al. 2022

The Galactic Center

The GC region harbours a central compact radio source, Sgr A*, that coincides with the **SMBH at the dynamical center of the Galaxy**, with a mass of 4.6 x 10^6 $M_\odot$ (Gillessen et al. 2017).

SgrA* is surrounded in the inner few pc by massive clusters of young star. At radii of ~200 pc there is a **twisted torus-like structure** rich in molecular gas and dust, the Central Molecular Zone, with ρ, T, and turbulent velocities up to 100 times larger than in the disk (Heywood et al. 2022). The CR density is also > 100 times larger (Oka et al. 2019).

The GC hosts also several **giant molecular clouds** with strong star formation taking place (e.g. Sgr B2), together with a number of SNRs and PWNe.

At several 100s of pc, large scale outflows are found, including radio lobes or bubbles, and filamentary structures of unknown origin (see e.g. Barkov et al. 2019)

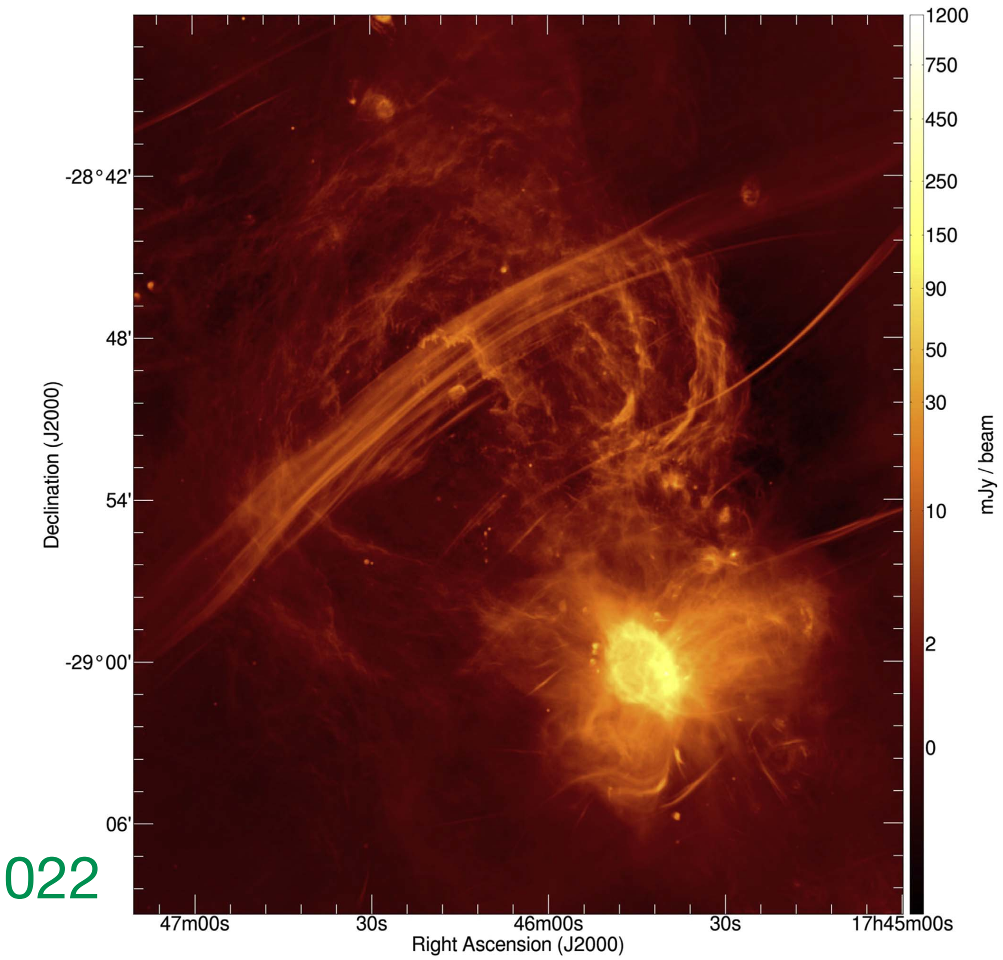

Heywood et al. 2022

The Galactic Center

The origin of the GeV and TeV emission towards the inner regions of the GC is unknown. Several scenarios have been discussed: the SMBH itself (Aharonian & Neronov 2005), the PWN G359.95-0.04 at a few arcsec distance from the GC (Wang et al. 2006; Hinton & Aharonian 2007), or the central diffuse region around the GC (Chernyakova et al. 2011).

H.E.S.S. revealed for the first time the existence of a TeV point-like source in the inner regions of the GC (Aharonian et al. 2006), HESS J1745–290, about 13” away from Sgr A* (Acero et al. 2010) and an extended TeV-emitting GC ridge **correlated a complex of giant MCs** within the central 200 pc of the Galaxy.

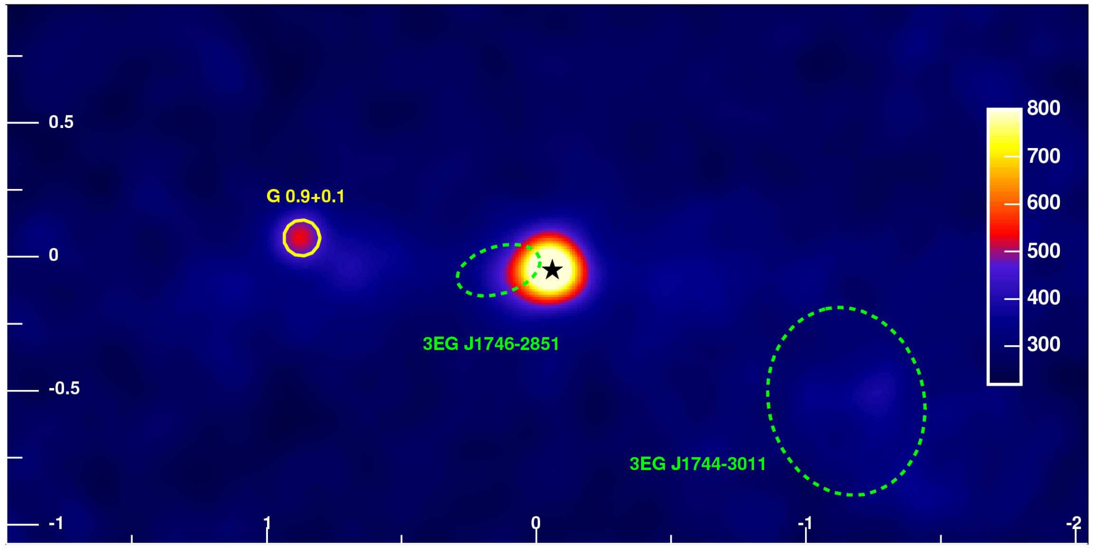

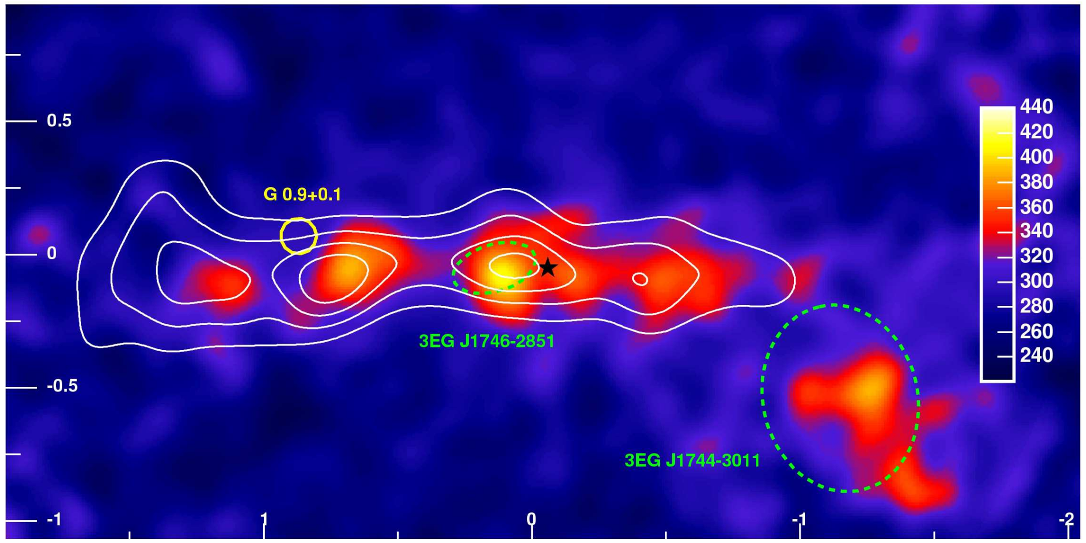

Aharonian et al. 2006

The Galactic Center

The origin of the GeV and TeV emission towards the inner regions of the GC is unknown. Several scenarios have been discussed: the SMBH itself (Aharonian & Neronov 2005), the PWN G359.95-0.04 at a few arcsec distance from the GC (Wang et al. 2006; Hinton & Aharonian 2007), or the central diffuse region around the GC (Chernyakova et al. 2011).

H.E.S.S. revealed for the first time the existence of a TeV point-like source in the inner regions of the GC (Aharonian et al. 2006), HESS J1745–290, about 13” away from Sgr A* (Acero et al. 2010) and an extended TeV-emitting GC ridge **correlated a complex of giant MCs** within the central 200 pc of the Galaxy.

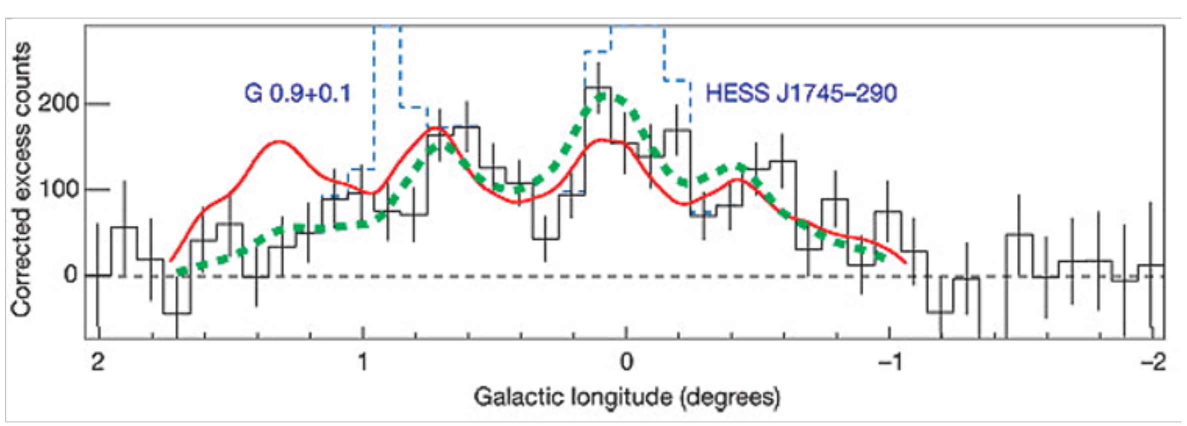

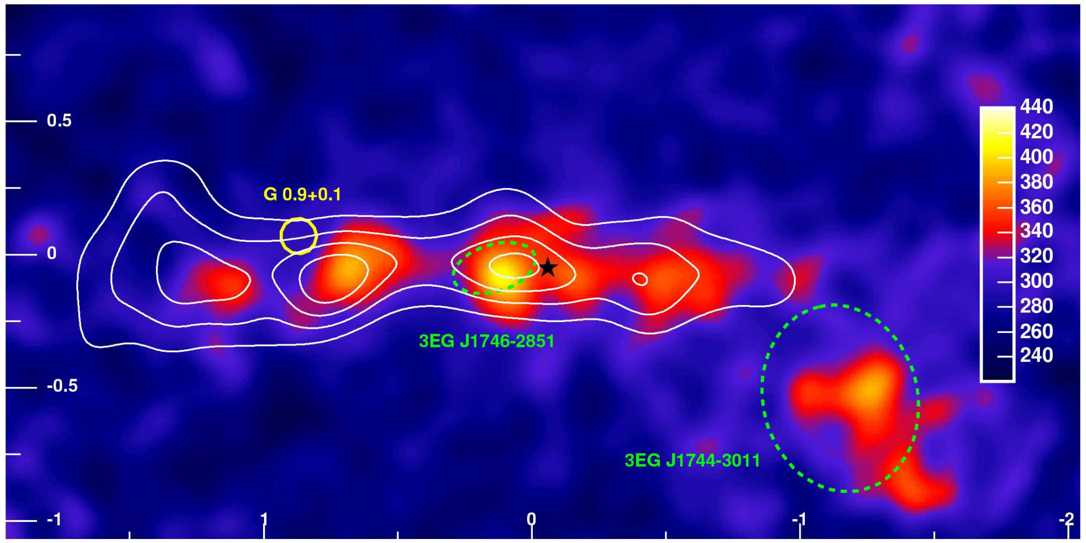

Aharonian et al. 2006

A PeVatron in the Galactic Center

The CR radial profile points towards **an accelerator located in the inner 10 pc of the GC, possibly Sgr A* itself**, indicating a quasi-continuous injection of protons (1/r profile) that diffuse into the CMZ.

The spectrum of the diffuse emission is **hard** (index 2.3) and **does not show any signature for a cutoff up > 50 TeV.** Assuming pp interactions, this implies proton energies **up to ~1 PeV** => a PeVatron

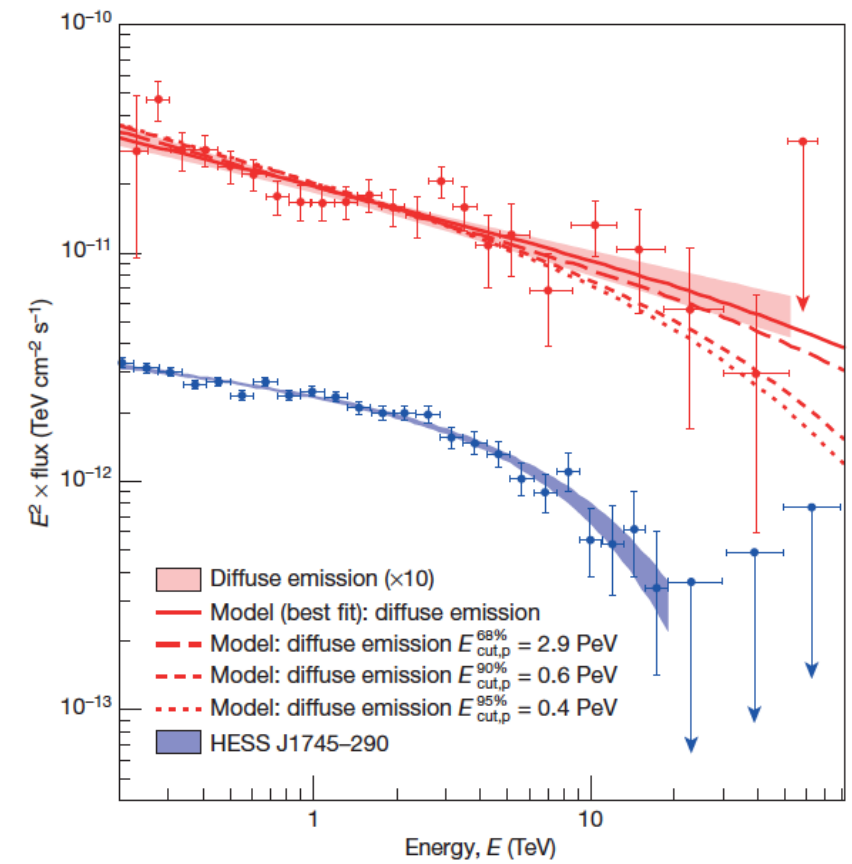

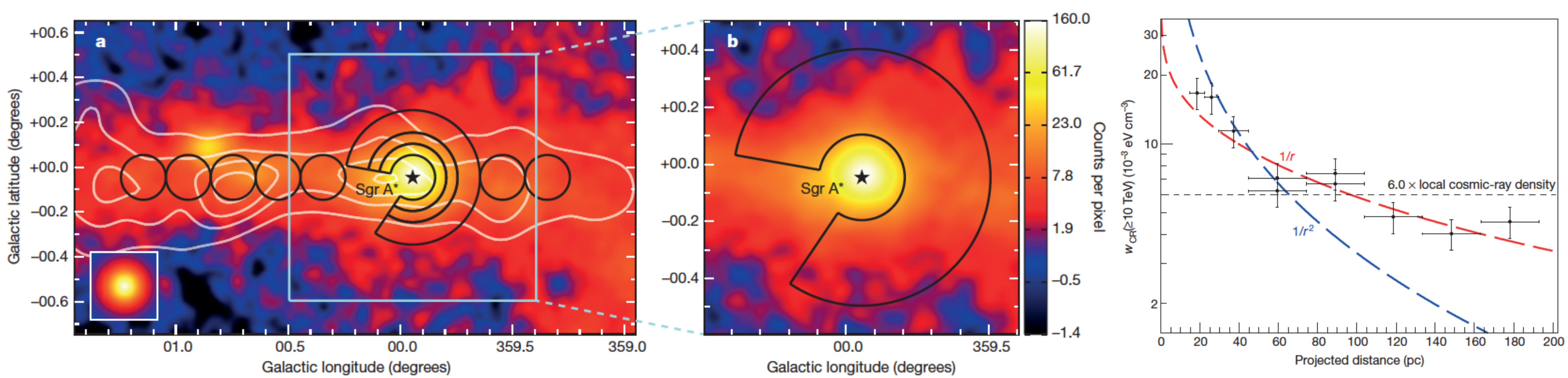

H.E.S.S. coll. 2016

A PeVatron in the Galactic Center

The SMBH Sgr A* **may have operated at a much higher accretion rate** than as of the (moderate) levels observed today

An average acceleration rate of 10^{39} erg/s E>10 TeV protons over the last 10^6 -10^7 years would be sufficient to **explain the flux of CRs around the "knee"**, making Sgr A* a viable **alternative to SNR as a source of PeV Galactic cosmic rays.**

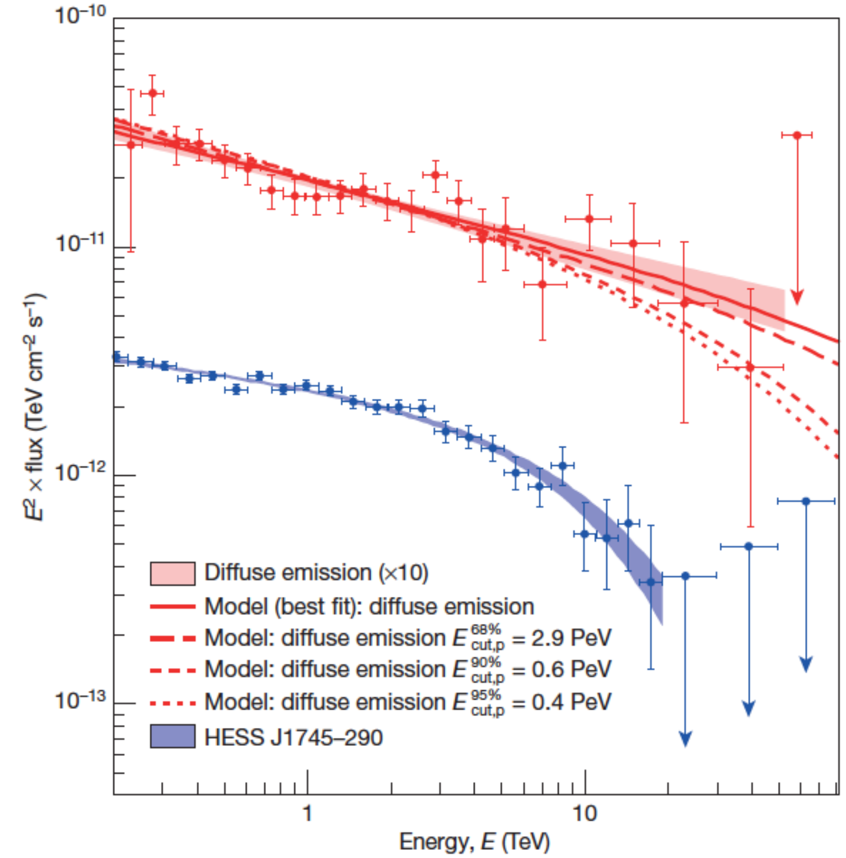

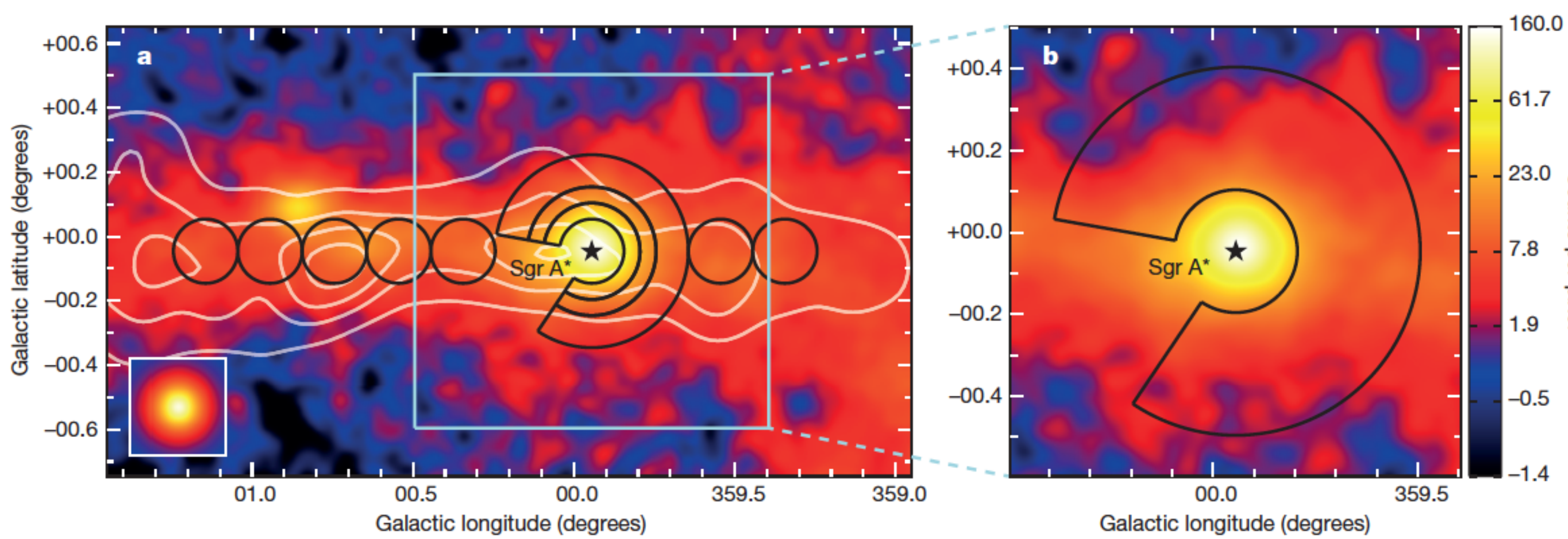

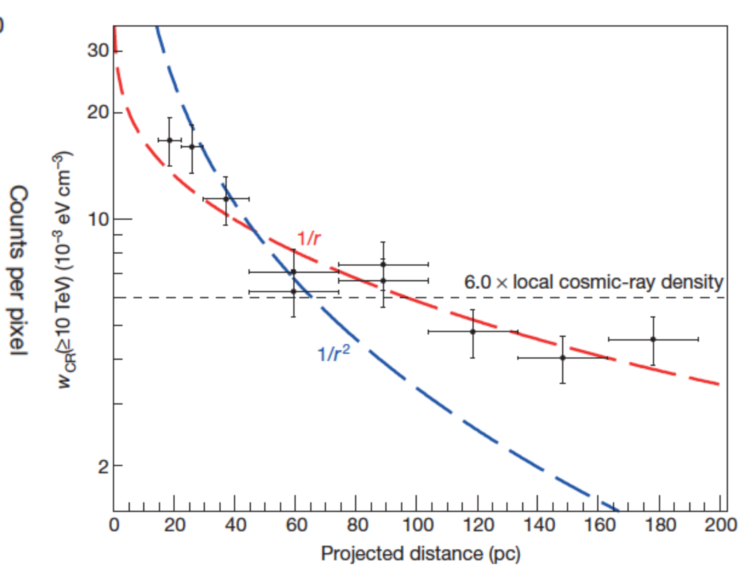

H.E.S.S. coll. 2016

Galactic Center

MAGIC observed the GC region for about100 h over five years, from 2012 to 2017, collected large zenith angles ~60 - 70 deg) => leading to a **larger energy threshold**, but also an **increased effective collection area**. (Acciari et al. 2020).

A significant detection is obtained for Sgr A*, the “Arc” PWN and the SNR G0.9+0.1, together with an extended component for the Galactic Ridge, perfectly compatible with the H.E.S.S. maps. The derived **CR profile peaks at the GC** position with a profile index of ~1.2, **consistent with a 1/r profile**

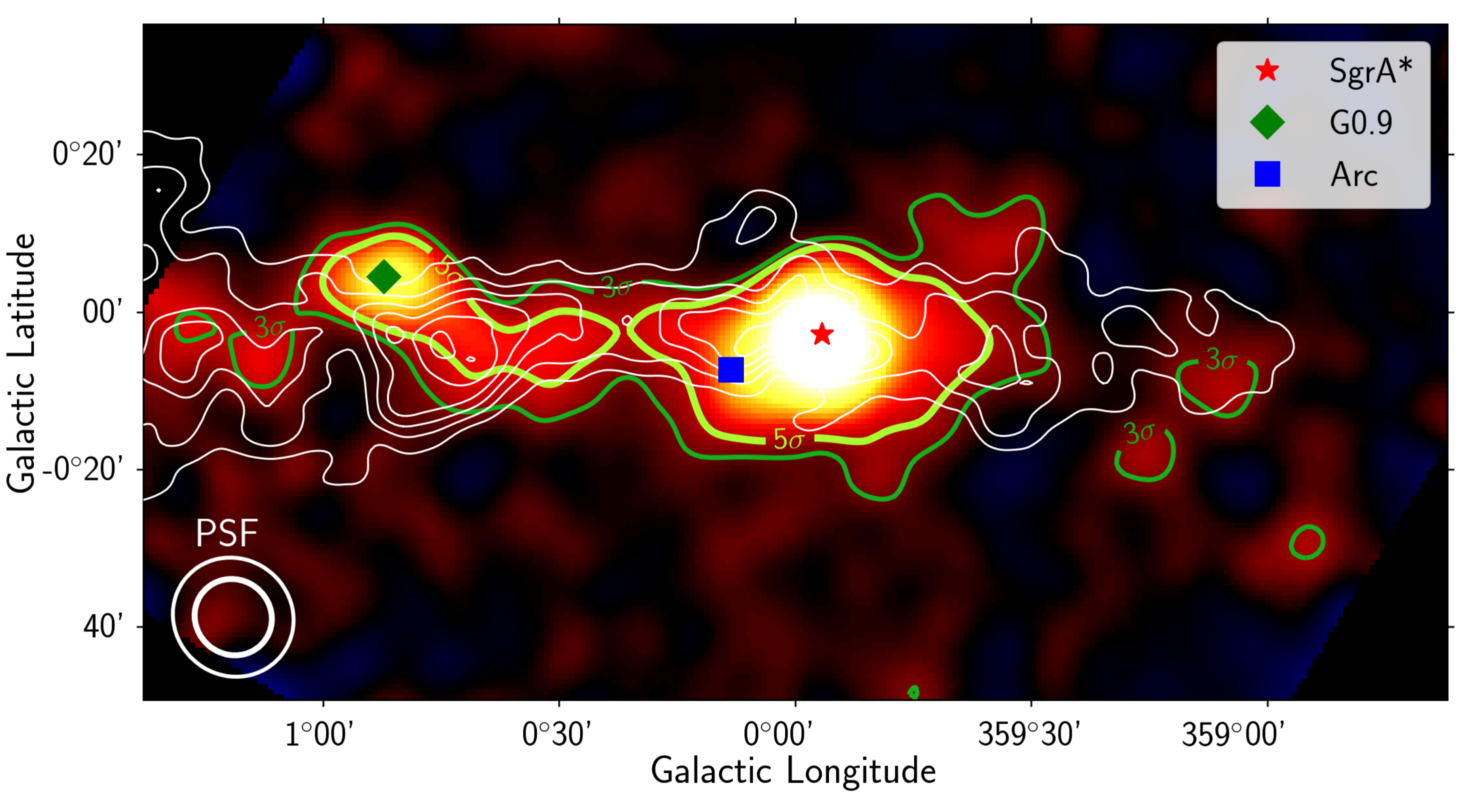

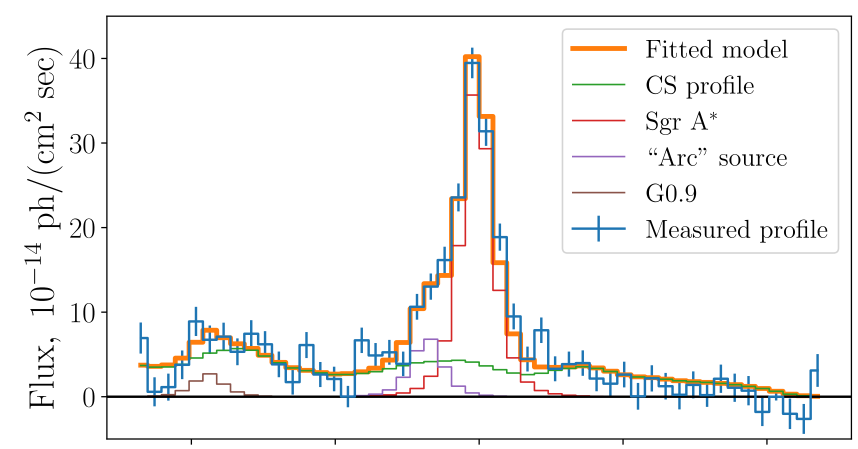

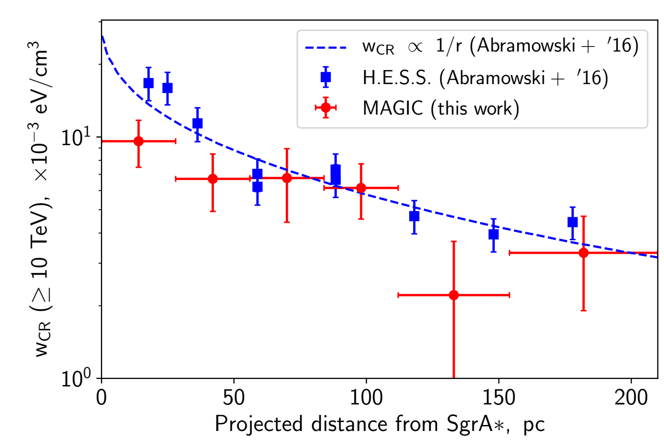

Acciari et al. 2020

Galactic Center

On spectral grounds, **MAGIC data is well-fit with a PL for both Sgr A* and the Galactic Ridge**, with a spectral **index ~2** and an **2σ indication of a exp cut-off at ~20 TeV**. The 1σ confidence range for the cut-off energy spans from 10 TeV to 80 TeV, corresponding to proton energies of ≈0.1–1 PeV, still (marginally) **compatible with the PeVatron scenario**.

Name	Spec. type	N, 10^{-25} eV^{-1} cm^{-2} s^{-1}	Γ	E_{cut}, TeV
Sgr A*	PLC	$5.39^{+0.56}_{-0.46}$ stat.$^{+1.61}_{-1.19}$ sys.	$-1.98^{+0.11}_{-0.10}$ stat.$^{+0.18}_{-0.17}$ sys.	$12.4^{+5.5}_{-3.2}$ stat.$^{+3.3}_{-0.2}$ sys.
G0.9+0.1	PL	$0.93^{+0.20}_{-0.17}$ stat.$^{+0.26}_{-0.12}$ sys.	$-2.32^{+0.13}_{-0.15}$ stat.$^{+0.20}_{-0.12}$ sys.	–
Arc	PL	$0.52^{+0.15}_{-0.15}$ stat.$^{+0.16}_{-0.09}$ sys.	$-2.29^{+0.17}_{-0.19}$ stat.$^{+0.23}_{-0.13}$ sys.	–
Diffuse	PLC	$9.32^{+2.39}_{-1.63}$ stat.$^{+2.53}_{-1.97}$ sys.	$-1.98^{+0.26}_{-0.21}$ stat.$^{+0.16}_{-0.15}$ sys.	$17.5^{+59.3}_{-9.55}$ stat.$^{+4.5}_{-1.9}$ sys.

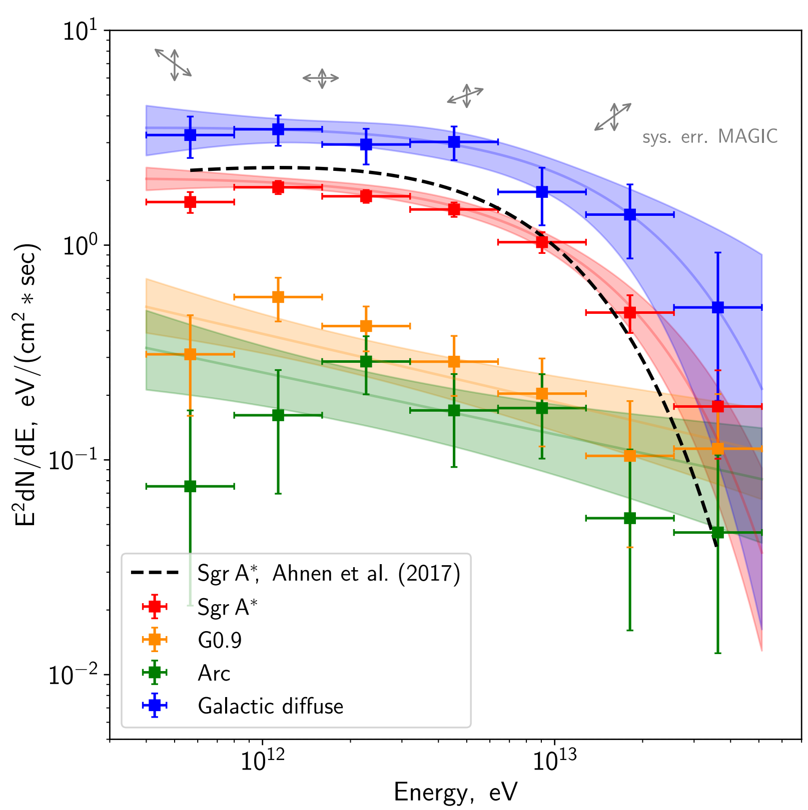

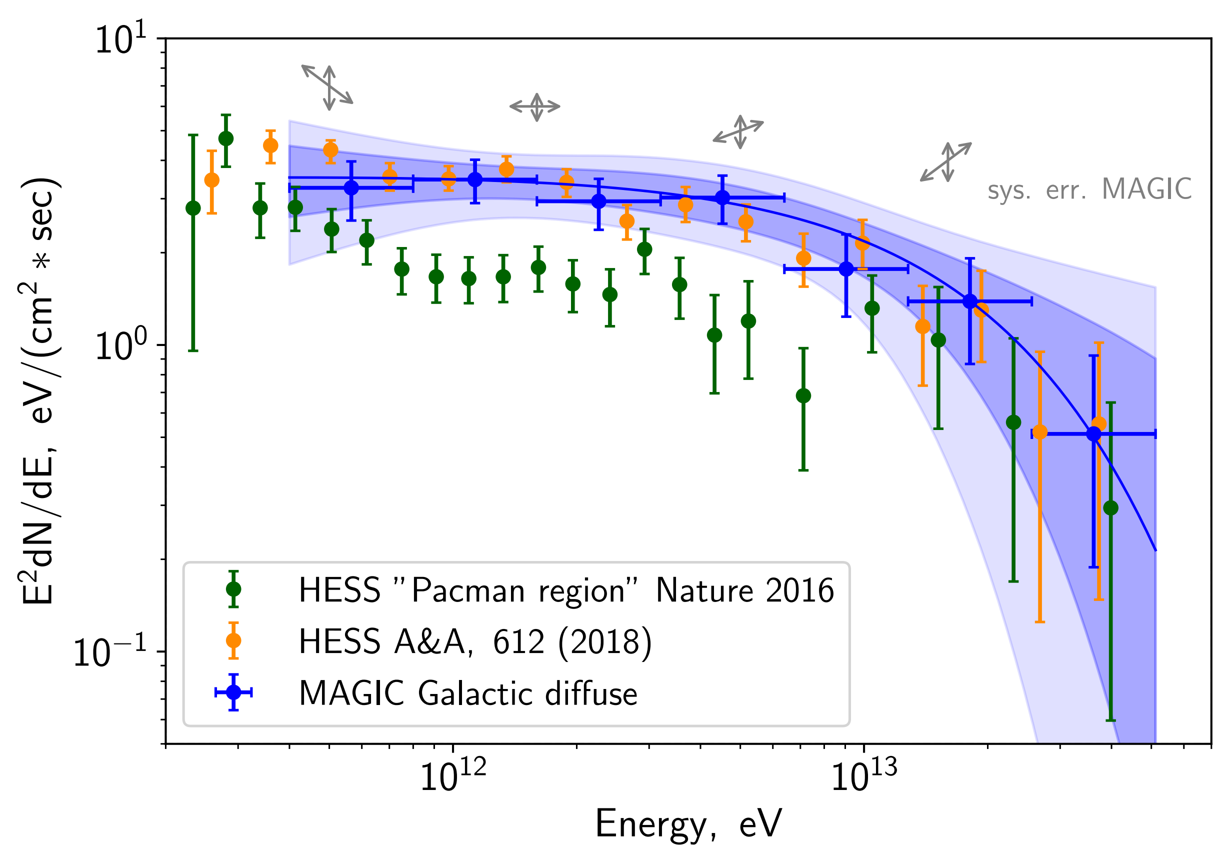

Galactic Center

VERITAS also confirmed recently the H.E.S.S. results, following a 125h of dedicated observations of the GC region under **large zenith angle conditions** (Adams et al. 2021).

The point-like source VER J1745–290 is detected at high statistical significance (38σ), with its location consistent with Sgr A*, and a spectral distribution following a PL with **index ~2.1**, and an **exp-cutoff at ~10.0 TeV**.

The extended GC ridge is also clearly detected (9.5σ), and is best fit by a **PL with an index of 2.2 with no evidence of a cutoff up to 40 TeVs**.

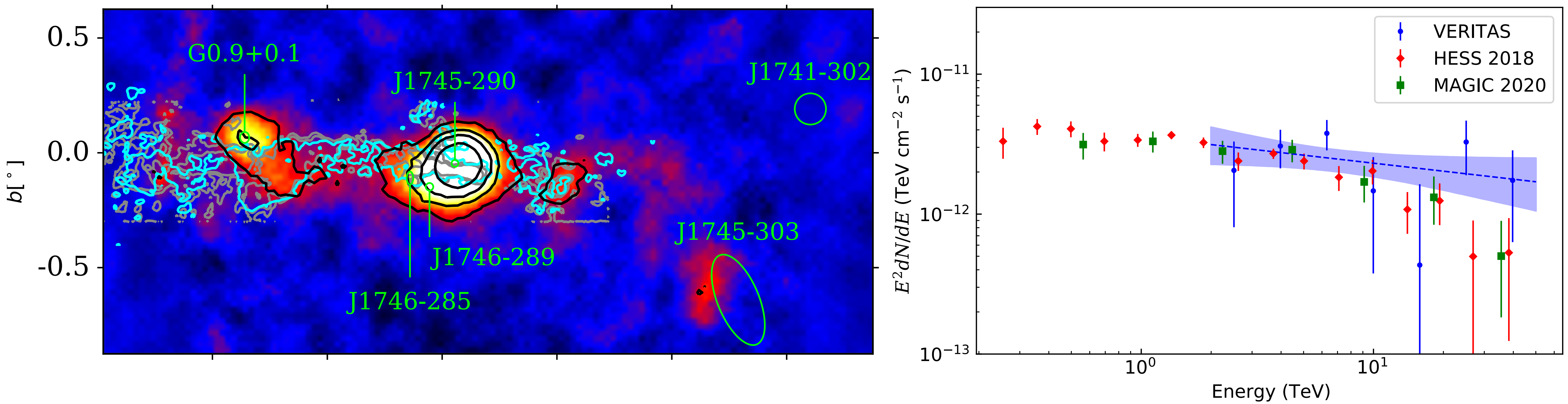

Adams et al. 2021

Galactic Center

Very recently the LST-1 first prototype of the CTAO array has also reported on observations of the GC under large zenith angle mode, during its scientific commissioning phase (Abe et al. 2023).

LST-1 data account for **~39h observations** collected in 2021 and 2022. A preliminary spectral analysis of these data **confirms the detection of Sgr A* and SNR G0.9+0.1** at high significance, with **Sgr A* described with a PL** (index ~ 2.14 and 2.30) **+ exp cut-off** (E_c ~ 20 TeV)

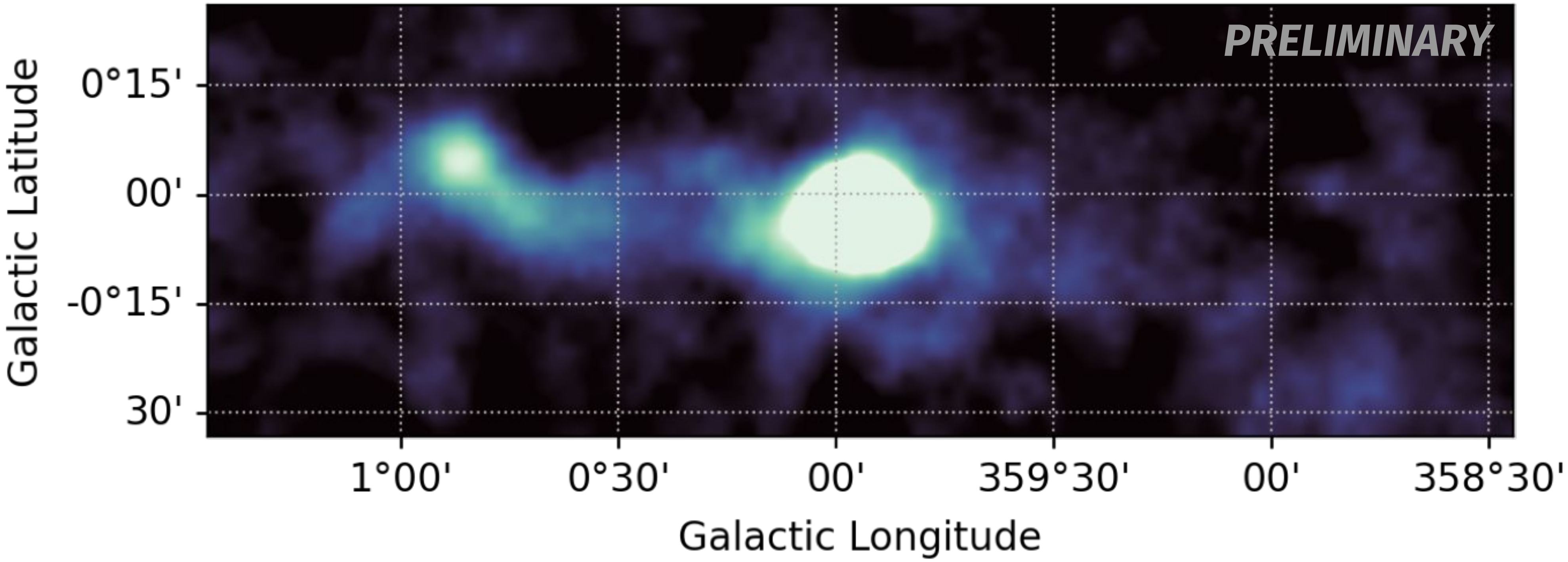

Abe et al. 2023

SNRs @ VHE gamma-rays

SNRs are the result of supernova explosions produced by the **collapse of a massive star** (> 8 $M_\odot$, core-collapse SNe) or in a **WD in a binary system that exceeds the Chandrashekar limit** (>1.4 $M_\odot$) when accreting from the companion star in a binary system (type Ia SNe).

The SN expels a up to a few $M_\odot$ at a speed of ~10^4 km/s. This corresponds to a **kinetic energy of about 10^{51} erg**. The **chemical composition of the ejected material** and the **ISM properties** into which the explosion evolves can

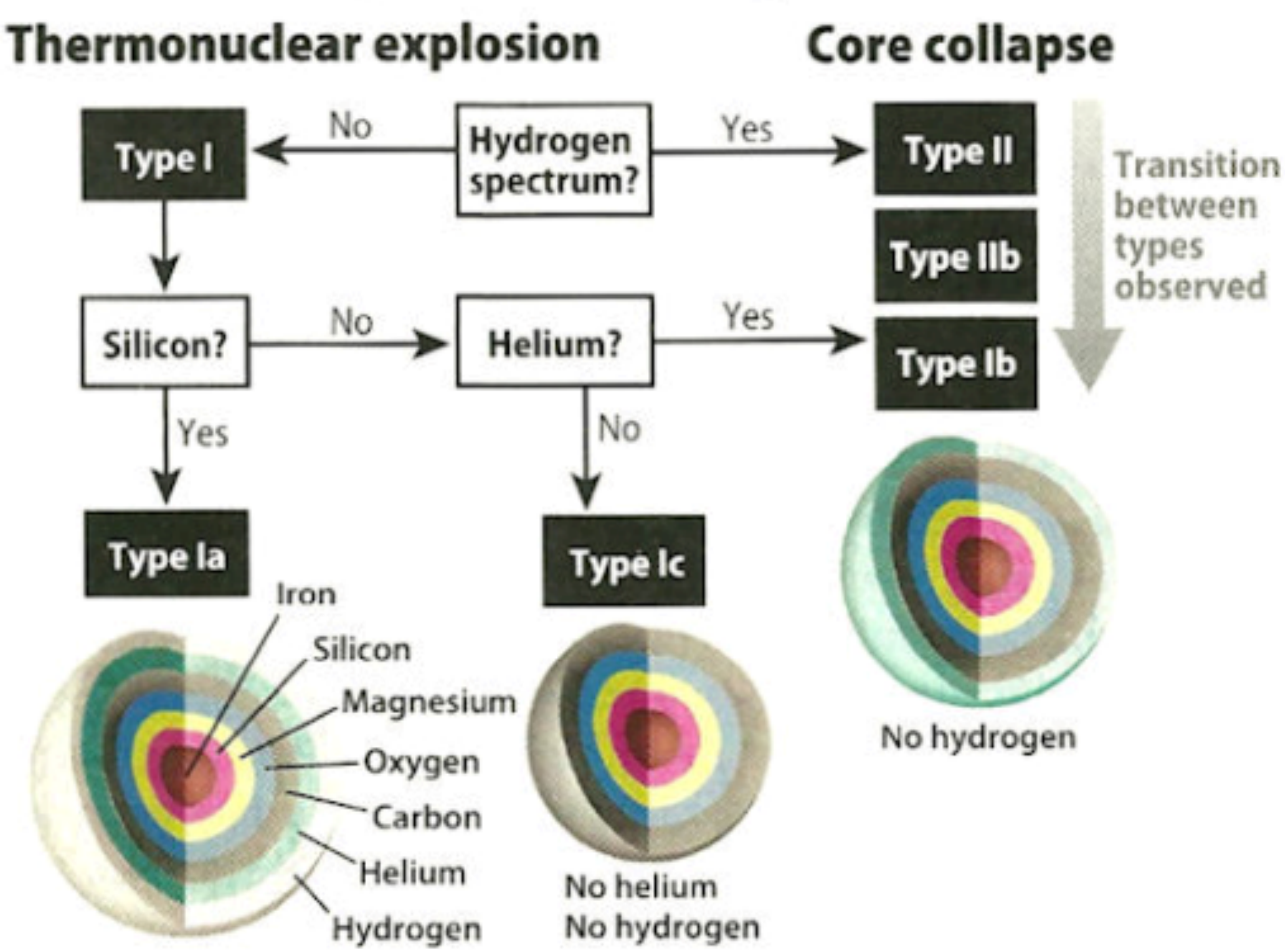

SNRs @ VHE gamma-rays

The **SNR evolution** mainly depends on $M_{ej} \lesseqgtr M_{sw}$

- "free expansion phase" (a few 100s yrs), $M_{ej} < M_{sw}$ and the SNR size evolves as $R \propto t$. The outflow is supersonic, and a strong shock develops.
- "Sedov-Taylor phase" (~20 to 40 kyrs), $M_{ej} \leq M_{sw}$ the **deceleration of the shell** becomes significant, and a reverse shock is formed towards the SNR ejecta). In this phase $R \propto t^{2/5}$. Both the forward and reverse shock can accelerate particles, leading to non-thermal emission from radio to gamma-rays.
- "radiative phase" $M_{ej} << M_{sw}$, the shell expands at subsonic velocities, and the SNR eventually dissolves into the ISM.

Cas A, Lee et al. 2014

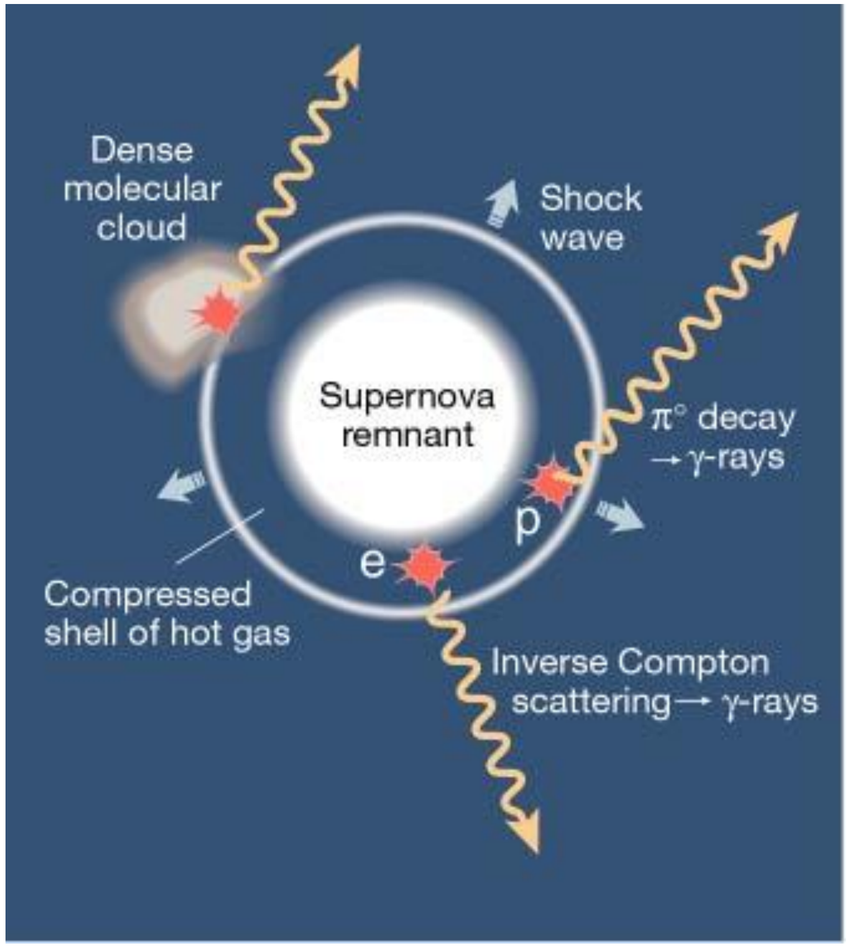

SNRs @ VHE gamma-rays

The first γ-ray instruments (SAS-2, COS-B in the 1970s, EGRET on board CGRO in the 1990s) **were already able to detect these objects**. On the other hand, **the limited angular resolution** of these instruments and the crowding of the galactic fields did not allow the γ-ray emission to be associated with SNRs.

The first certain associations were made with Cherenkov instruments; HEGRA observed a source associated with SNR W28, while H.E.S.S. was able to resolve the shell morphology of SNR RX J1713.7-3946 [Aharonian et al. 2006].

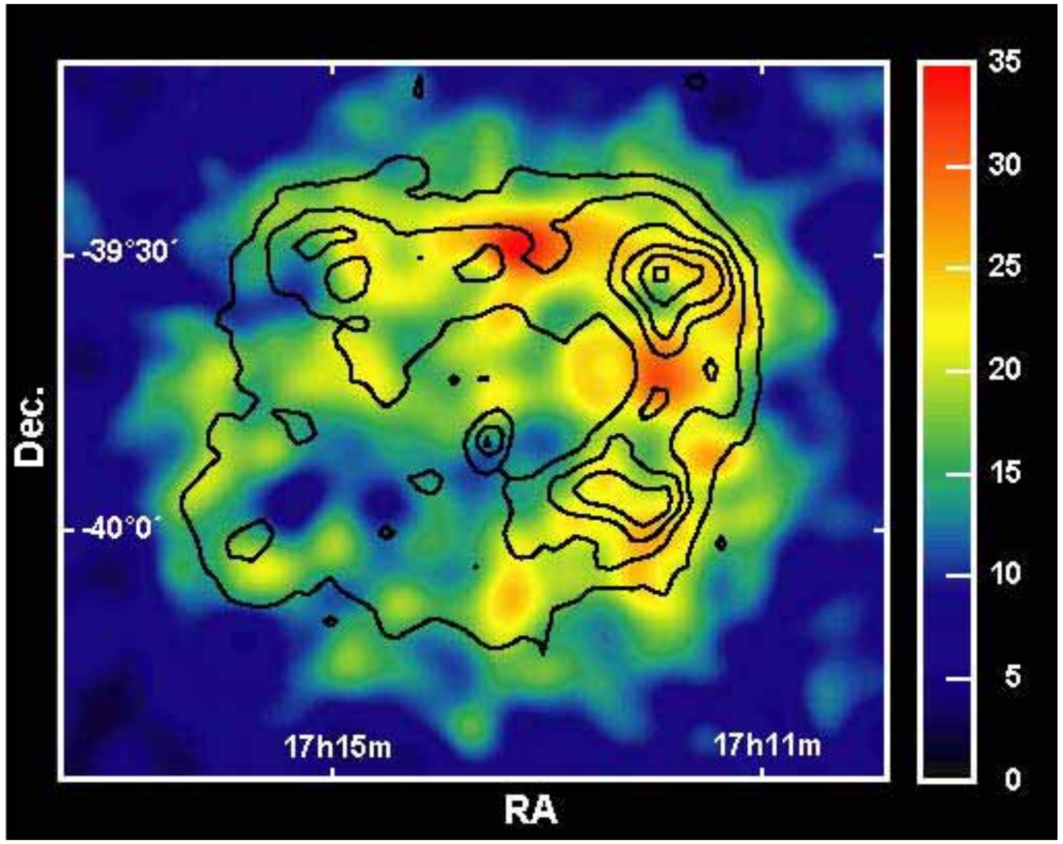

Aharonian et al. 2006

SNRs @ VHE gamma-rays

SNR Name	FERMI-LAT	AGILE	HESS	MAGIC	VERITAS
G359.1-0.5	(a) - [97]*	—	[13]*	—	—
HESS J1731-347	[4] - [84]*	—	[86]*	—	—
CTB 37B	(b) - [148]*	—	[10]*	—	—
CTB 37A	(a,b*) - [53] - [48]*	—	[11]*	—	—
RX J1713.7-3946	(a,b) - [66]*	—	[15]*	—	—
SN 1006 (NE)	[150] - [58]*	—	[3]*	—	—
SN 1006 (SW)	[150] - [58]*	—	[3]*	—	—
G318.2+0.1	—	—	—	—	—
RCW 86	(b^*) [19]*		[88]*	—	—
G298.6-0.0	(a^*, b^*)	—	—	—	—
Vela Jr.	(a^*, b^*) - [137]	—	[87]*	—	—
Puppis A	(a,b^*) - [149]*	—	[90]*	—	—
IC 443	(a,b) - [6]*	[138]*	—	[25]*	[1]*
Tycho	(a,b) - [33]*	—	—	—	[33]*
Cas A	(a,b) - [17]*	—	—	[17]*	[113]*
Gamma Cygni	(a,b) - [71]*	—	—	—	[28]*
Cygnus Loop	(a^*, b^*) - [125]*	—	—	—	—
W51 C	(a,b) - [101]*	—	—	[27]*	—
W49 B	(a,b) - [92]*	—	[92]*	—	—
W44	(a,b^*) - [6]*	[51]	—	—	—
W41	(a^*) - [91]	—	[91]*	[26]*	—
W28 north	[61]*	[79]	[61]*	—	—
W28 A	[61]*	—	[61]*	—	—
W28 B	[61]*	—	[61]*	—	—
W28 C	[61]*	—	[61]*	—	—
G349.7+0.2	(a,b^*) - [89]*	—	[89]*	—	—
HESS J1912+101	—	—	[82]*	—	—
HESS J1534-571	[31]*	—	[31]*	—	—
MSH 17-39	(a^*) - [56]	—	—	—	—
HB 21	(a^*) - [122]	—	—	—	—
HESS J1614-518	—	—	[82]*	—	—
W30	(a^*,b) - [21]	—	[16]*	—	—
3C 391	(a,b^*) - [54]*	—	—	—	—
CTB 109	(a^*, b^*) - [55]	—	—	—	—
G337.0-0.1	(a,b^*) - [56]*	—	—	—	—
S147	(a,b^*) - [107]*	—	—	—	—
Kes17	(a^*, b^*) - [77]	—	—	—	—

adapted from
Crestan et al. 2023

SNRs @ VHE gamma-rays

SNRs have long been suggested to be a major contributor to **Galactic CRs** (Baade & Zwicky 1934). This hypothesis can be tested with observations **in the gamma-ray band**. Since the CR spectrum shows that some Galactic sources can accelerate particles to at least 1 PeV, this should result in a gamma-ray spectrum that extends up to (and beyond) 100 TeV

SNRs are indeed strong non-thermal emitters (from radio to γ-ray) implying **efficient particle acceleration** (shocks). In addition, their **energy reservoir** matches the power needed to sustain the galactic CR population:

$$E_{CR} = w_{CR} \times V_{disk} \approx 1\ \mathrm{eV/cm^3} \times \pi (R/15\ \mathrm{kpc})^2 \times (\mathrm{h}/1\ \mathrm{kpc}) \approx 3 \times 10^{55} \mathrm{erg}$$

CR confinement time: $\tau_{disk} \approx 10^7 \mathrm{yrs}$ (from CR isotope ratios measurements)

$$\Rightarrow\ P_{CR} = E_{CR}/\tau_{disk} \approx 10^{41} \mathrm{erg/s}$$

$$P_{SN} = \nu_{SN} \times E_{SN} \approx \frac{1}{30\ \mathrm{yrs}} \times 10^{51} = 10^{42} \mathrm{erg/s}$$

SNR can sustain the bulk Galactic CR if they convert ~ 10% of the SN energy is converted into accelerated particles

SNRs @ VHE gamma-rays

Gamma-rays from SNR: leptonic or hadronic?

- accelerated **electrons** + B-fields gives yield to synchrotron emission, which can reach the X-ray band for E_e ~ few TeV. The same electron population can up-scatter local radiation fields through IC, giving rise to **gamma-ray emission**. In case of a dense ISM, Bremsstrahlung can also be expected.
- if **hadrons** are also accelerated, they scatter inelastically against the nuclei of the medium in "pp interactions", producing neutral pions, which decay into two γ-ray photons. **Secondary electrons** produced by pp interactions can also produce γ-ray emission through IC and Bremsstrahlung mechanisms.

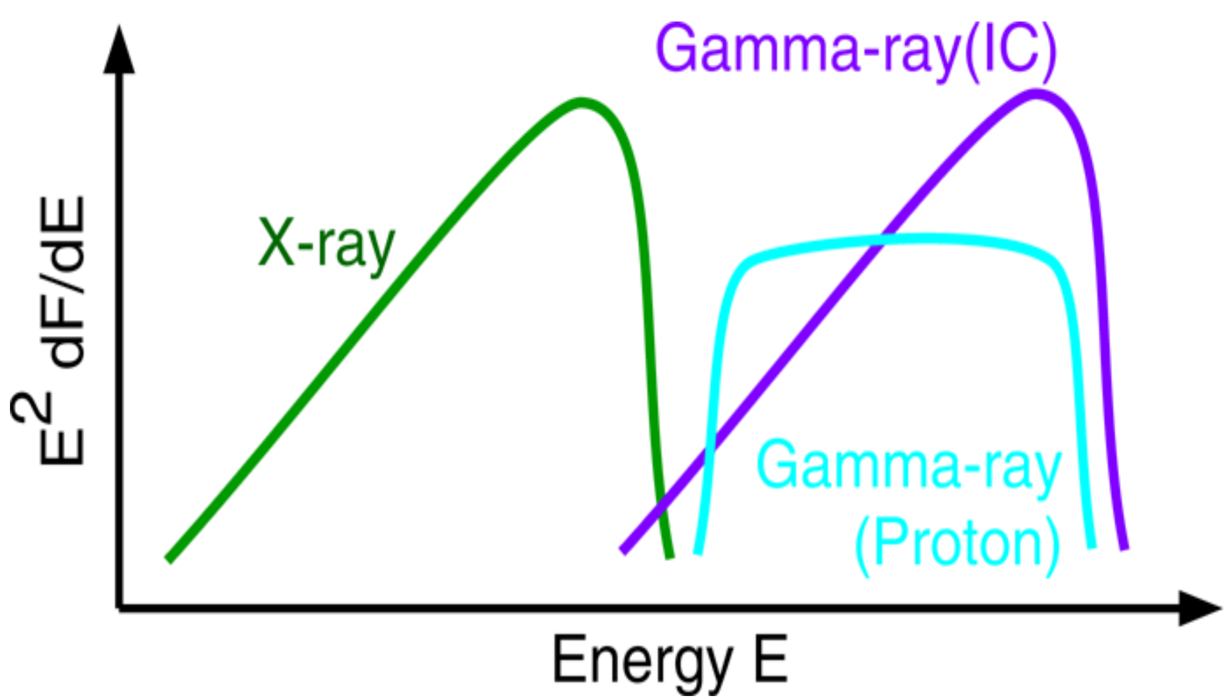

- proton-proton $E_\gamma \approx 0.1 E_p$
- IC on CMB $E_\gamma \approx 1 \left(\frac{E_e}{20\text{TeV}}\right) \text{TeV}$
- Bremsstrahlung $E_\gamma \approx E_e$

SNRs @ VHE gamma-rays

Gamma-rays from SNR: leptonic or hadronic?

- accelerated **electrons** + B-fields gives yield to synchrotron emission, which can reach the X-ray band for E_e ~ few TeV. The same electron population can up-scatter local radiation fields through IC, giving rise to **gamma-ray emission**. In case of a dense ISM, Bremsstrahlung can also be expected.
- if **hadrons** are also accelerated, they scatter inelastically against the nuclei of the medium in "pp interactions", producing neutral pions, which decay into two γ-ray photons. **Secondary electrons** produced by pp interactions can also produce γ-ray emission through IC and Bremsstrahlung mechanisms.

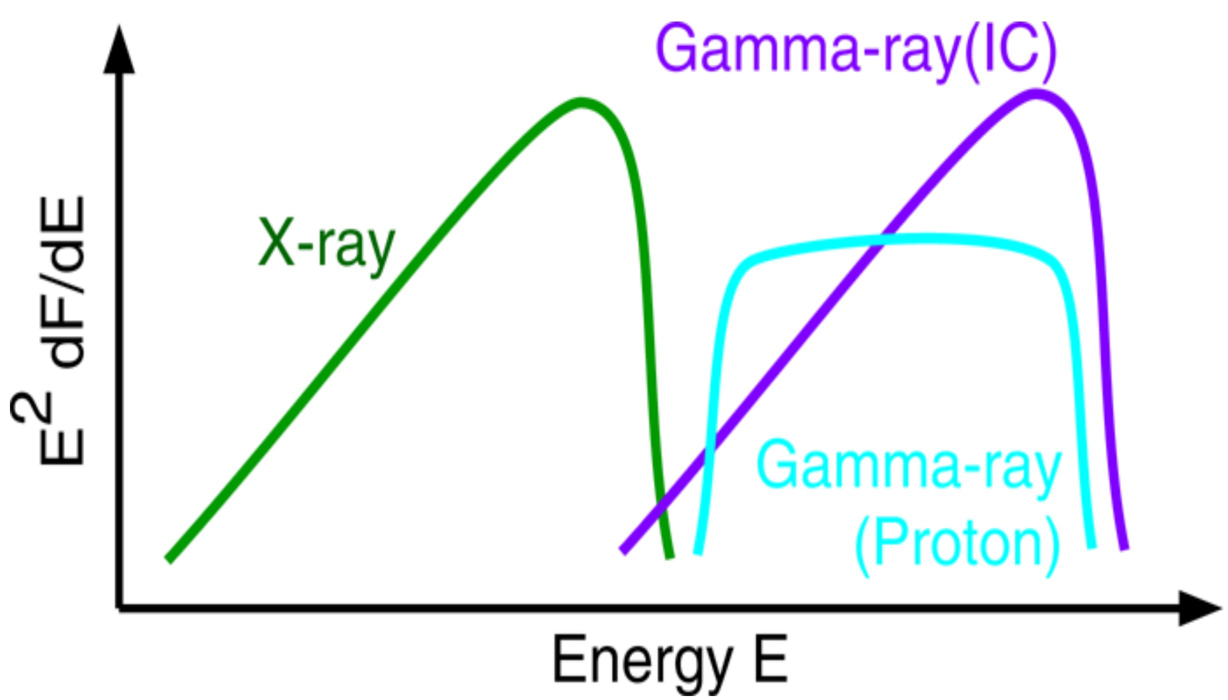

$$E_{p,e}^{-\mathrm{P}} \rightarrow E_{\gamma}^{-\Gamma}$$

- proton-proton $\Gamma = P$
- IC on CMB $\Gamma = \left(\frac{P+1}{2}\right)$
- Bremsstrahlung $\Gamma = P$

SNRs @ VHE gamma-rays

Young SNRs, with ages < few × 10^3 yrs, **display shell-like γ-ray morpholgies,** similar to what observed in X-rays. **γ-ray spectra are typically hard** (index ≲ 2) peaking around a few TeV, followed by a rapid (super/exponential) decrease. Young SNRs show similar γ-ray luminosities, which are well-modelled in a **leptonic scenario** with a **single e^- population.** Some well-known young SNRs are RX J1713.7-3946, RX J0852.0-4622, RCW 86, and the "historical SNRs": Cas A, Tycho, SN 1006 and Kepler SNRs (the latter one recently detected by H.E.S.S.)

Evolved SNRs (above 10^4 yrs) can **interact with nearby molecular clouds** (MCs), with $M_c > 10^3 M_\odot$. leading to γ-rays through **proton-proton interactions**. The spectra of these objects have a **soft index** (>2.5) and are **more easily observed in the GeV than in the TeV band.** γ-ray luminosities are ≥1035 erg/s. Well-known interacting SNRs are W44, W28, IC 443, and W51C.

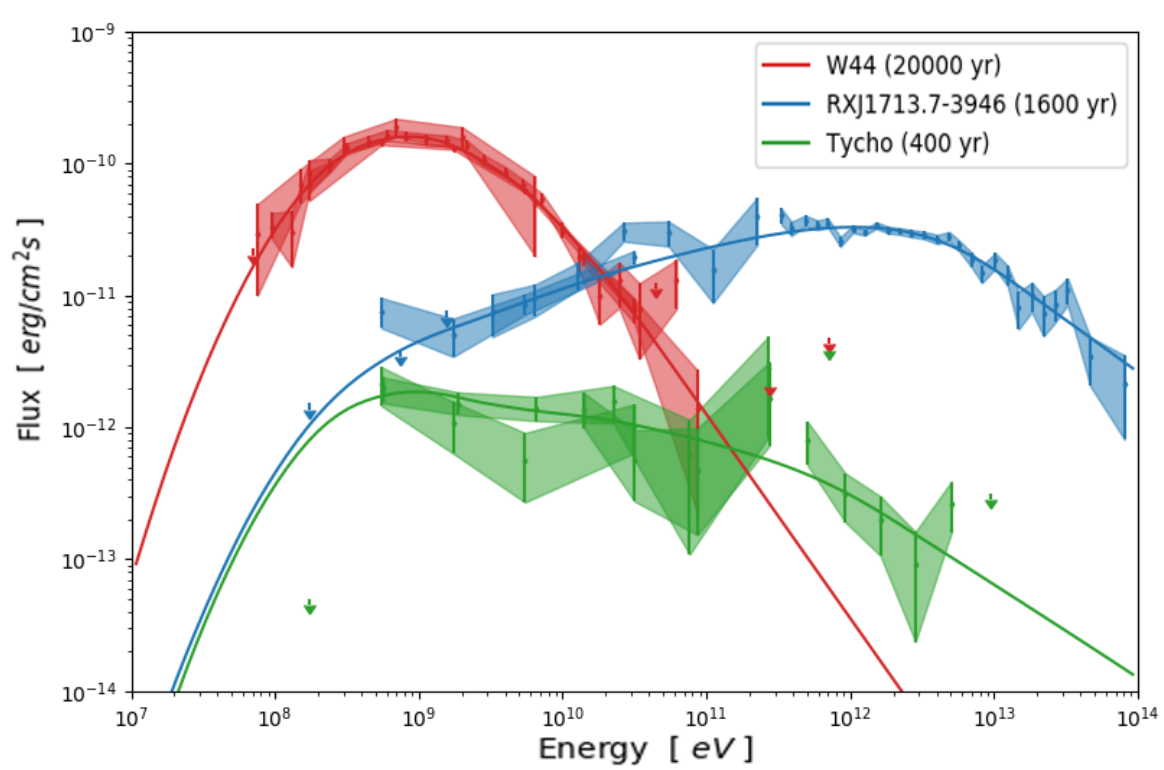

SNRs @ VHE gamma-rays

Young SNRs: the case of RX J1713.7–3946

RX J1713.7–3946 is a young SNR (about 1625 yrs), close (~1 kpc), and large (angular diamter of ~ 0.6 deg) discovered with ROSAT (Pfeffermann & Aschenbach 1996), and considered a "text book" example of X-ray bright and radio dim shell-type SNRs.

In gamma-rays, is **one of the brightest VHE gamma-ray sources** in the sky, an ideal target to study the acceleration of CRs in SNRs, and a "standard candle" in the debate about the **hadronic or leptonic origin of the γ-ray emission from SNRs**

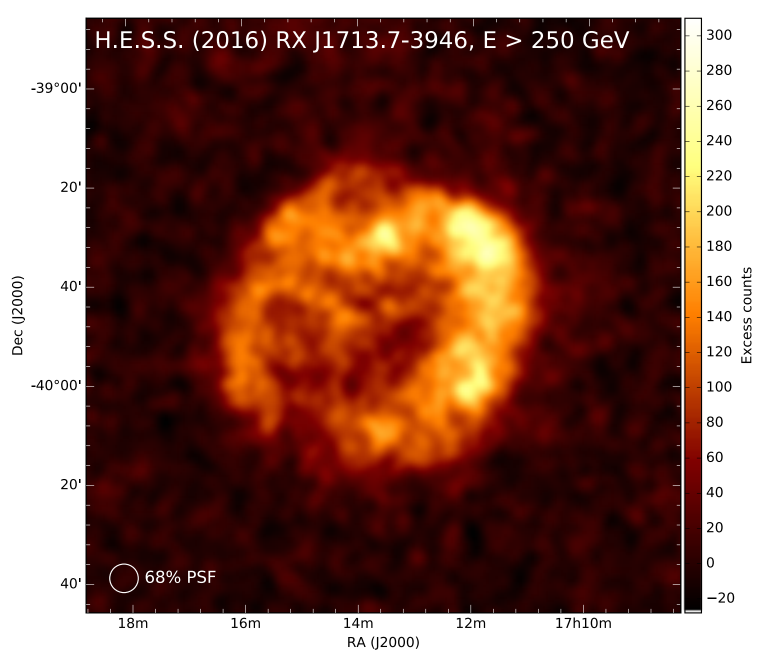

H.E.S.S. coll. 2018

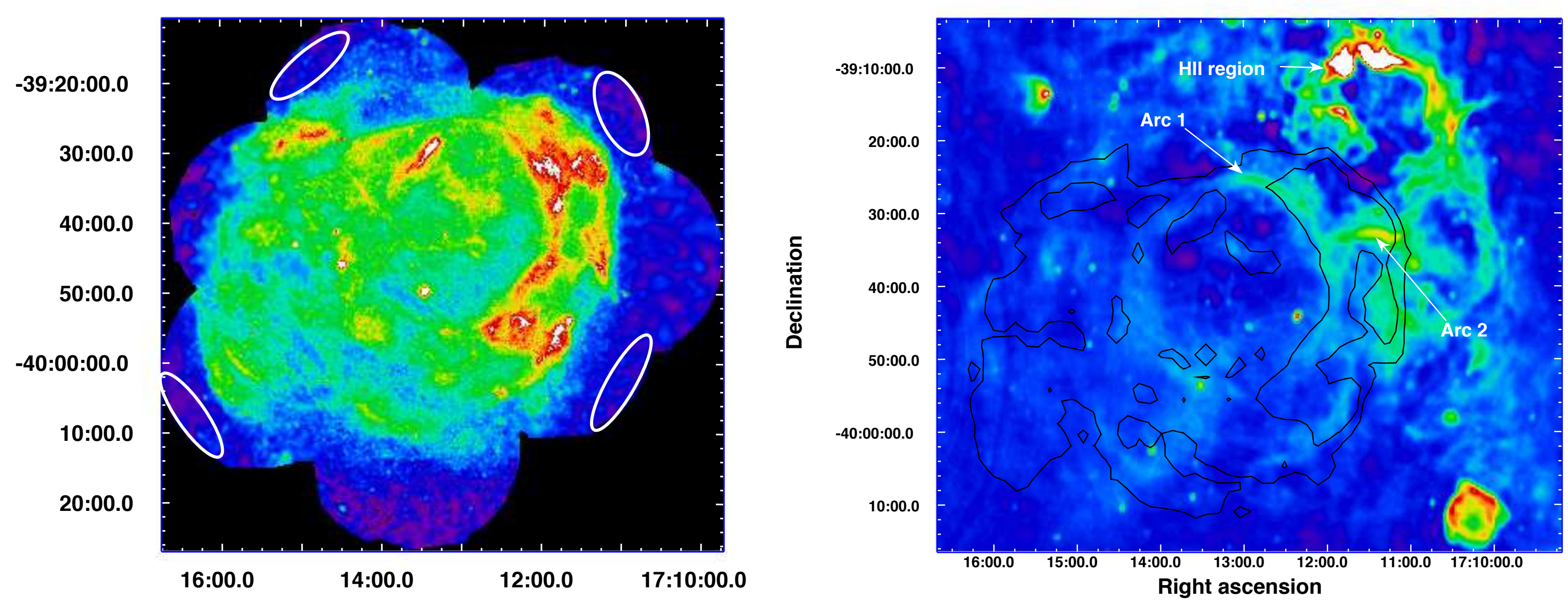

Acero et al. 2018

SNRs @ VHE gamma-rays

The **most precise measurements of RXJ 1713** have been obtained with H.E.S.S. (A detailed morphological study revealed a **larger gamma-ray extension than the synchrotron X-ray boundaries** in the brightest sectors

Such $R_\gamma > R_X$ could be an indication of **CR escape from the SNR**

(Aharonian & Atoyan 1996; Gabici et al. 2009; Malkov et al. 2013), which could act as "CR precursor" ahead of the shock ($d_{prec} \sim D_{upstream} / u_{shock}$) characteristic of DSA acceleration (Malkov et al. 2005; Zirakashvili & Aharonian 2010, Bell et al. 2013)

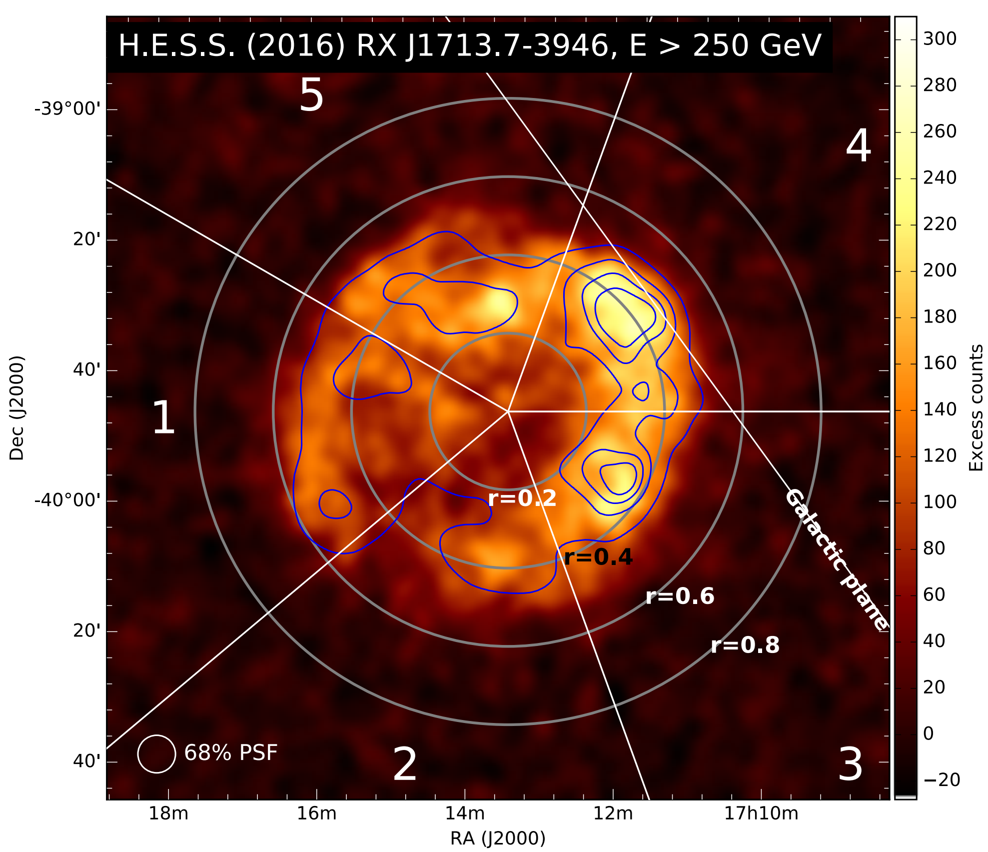

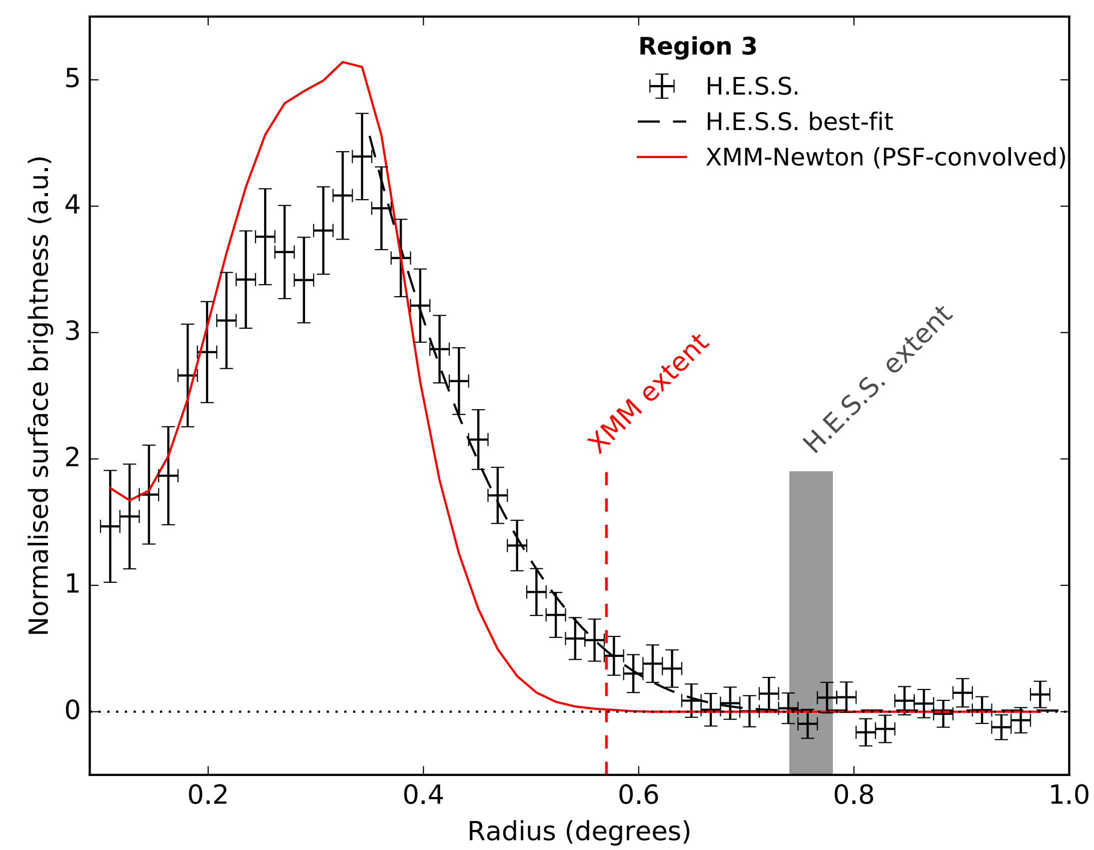

H.E.S.S. coll. 2018

SNRs @ VHE gamma-rays

The SED of RX J1713.7−3946 can be fit with present age parent particle spectra in both a hadronic and leptonic scenario, without the need for assumptions on the particle acceleration process.

A broken PL with a **break at 1-3 TeV is needed** in both scenarios. For leptons, the break can be the result of synchrotron cooling in a high B-field (~70 microG). For protons, the break could be due to E-dependent diffusion of protons in the clumps, where high-E protons interact deeper in the clouds and emit more efficiently than low-E protons (Zirakashvili & Aharonian 2010, Gabici & Aharonian 2014)

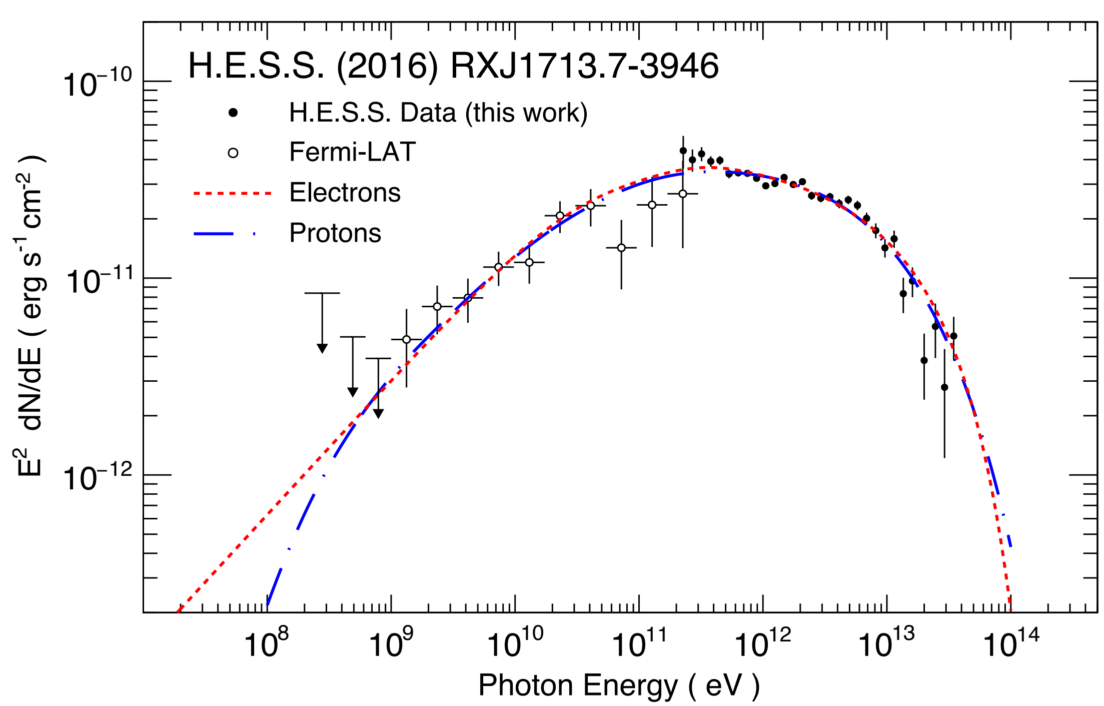

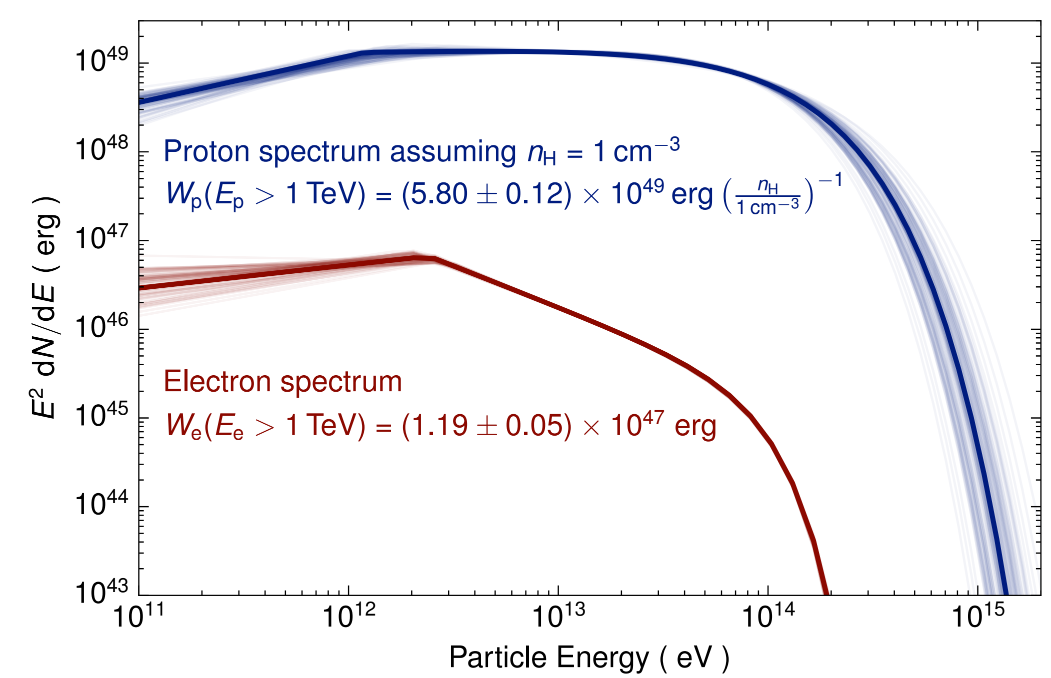

H.E.S.S. coll. 2018

SNRs @ VHE gamma-rays

The brightness of RX J1713.7−3946 and its relatively large angular size allows the H.E.S.S. measurements of key **physical parameters** defining different spatial regions

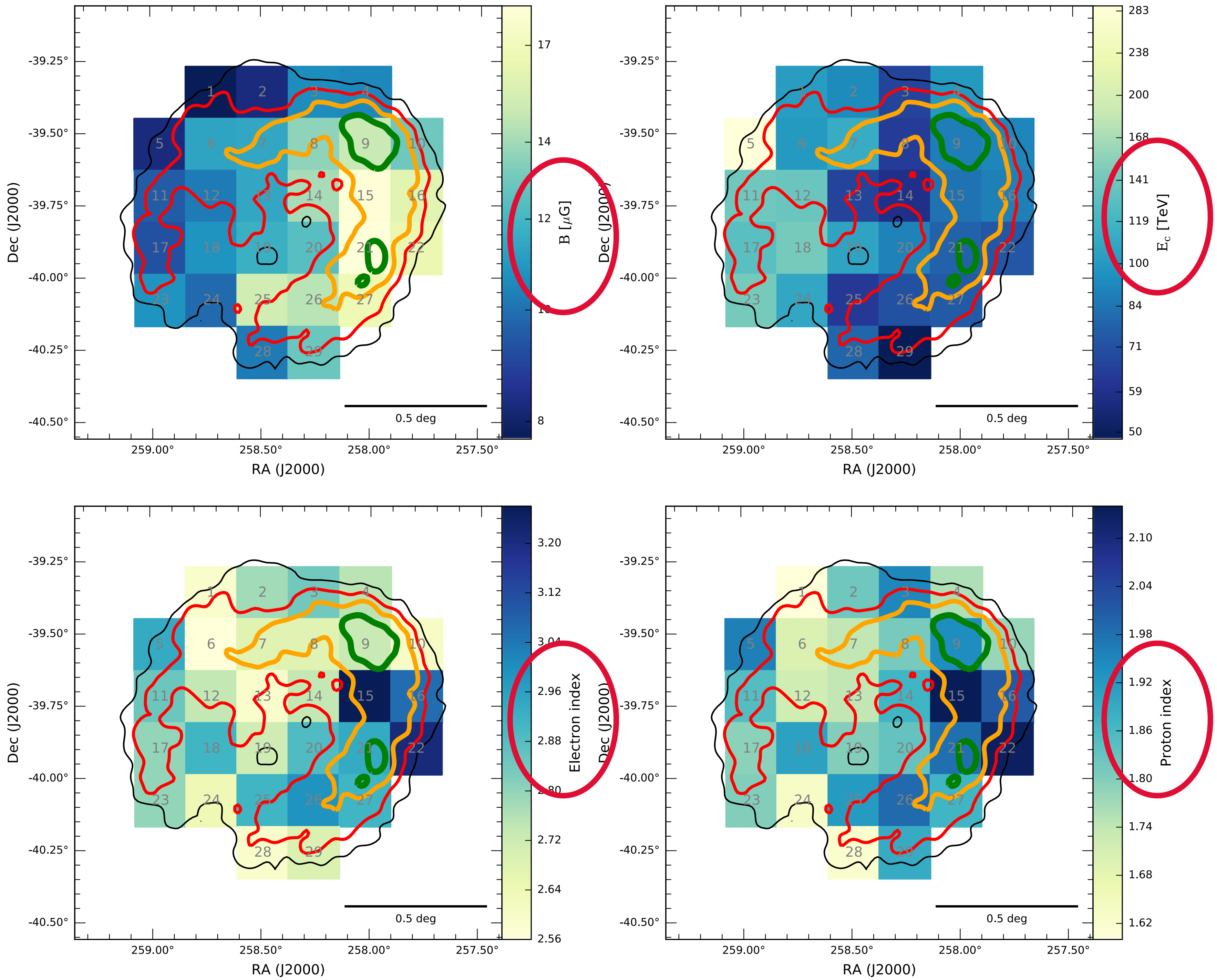

H.E.S.S. coll. 2018

SNRs @ VHE gamma-rays

The brightness of RX J1713.7−3946 and its relatively large angular size allows the H.E.S.S. measurements of key **physical parameters** defining different spatial regions

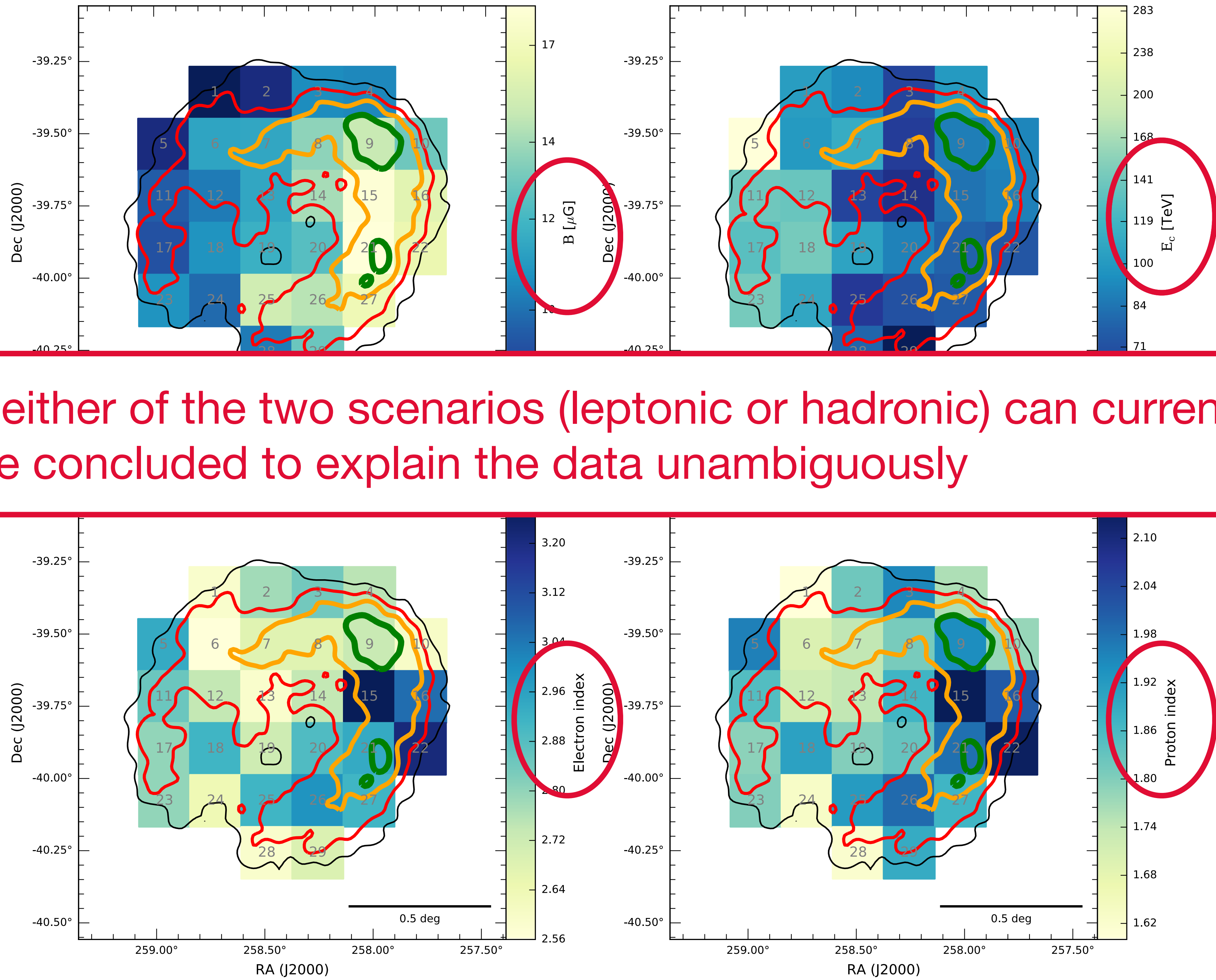

Neither of the two scenarios (leptonic or hadronic) can currently be concluded to explain the data unambiguously

H.E.S.S. coll. 2018

SNRs @ VHE gamma-rays

The brightness of RX J1713.7−3946 and its relatively large angular size allows the H.E.S.S. measurements of key **physical parameters** defining different spatial regions

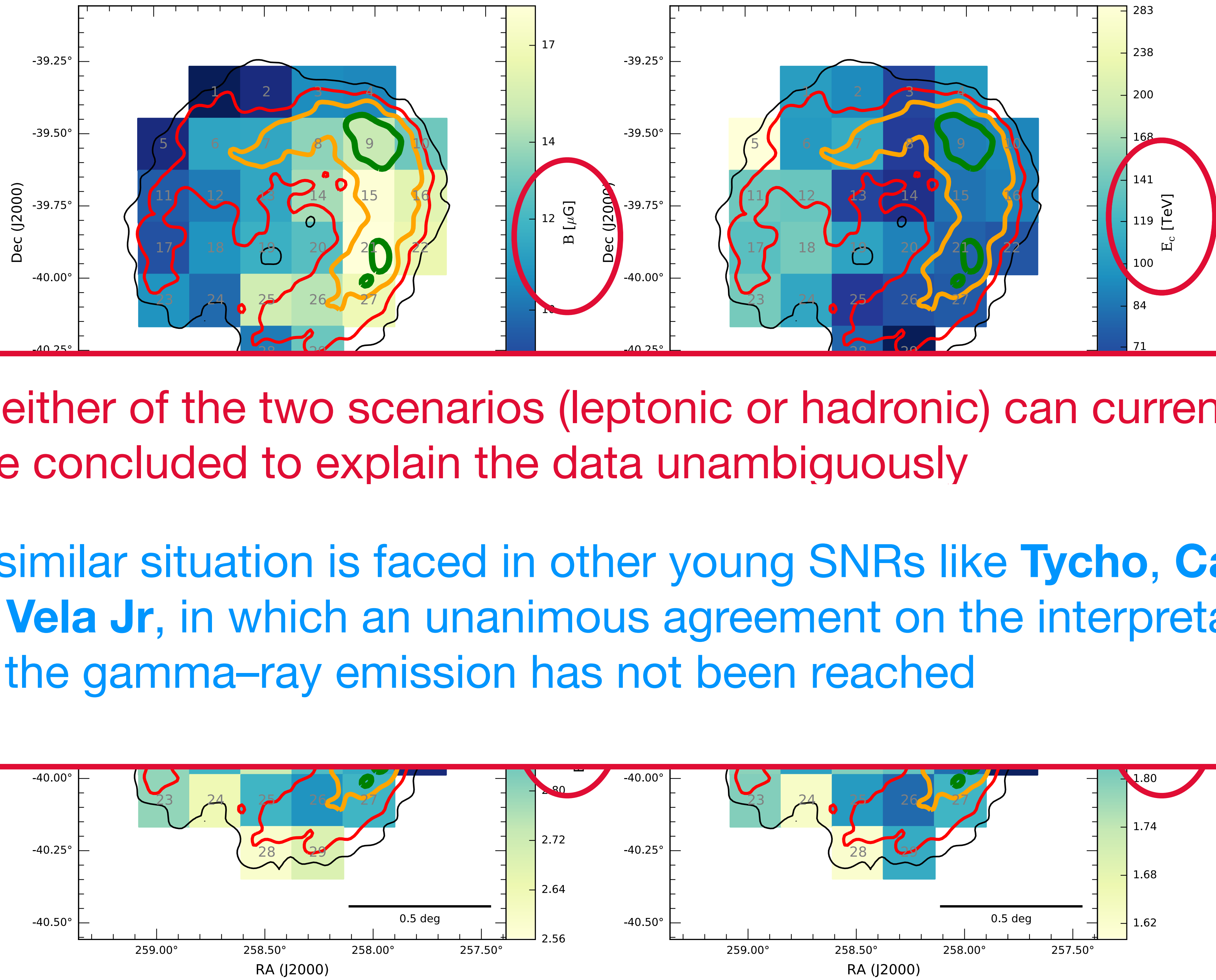

Neither of the two scenarios (leptonic or hadronic) can currently be concluded to explain the data unambiguously

A similar situation is faced in other young SNRs like **Tycho**, **Cas A** or **Vela Jr**, in which an unanimous agreement on the interpretation of the gamma–ray emission has not been reached

H.E.S.S. coll. 2018

SNR interaction with dense MCs

Evidence for SNR/MC interactions has been found in a number of gamma-ray emitting SNRs (Slane et al. 2014). The **gamma-ray emission** has been interpreted as the result of *pp* interactions, which are **strongly enhanced** due to the presence of a thick target (Aharonian et al. 1994).

This is expected -> massive stars originate in dense regions => dense MCs. These stars end rapidly in SNRs, which evolve **in the vicinity of the parent cloud**. The SNRs accelerate CRs, which can then interact into the cloud and produce gamma-rays.

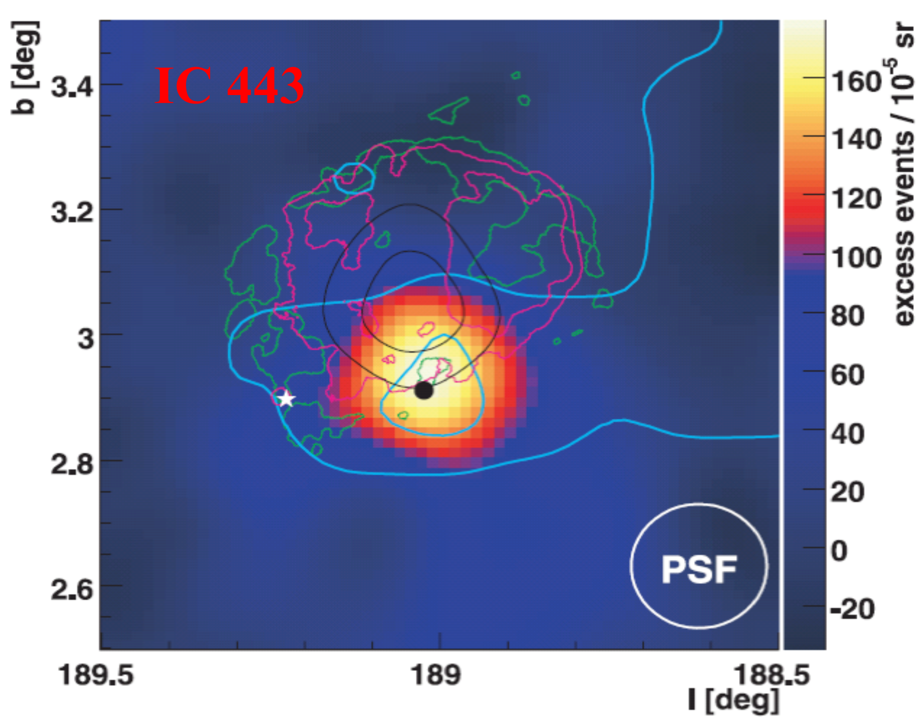

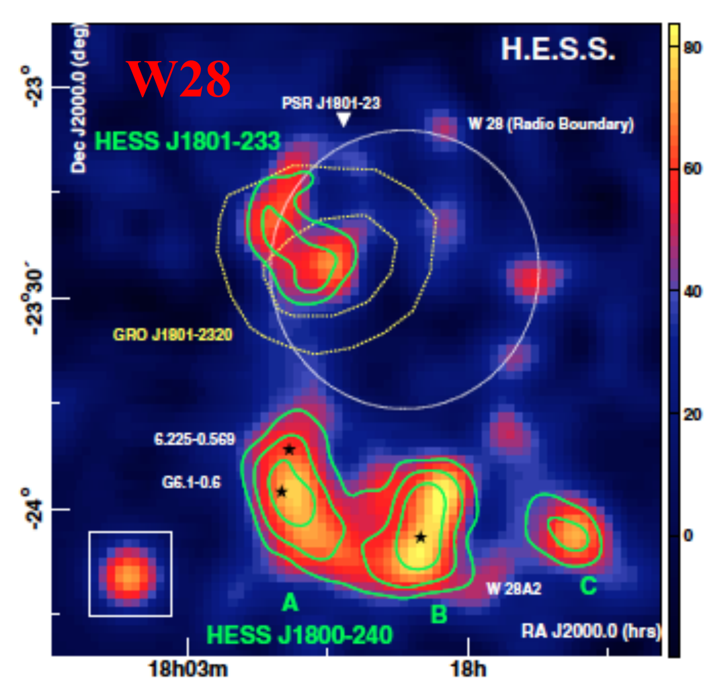

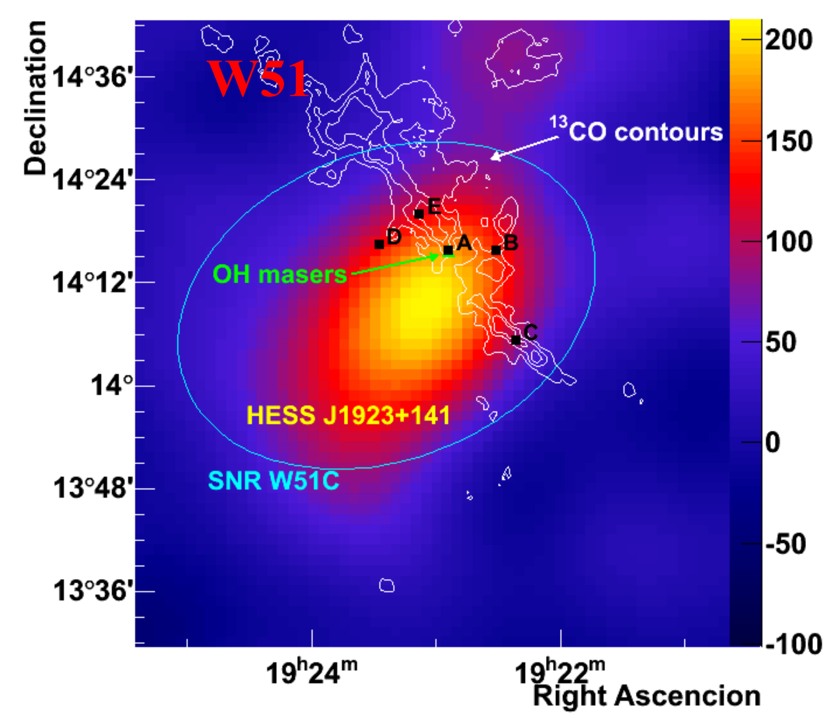

SNRs @ VHE gamma-rays

SNR interaction with dense MCs

Evidence for SNR/MC interactions has been found in a number of gamma-ray emitting SNRs (Slane et al. 2014). The **gamma-ray emission** has been interpreted as the result of *pp* interactions, which are **strongly enhanced** due to the presence of a thick target (Aharonian et al. 1994).

- W51C: *Fermi*-LAT observations of reveal a spectrum that is **consistent with π^0-decay**, with dominant **Bremsstrahlung** and **IC** emission **ruled out** on energetic grounds (Abdo et al. 2009). NOTE: Recently LHAASO reported UHE emission coincident with W51, up to 300 TeV (Chen et al. 2023)
- W41, MSH 17–39, G337.7–0.1 and Kes 79: Detailed studies have revealed **gamma-ray spectra indicative of hadronic emission**, with leptonic scenarios requiring total electron energies in excess of 10^{51} erg (Castro et al. 2013) (Auchettl et al. 2014)
- W28: **Discrete TeV sources** outside the remnant have been suggested to originate from **particles escaping the SNR** and interacting with adjacent clouds (Aharonian et al. 2008).
- IC 443: **Escaping CRs interacting with external MCs** has been suggested to explain the observed gamma-ray flux (Albert et al. 2007, Acciari et al. 2009)

The "Pion bump"

W44 and IC 443 show clear evidence of a kinematic "pion bump" in their spectra, firmly establishing the presence of energetic ions in these remnants (Abdo et al. 2010; Giuliani et al. 2011; Ackermann et al. 2013).

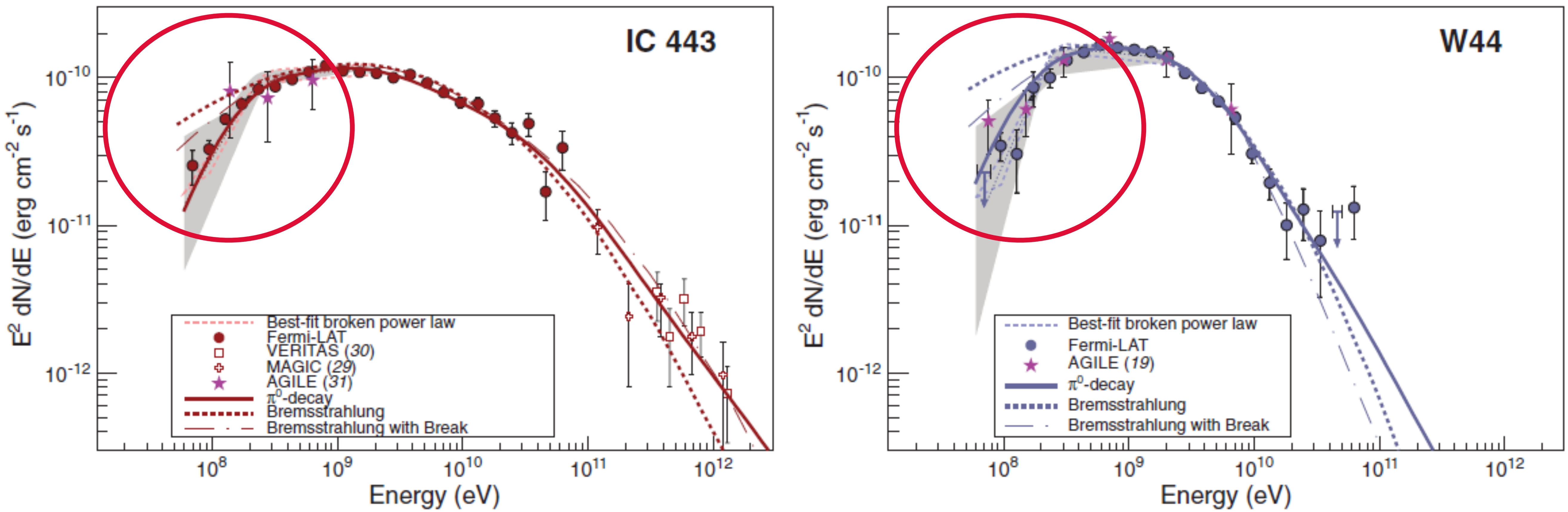

Ackermann et al. 2013

SNRs @ VHE gamma-rays

The “Pion bump”

W44 and IC 443 show clear evidence of a kinematic “pion bump” in their spectra, firmly establishing the presence of energetic ions in these remnants (Abdo et al. 2010; Giuliani et al. 2011; Ackermann et al. 2013).

SNR are proved CR accelerators. However, open questions remain about the **maximum attainable CR energy (PeV?)** the **acceleration efficiency**, the **electron-to-proton ratio** for the injected particles, and the eventual **escape of CRs** from the acceleration region.

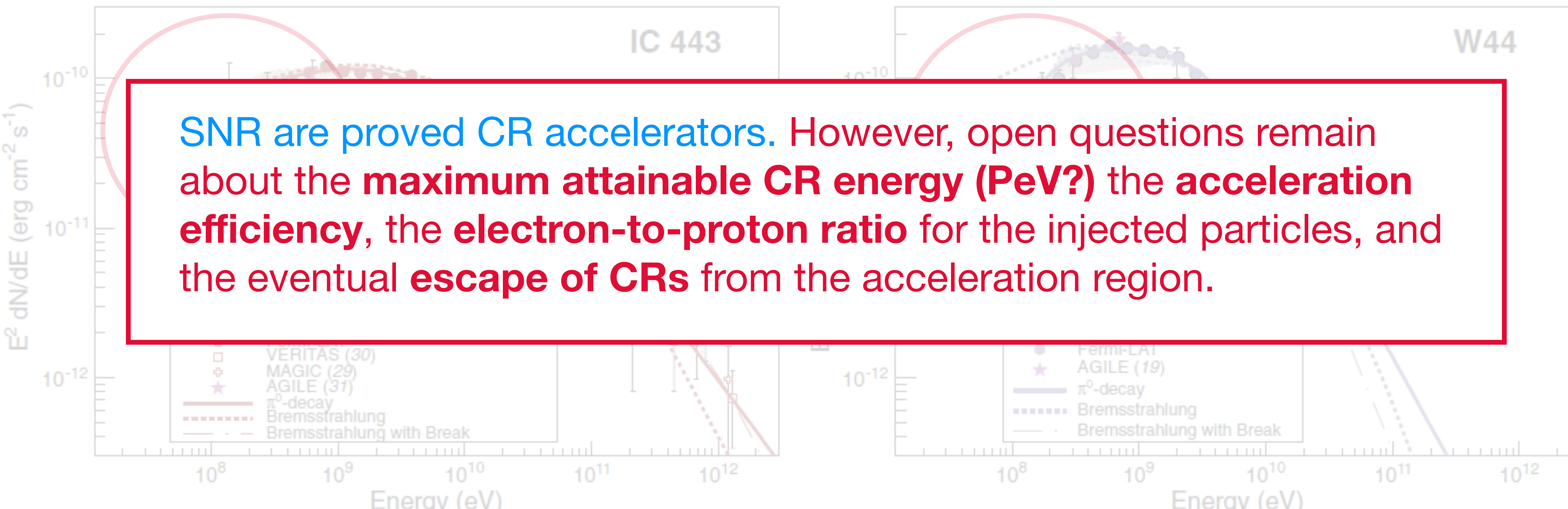

Ackermann et al. 2013

PSRs @ VHE gamma-rays

PSRs @ VHE gamma-rays

Pulsars (PSRs) are born in supernova explosions, and are composed of a rapidly spinning and strongly magnetized neutron star that emits **beams of e.m. radiation modulated at the stellar rotational period**.

PSR radiation spans a **wide range of frequencies**: from radio to VHE gamma-rays. More than **3000 PSRs have been detected in radio**, and > **300 have been reported at HEs** by the *Fermi*-LAT (Smith et al. 2023).

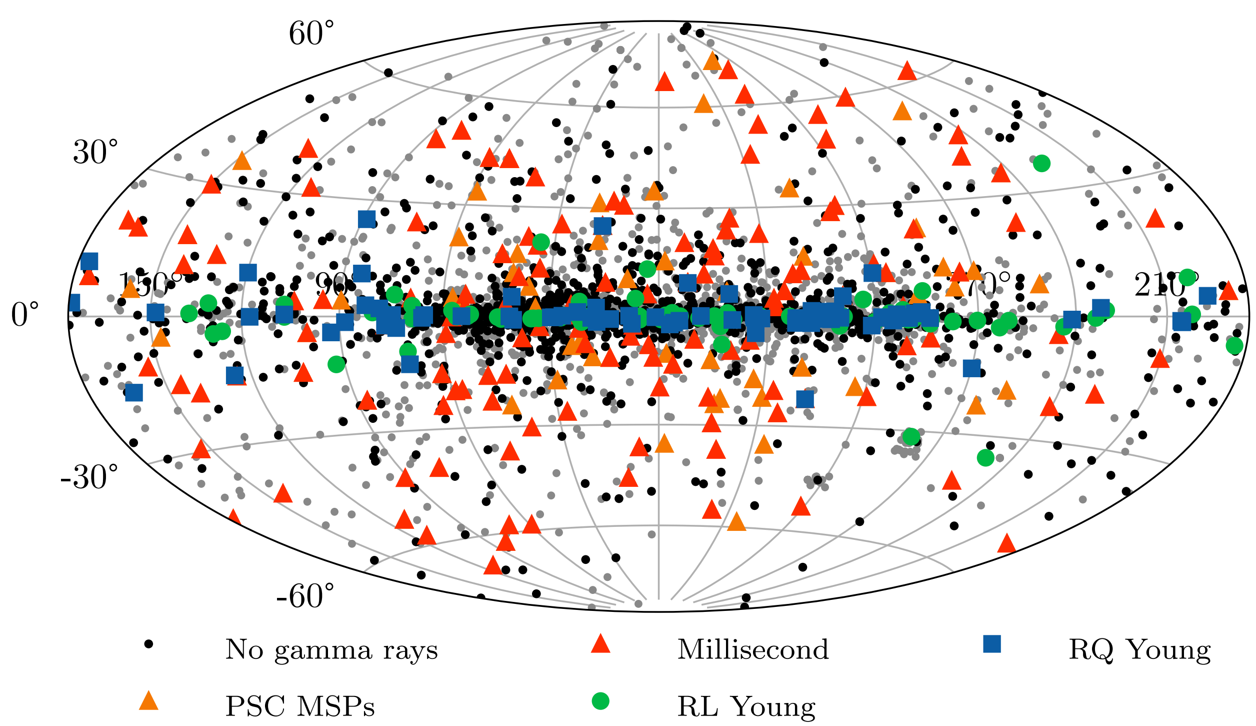

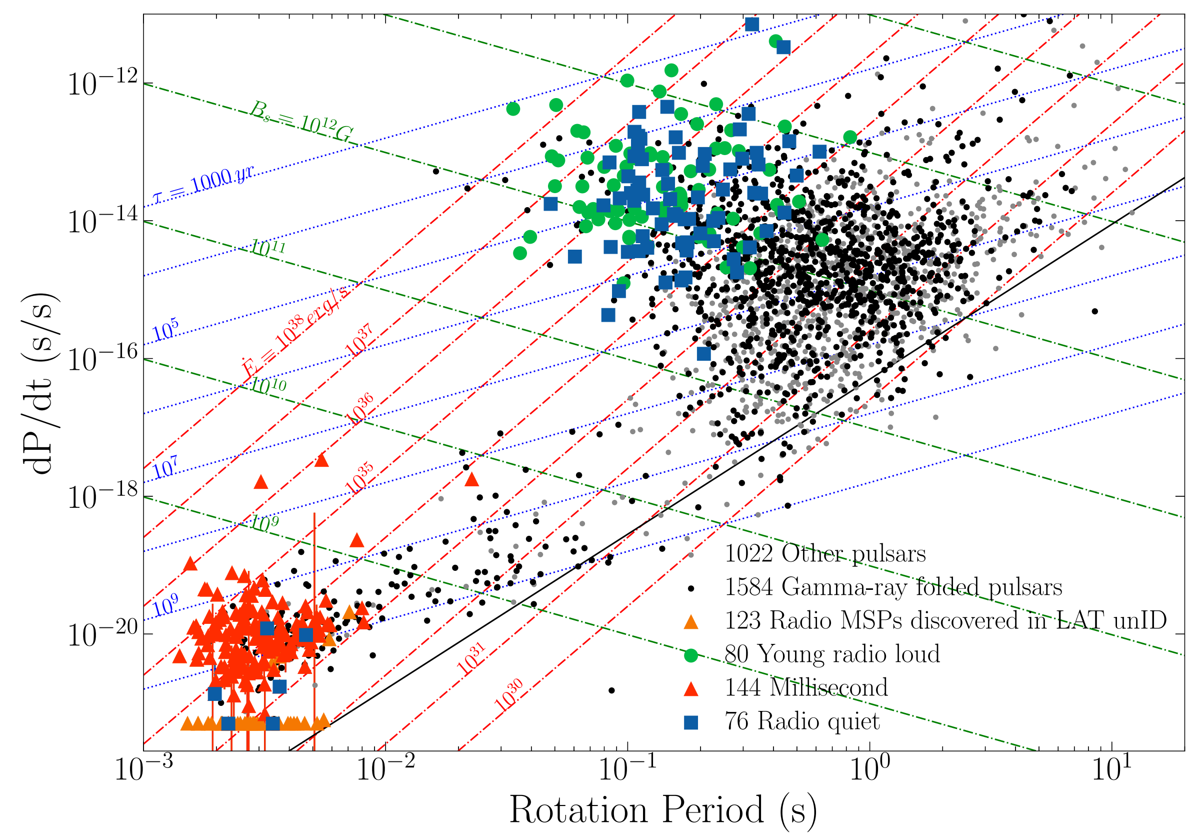

Smith et al. 2023

PSRs @ VHE gamma-rays

Pulsars (PSRs) are born in supernova explosions, and are composed of a rapidly spinning and strongly magnetized neutron star that emits **beams of e.m. radiation modulated at the stellar rotational period**.

PSR radiation spans a **wide range of frequencies**: from radio to VHE gamma-rays. More than **3000 PSRs have been detected in radio**, and > **300 have been reported at HEs** by the *Fermi*-LAT (Smith et al. 2023).

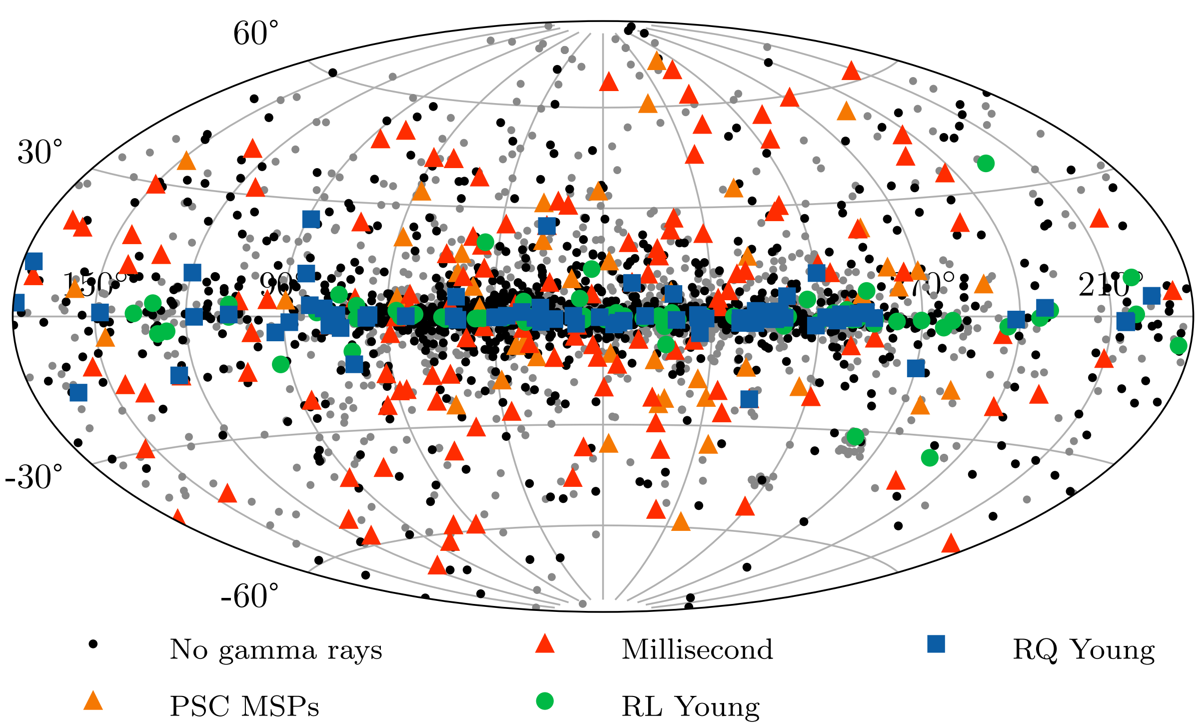

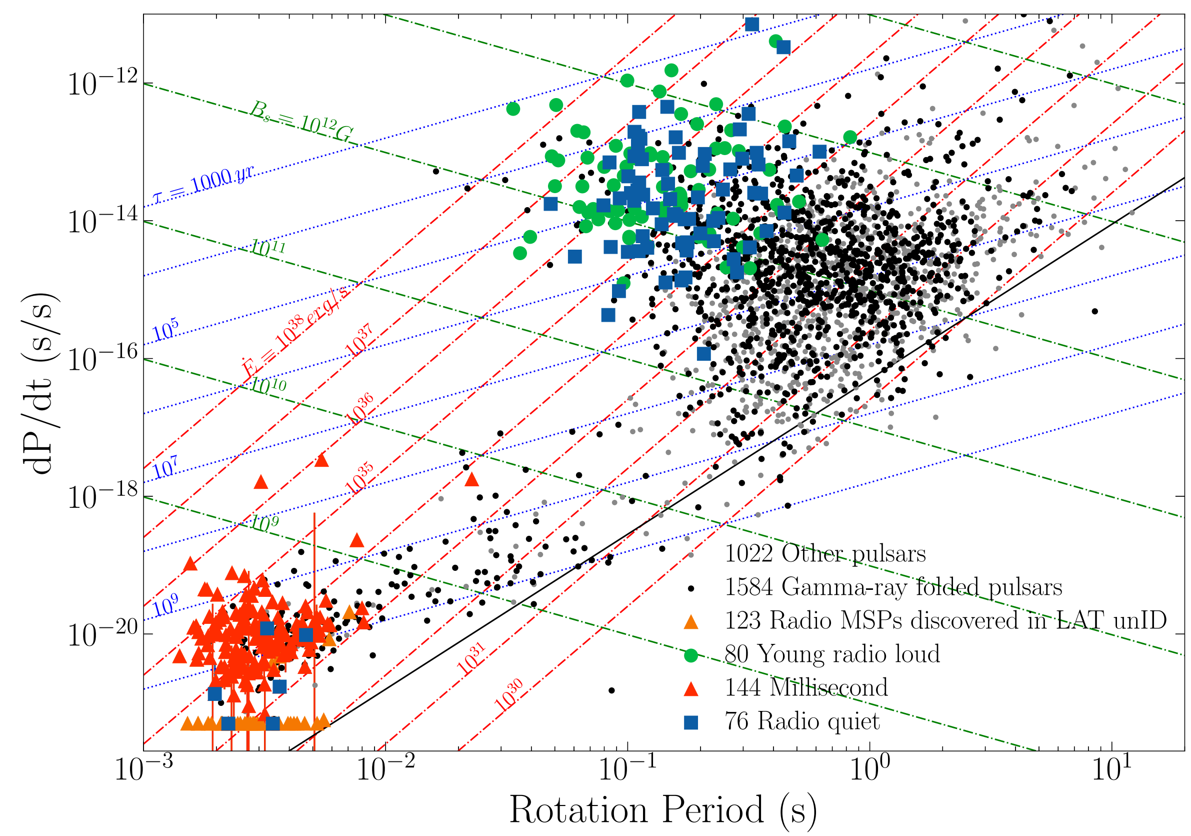

Smith et al. 2023

PSRs @ VHE gamma-rays

Some of the **key observational results** from the third *Fermi*-LAT PSR catalog (Smith et al. 2023):

- Spectra can be fitted by a **PL** with an **exponential cutoff at ~1–5 GeV**
- The rotational energy-loss rate varies from **~3×10^{33} erg s^{-1} to 5×10^{38} erg s^{-1}**
- Efficiencies for conversion to gamma-ray emission: from **~0.1% to ~1**.
- **~ 75% of the pulsars have two peaks**, separated by ~0.2 in phase.
- For most PSRs, **gamma-ray emission appears to come mainly from the outer magnetosphere**, polar-cap emission still plausible for a few
- Associations reveal that many of these pulsars power PWNe.
- **Gamma-ray-selected** young pulsars are **born at a rate comparable** to that of the **radio-selected ones**. The **birthrate** of all young gamma-ray-detected pulsars is a **substantial fraction of the expected Galactic supernova rate**

PSRs @ VHE gamma-rays

Several models have been considered for the HE emission detected from PSRs, distinguished on **different assumptions of the geometry and location of the 'gap regions'** (regions where the electric field is not totally screened by the plasma and efficient particle acceleration can take place)

- **Polar cap models**: emission from HE particles is assumed to originate close to the NS surface. Particles are accelerated by large E-fields near the magnetic poles up to a few stellar radii.
- **Slot gap models**: the radiation comes from narrow gaps close to the last open field lines, with the gaps extending from the NS surface up to high altitudes
- **Outer gap models**: the gap region extends from the null-charge surface, where the Goldreich-Julian charge density is zero up to high altitudes, also close to the last open field lines

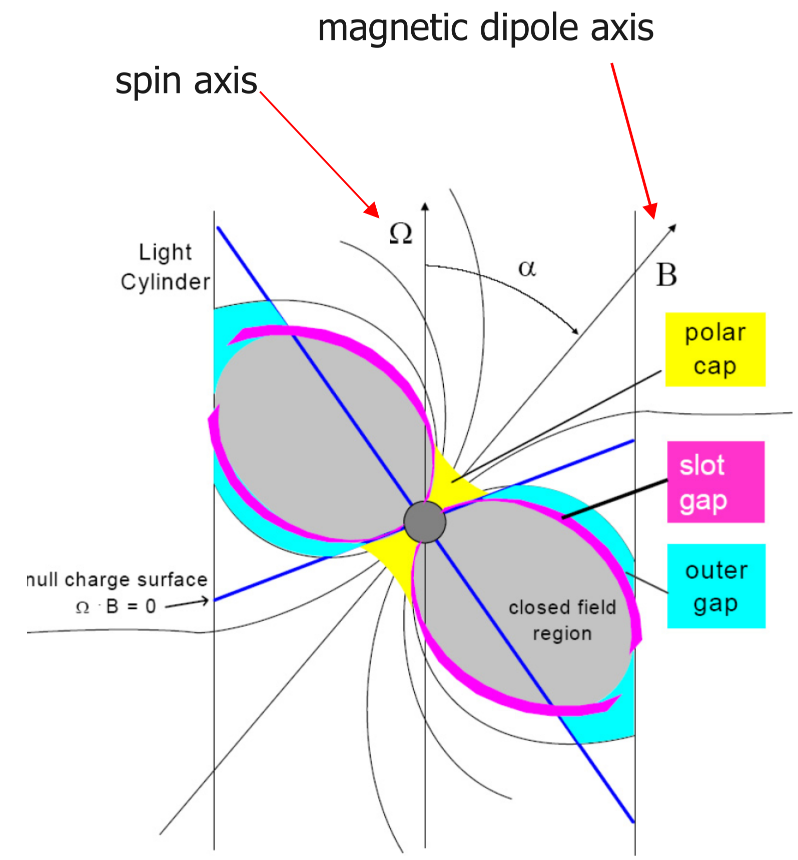

Harding et al. 2011

To explain HE emission one has to take detailed particle transport and radiation mechanisms into account. These mechanisms include curvature radiation, synchrotron radiation, and IC scattering

PSRs @ VHE gamma-rays

Several models have been considered for the HE emission detected from PSRs, distinguished on **different assumptions of the geometry and location of the 'gap regions'** (regions where the electric field is not totally screened by the plasma and efficient particle acceleration can take place)

- **Polar cap models**: emission from HE particles is assumed to originate close to the NS surface. Particles are accelerated by large E-fields near the magnetic poles up to a few stellar radii.
- S… g… e…
- O… n… charge density is zero up to high altitudes, also close to the last open field lines

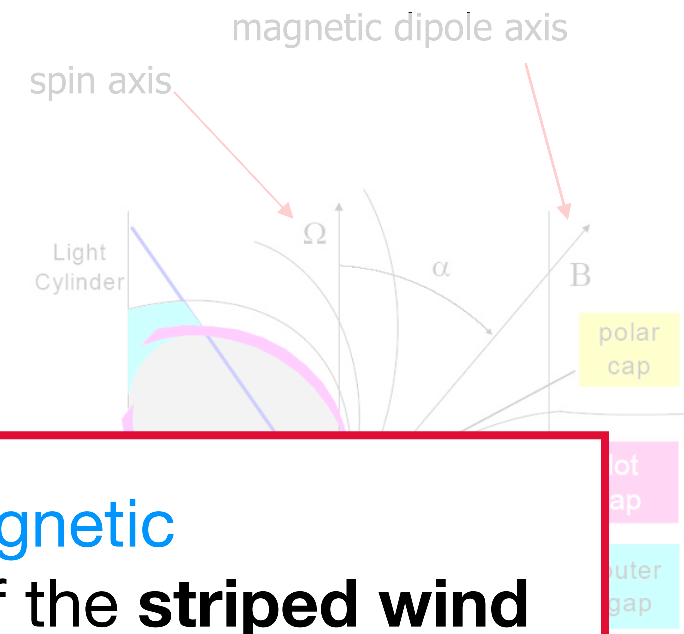

Harding et al. 2011

Particle acceleration can also take place through magnetic reconnection in the **equatorial current sheet** (CS) of the **striped wind beyond the LC**, which can then radiate synchrotron emission from optical to gamma-ray wavelengths

To explain HE emission one has to take detailed particle transport and radiation mechanisms into account. These mechanisms include curvature radiation, synchrotron radiation, and IC scattering

PSRs @ VHE gamma-rays

At 10's to 100's GeVs, IACTs have reported 4 PSRs in the recent years (Crab, Vela, PSR B1706 and Geminga). At VHEs, only two PSRs have been so far detected: the Crab (up to ~1.5 TeV, MAGIC) and the Vela PSR (**up to 20 TeV**)

MAGIC detection of pulsations from the Crab pulsar at energies up to ~ 25 GeV (MAGIC col. 2008)

VERITAS detected pulsed photons up to ~400 GeV from the Crab (VERITAS col. 2008)

MAGIC extended the energy of gamma-ray pulsations from the Crab up to 1.5 TeV (MAGIC col. 2016)

H.E.S.S. detected pulsed emission from the Vela PSR in the sub-20 GeV to 100 GeV range (HESS col. 2018)

H.E.S.S. detected pulsed emission from PSR B1706–44 up to 70 GeV (Spir-Jacob et al. 2019)

MAGIC reports pulsed emission from Geminga between 15 GeV and 75 GeV (MAGIC col. 2020).

Very recently, H.E.S.S. also reported pulsed emission from Vela at > 20 TeVs (HESS coll. 2023)

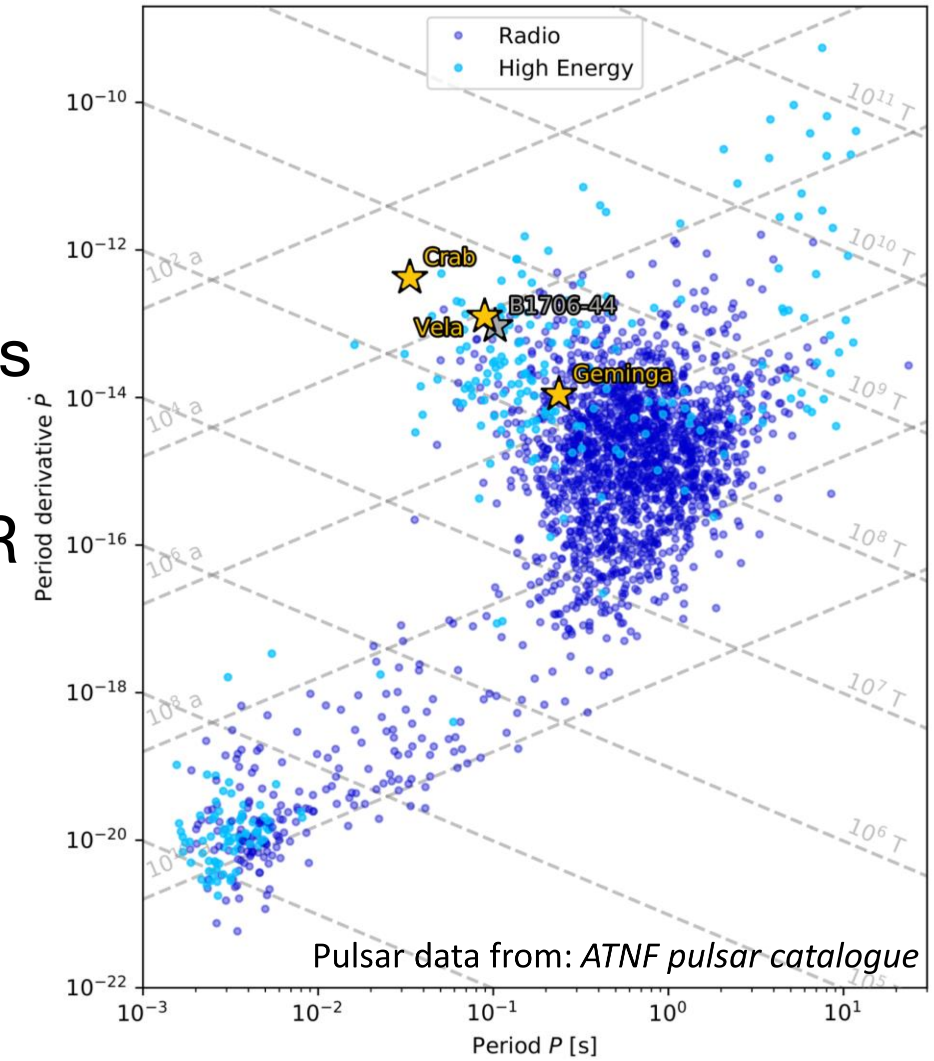

PSRs @ VHE gamma-rays

The measured spectra in the sub-100 GeV range for Vela, B1706–44 and Geminga seem to smoothly connect to that measured by *Fermi*-LAT, so it is not clear whether thisemission requires a separate spectral component.

The new VHE emission detected in the Crab, instead, can only be understood as an additional component adding a power-law tail, produced e.g. by IC scattering of secondary and tertiary e± pairs on IR-UV photons (Aharonian et al. 2012), or considering SSC scattering off synch. photons produced in the current sheet by the same population of synchrotron-emitting electrons (Mochol et al. 2015).

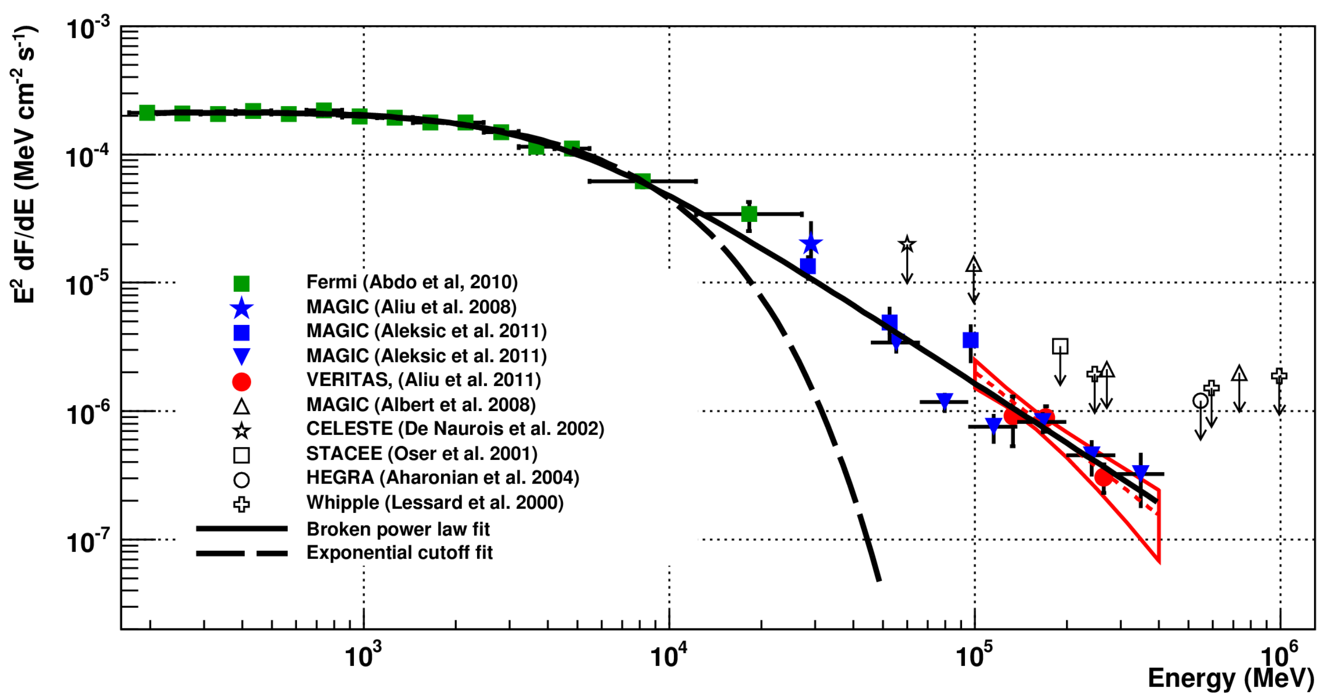

from Otte et al. 2012

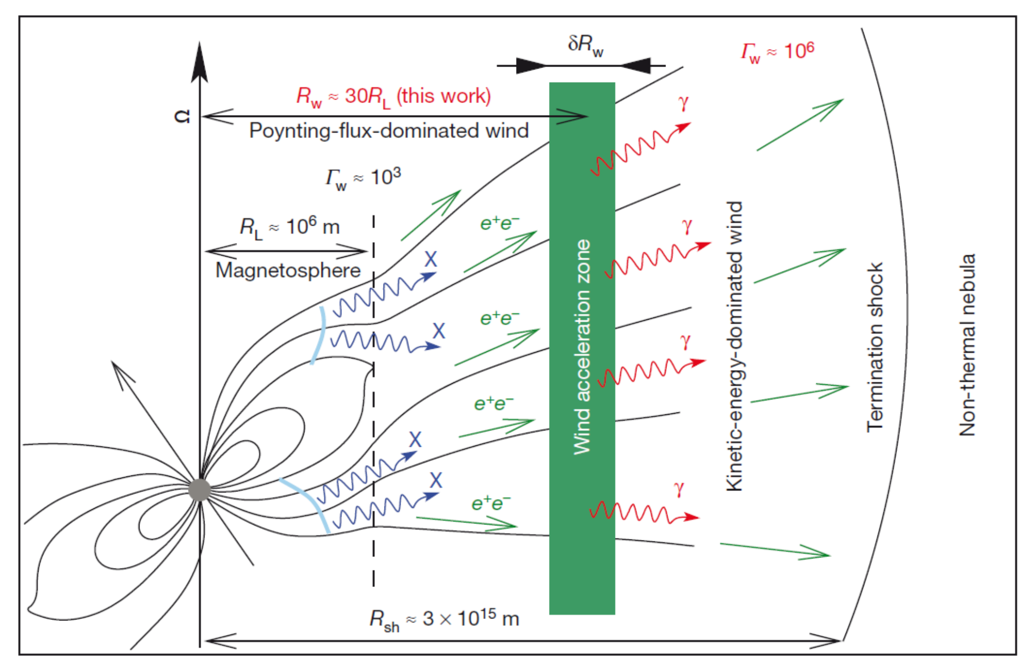

Aharonian et al. 2012

PSRs @ VHE gamma-rays

The measured spectra in the sub-100 GeV range for Vela, B1706–44 and Geminga seem to smoothly connect to that measured by *Fermi*-LAT, so it is not clear whether thisemission requires a separate spectral component.

The new VHE emission detected in the Crab, instead, can only be understood as an additional component adding a power-law tail, produced e.g. by IC scattering of secondary and tertiary e± pairs on IR-UV photons (Aharonian et al. 2012), or considering SSC scattering off synch. photons produced in the current sheet by the same population of synchrotron-emitting electrons (Mochol et al. 2015).

These models are however not exempt of **difficulties to explain some observational properties**, like the extension up to the multi-TeV domain without overshooting the GeV emission, or the correct description of the observed pulse profiles in the Crab

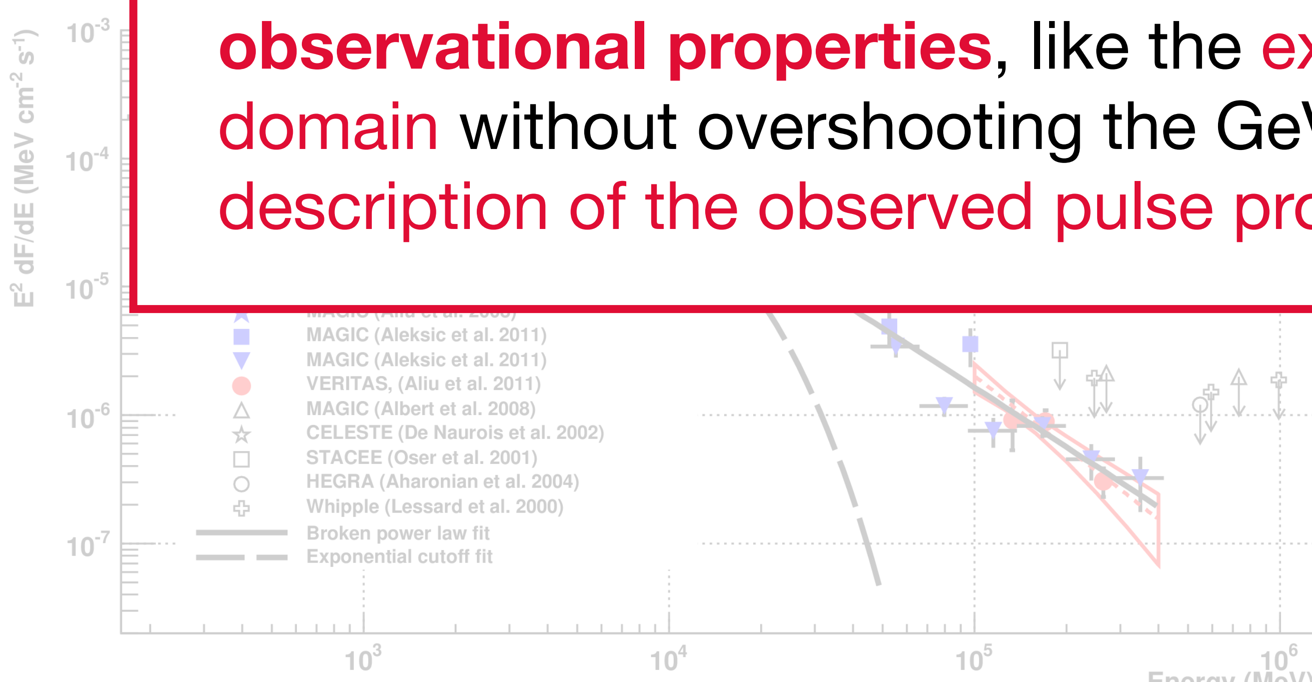

from Otte et al. 2012

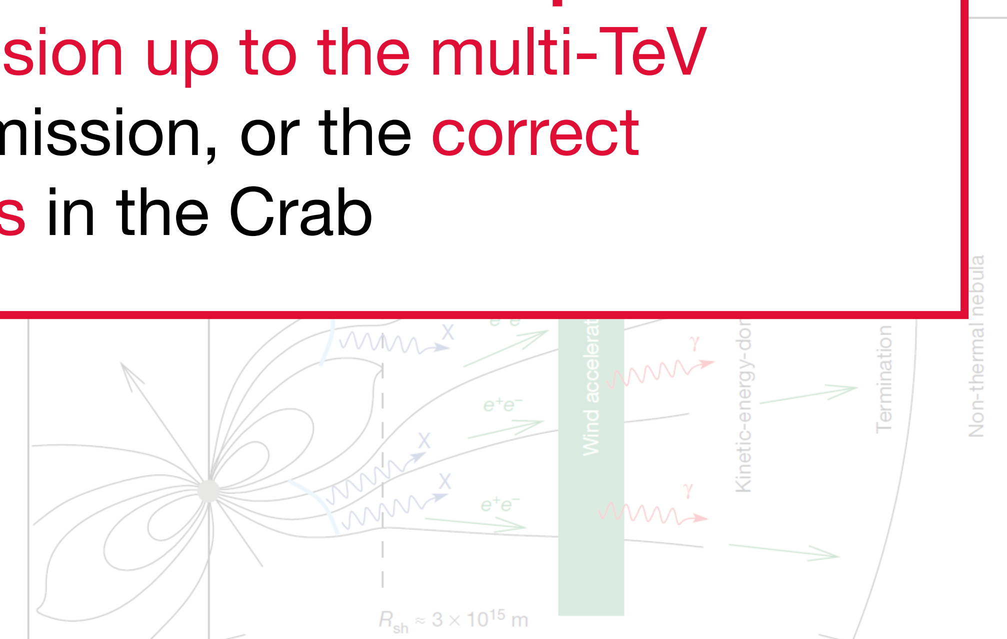

Aharonian et al. 2012

PSRs @ VHE gamma-rays

Very recently, the H.E.S.S. collaboration has reported on the detection of the Vela PSR **at multi-TeV energies** following the analysis of **80h observations** with the 12m HESS telescopes in search for TeV emission from P2. The highest significance level is found **above 5 TeV** and **reaching up to 20 TeV** energies, with the VHE spectrum displaying a very hard index ~1.4

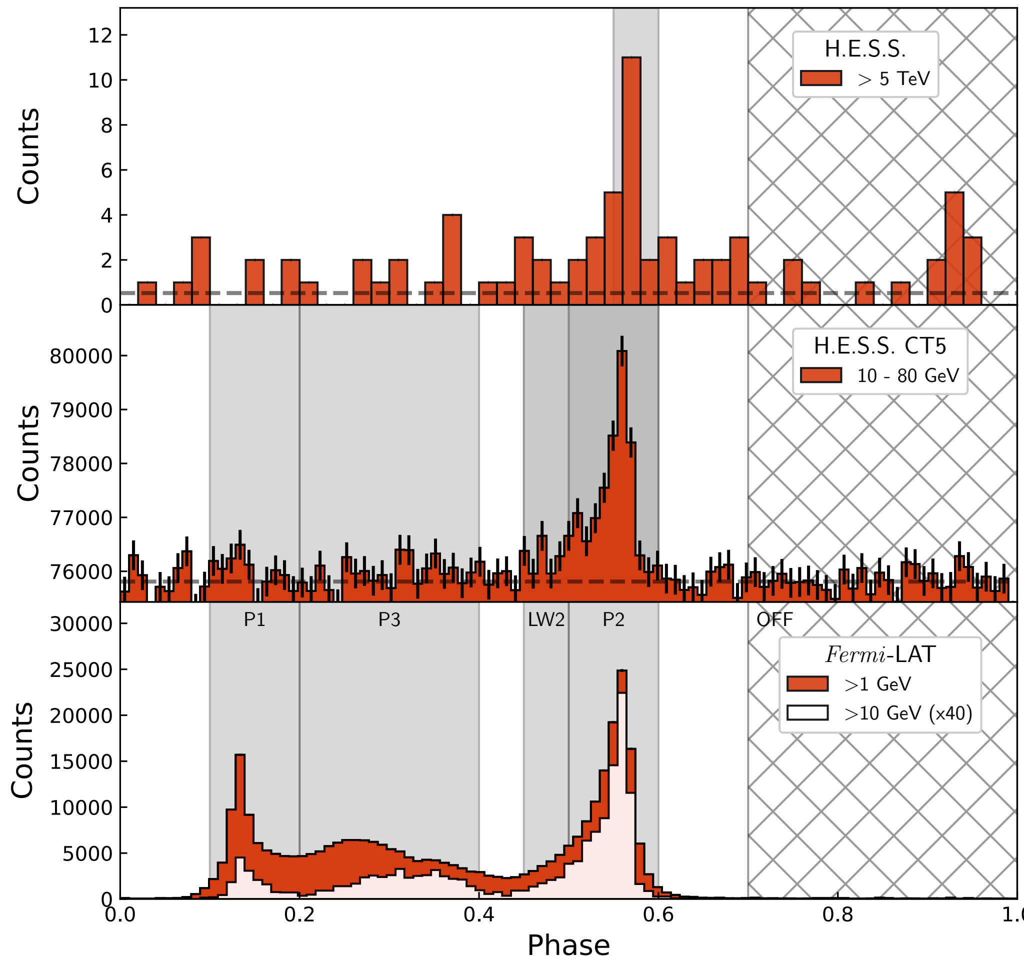

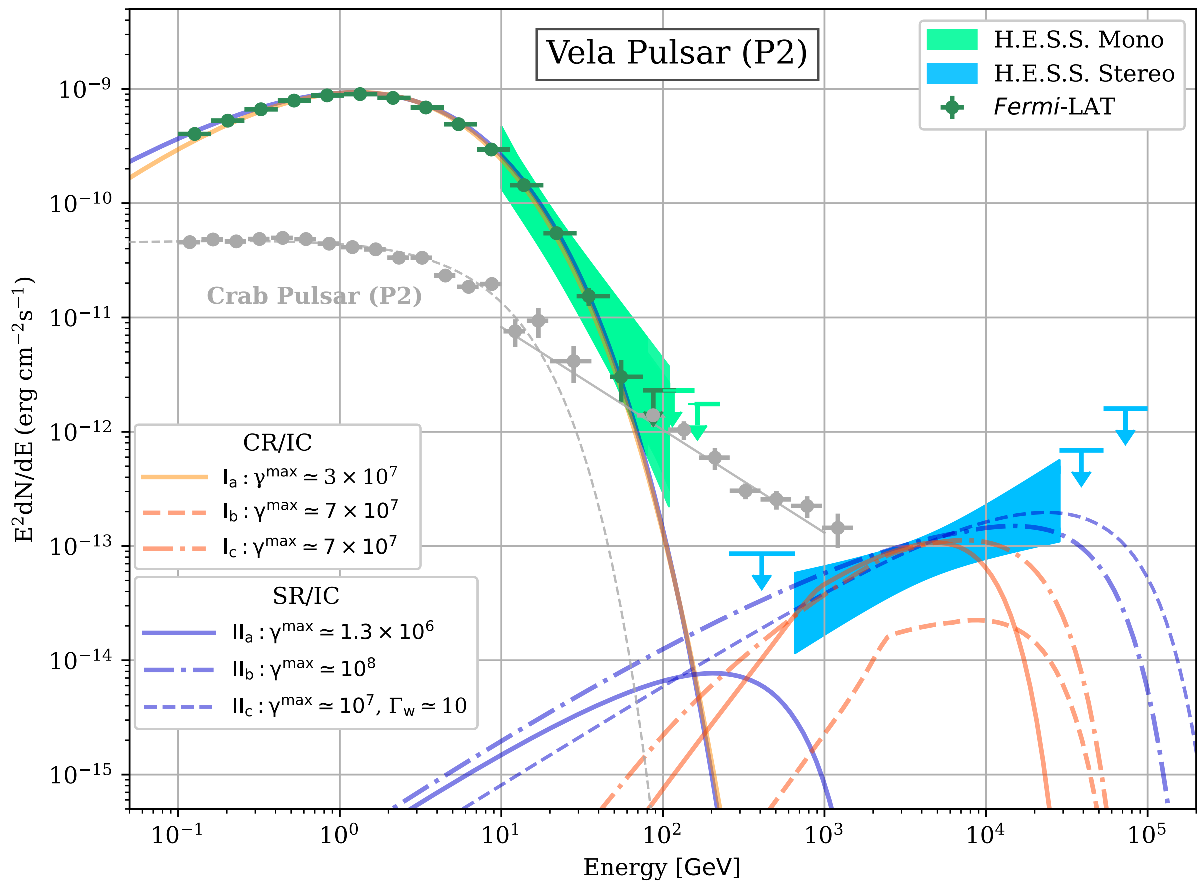

H.E.S.S. coll. 2023

PSRs @ VHE gamma-rays

Maximum particle energies at the level of $\gamma_e \sim 7 \times 10^7$ are derived, which rules out emission regions in the inner magnetosphere or at the light cylinder, where acceleration is limited by radiatie cooling (e.g. synchrotron).

The most likely process for producing the multi-TeV emission by energetic electrons, whatever the acceleration mechanism and emission regions are, is IC scattering of low-energy photons (e.g. non/thermal X-rays from the NS surface, or scattering on optical to the near-infrared photons (H.E.S.S. coll. 2023)

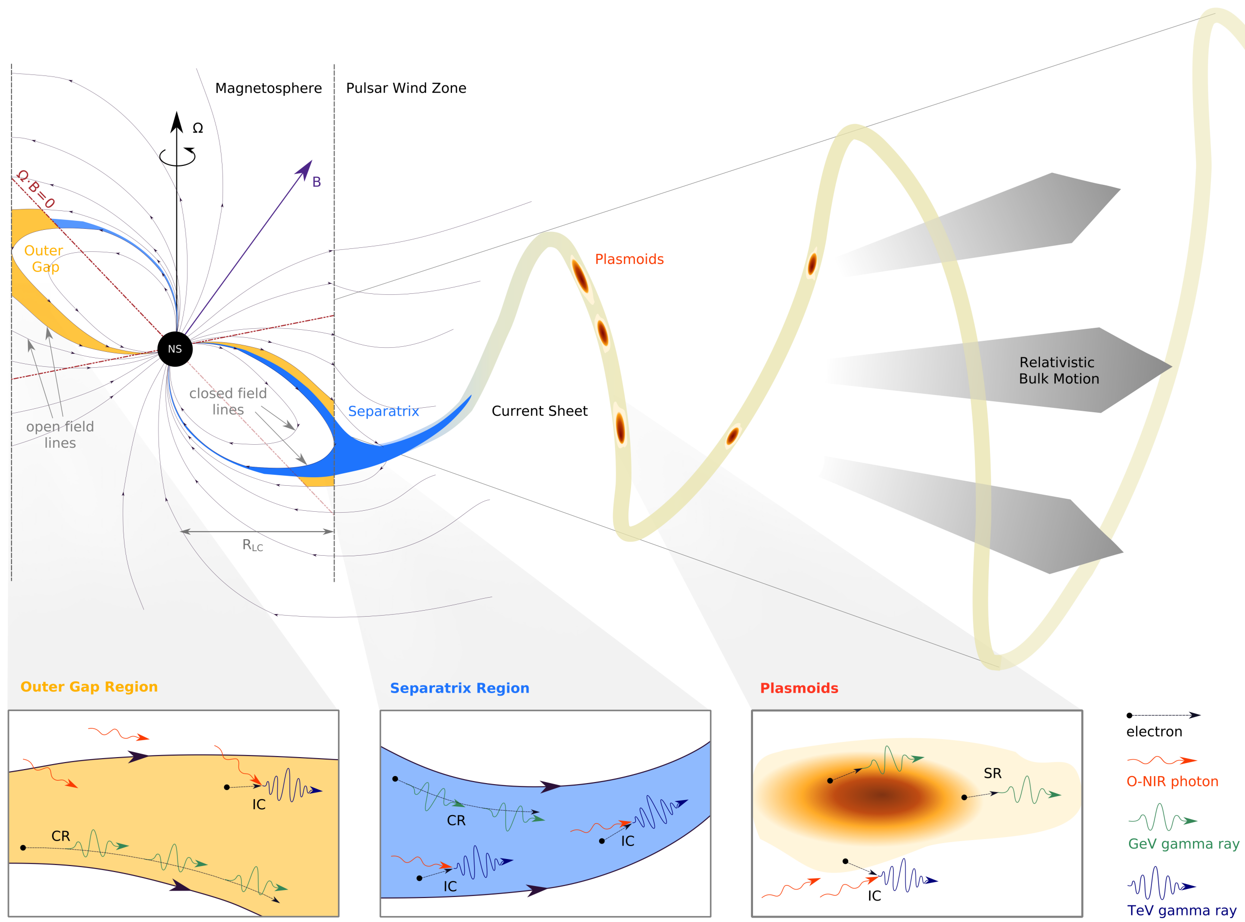

H.E.S.S. coll. 2023

3 - PWNe

PWNe @ VHEs

Pulsar wind nebulae (PWNe) are clouds of magnetised electron/positron plasma that can span many parsecs and are observed via their synchrotron (X-rays) or IC radiation (gamma-rays) emission (see Gaensler & Slane 2006 for a review)

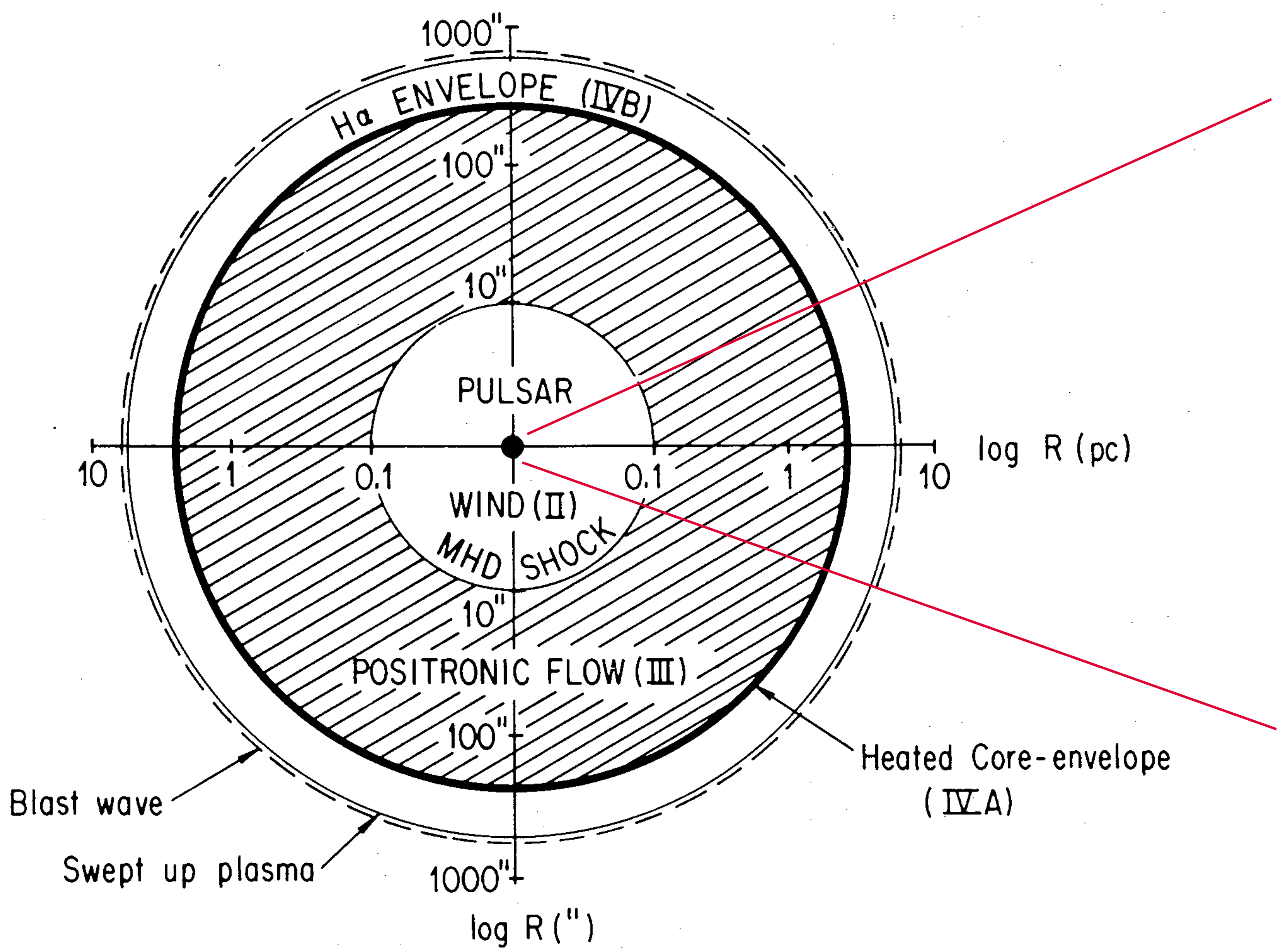

Pulsar wind structure in the Crab Nebula
Rees & Gunn (1974), Kennel & Coroniti (1984)

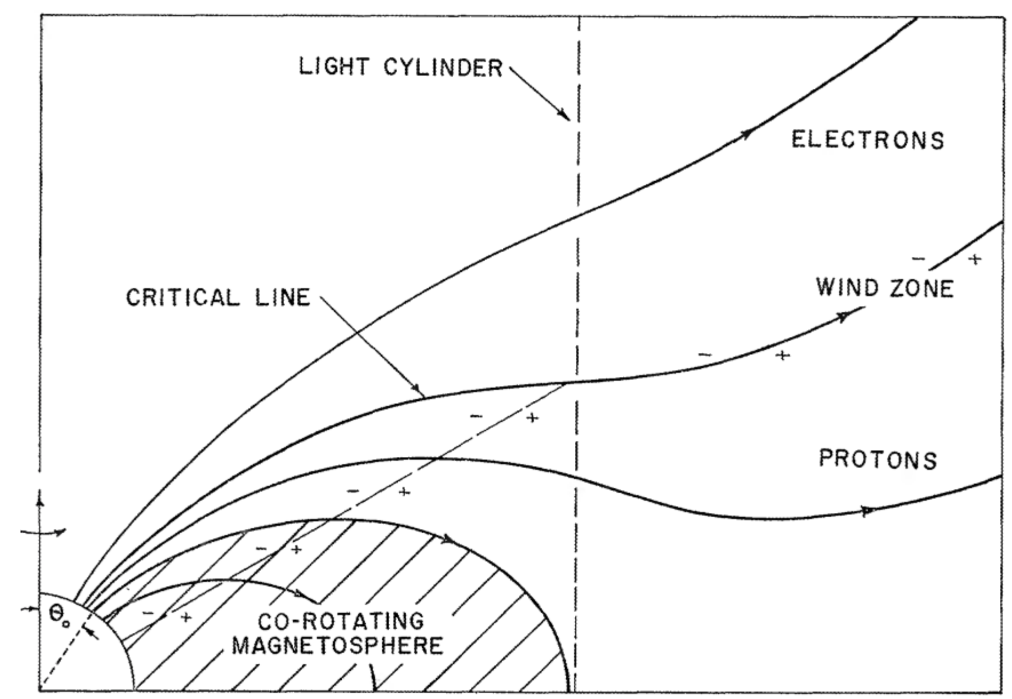

$$P_{\rm rad} = \frac{2}{3}\frac{\mu_\perp^2 \Omega^4}{c^3} \qquad \Delta\Phi = \frac{B_\star \Omega^2 R_\star^3}{2c^2}$$

$$\dot{N}_{GJ} = \frac{B_\star \Omega^2 R_\star^3}{ec}$$ (+ pair creation!)

PWNe @ VHEs

Since the **TeV detection of the Crab PWN in 1989 with the Whipple telescope** (Weekes et al. 1989), tens of Galactic sources have been associated with TeV PWN.

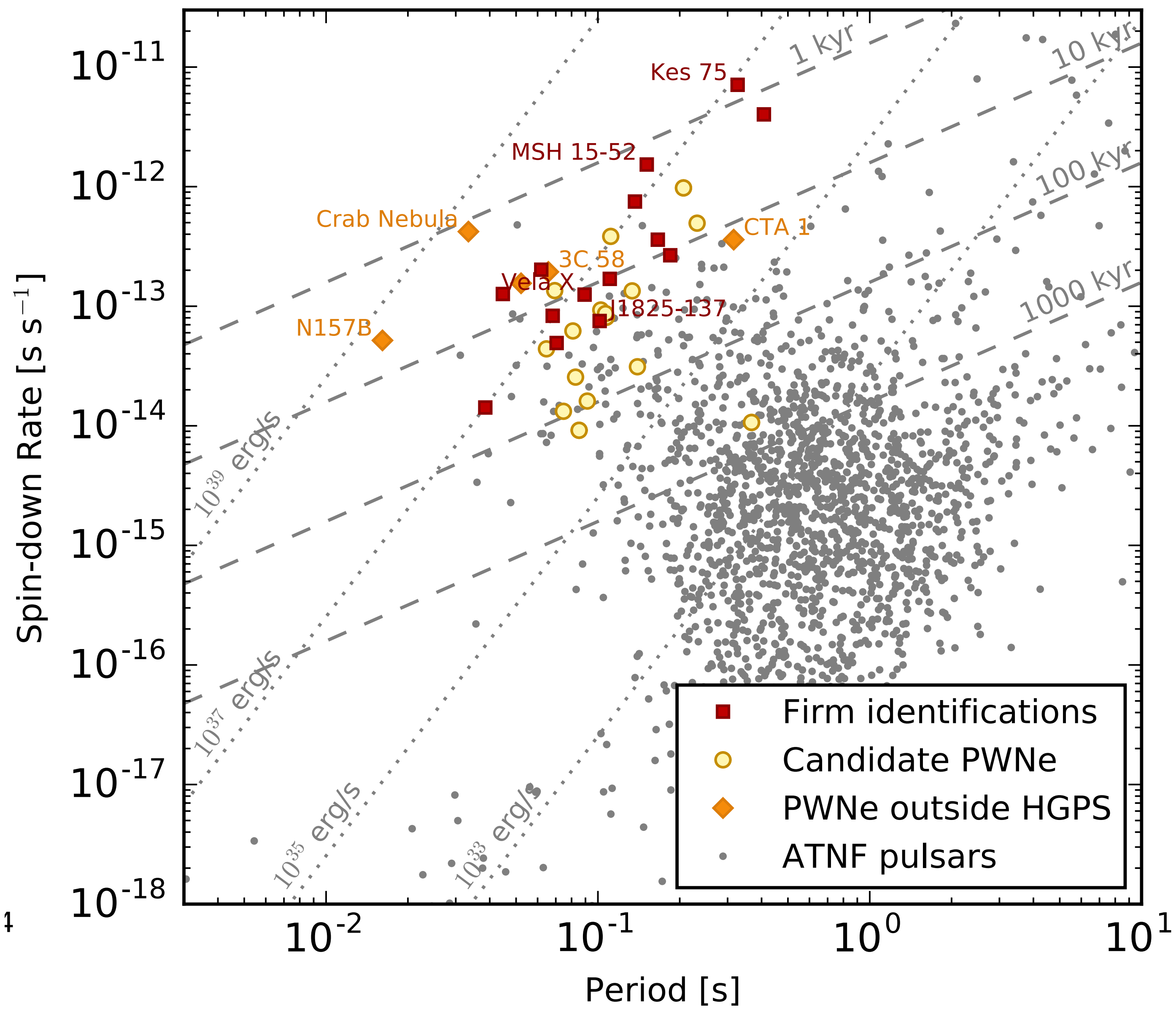

H.E.S.S. coll. 2018

PWNe @ VHEs

The Crab Nebula has been considered for decades the "standard candle" in VHE gamma-rays (we even speak on source fluxes in "Crab units"). Recently, the Crab Nebula spectrum has been revealed up to the UHE regime (Cao et al. 2021)

$$E_{max} = e\eta_E\eta_B^{1/2}\sqrt{\dot{E}/c} \approx 1.8\ \mathrm{PeV}\,\eta_{\mathrm{E}}\eta_{\mathrm{B}}^{1/2}\dot{\mathrm{E}}_{36}^{1/2}$$

$$\frac{B_{TS}^2}{4\pi} = \eta_B \frac{\dot{E}}{4\pi R_{TS}^2 c}$$

$$t_{acc} = \frac{E}{e\eta_E Bc}$$

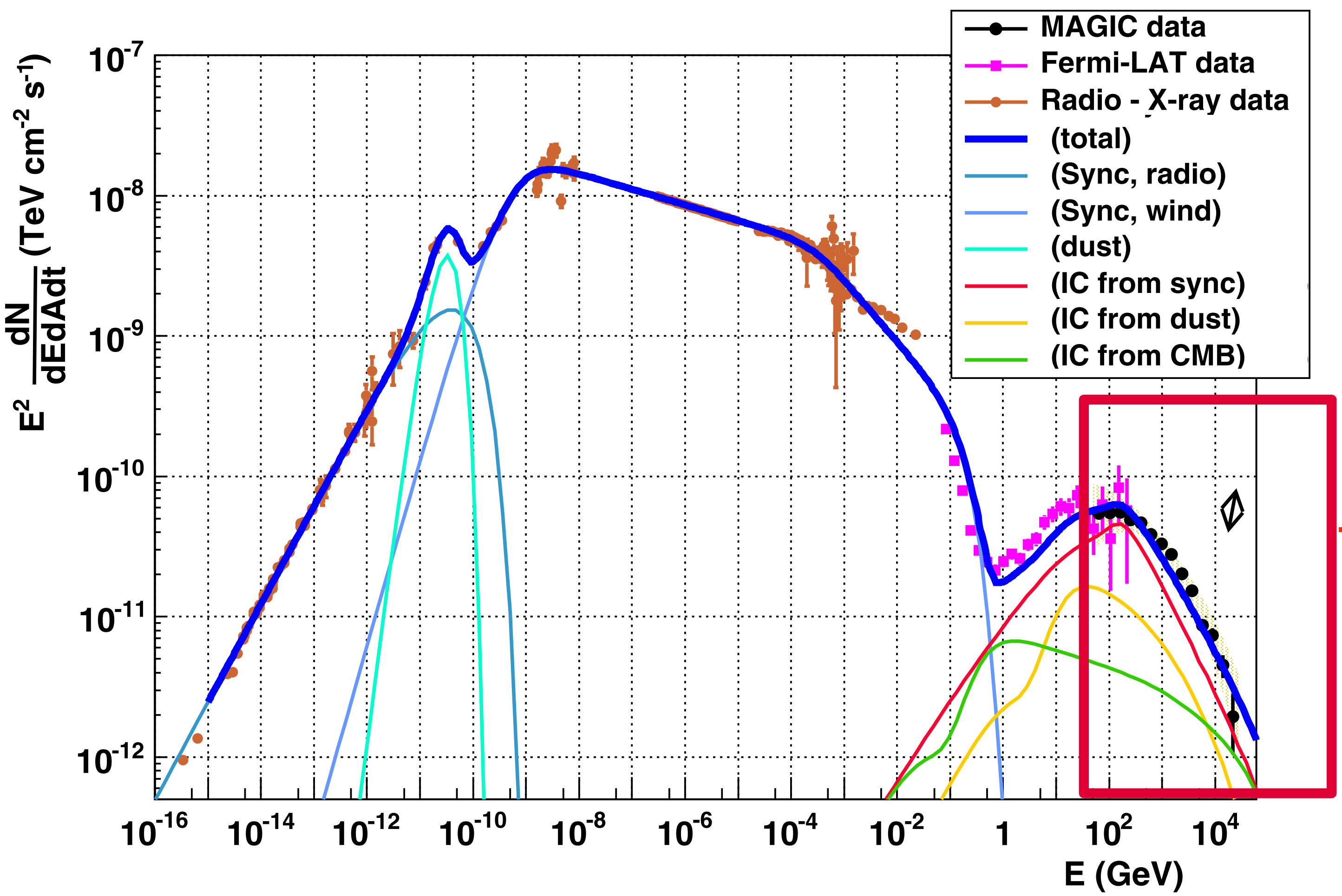

adapted from Aleksic et al. 2015

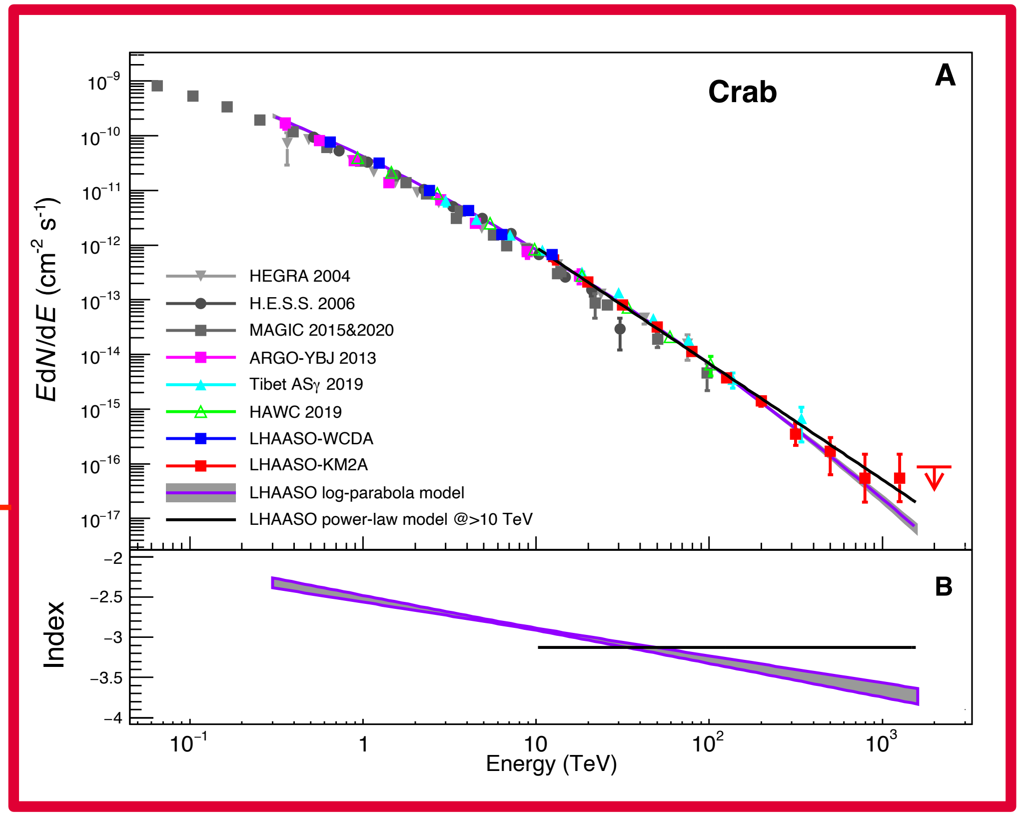

Cao et al. 2021

PWNe @ VHEs

The Crab Nebula has been considered for decades the “standard candle” in VHE gamma-rays (we even speak on source fluxes in “Crab units”). Recently, the Crab Nebula spectrum has been revealed up to the UHE regime (Cao et al. 2021)

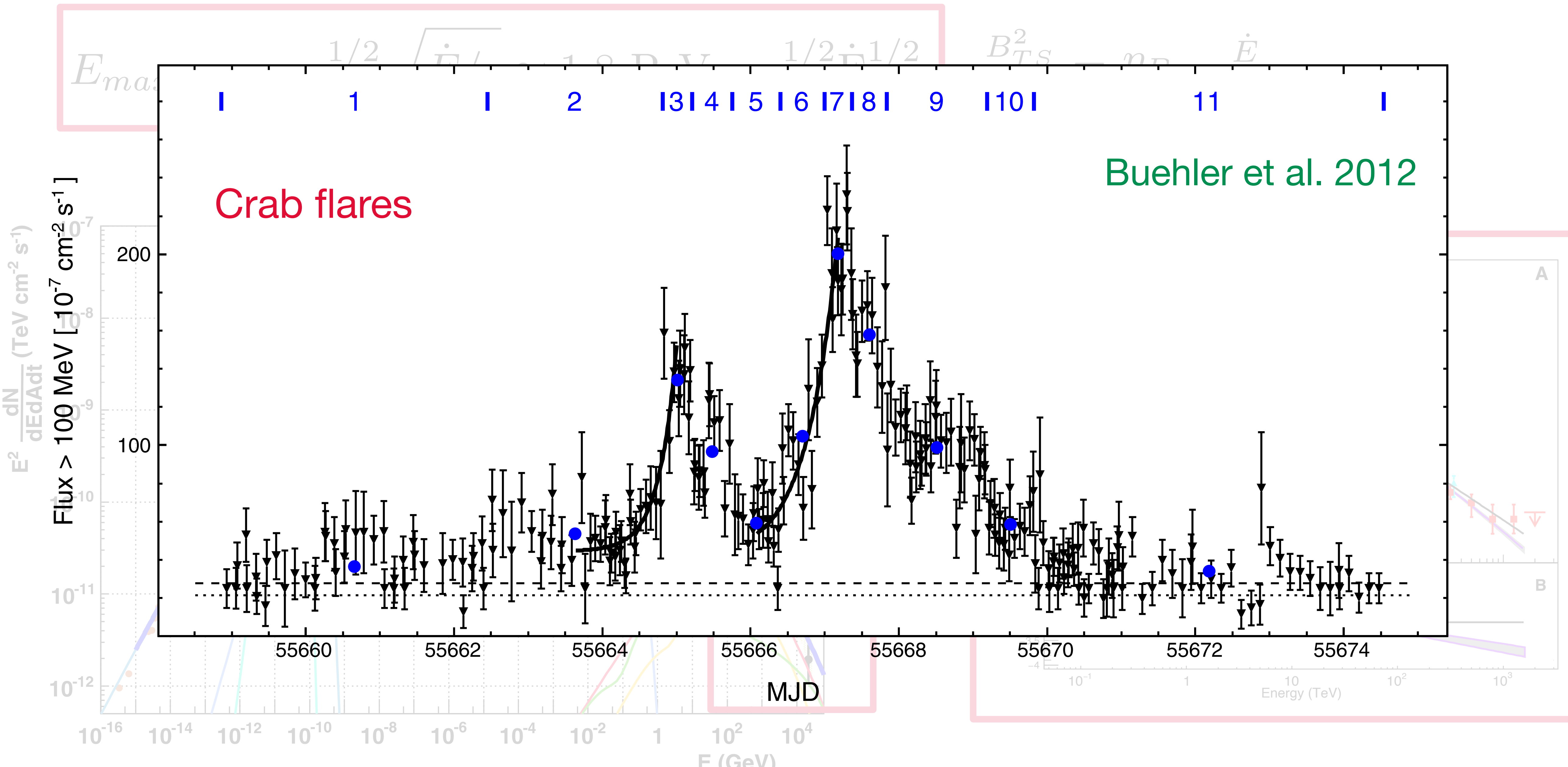

adapted from Aleksic et al. 2015

Cao et al. 2021

PWNe @ VHEs

Aharonian et al. 2006

HESS J1825-137

- First evidence of energy-dependent morphology at TeV gamma-rays.
- X-ray emitting particles cool faster than TeV emitting ones => sizes!
- Spectral evolution favors leptonic IC scenario.
- High gamma-ray luminosity **cannot be explained with a constant spin-down power** of the pulsar => requires **higher injection power** in the past.
- New HESS measurements reveals an extension beyond ~1.5 deg (100 pc)
- A dependence of the nebula extent with energy of $R \propto E^{\alpha}$ with $\alpha = -0.29$ disfavours a pure diffusion scenario for particle transport within the nebula

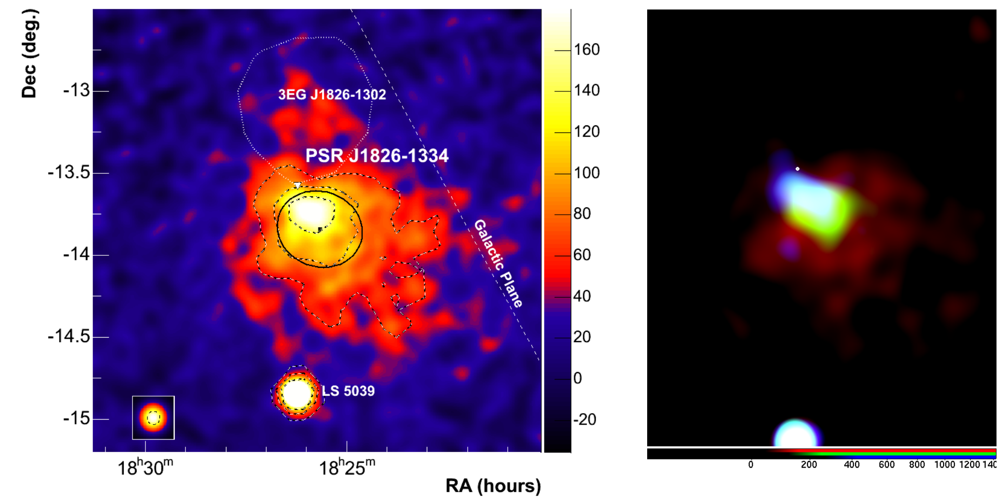

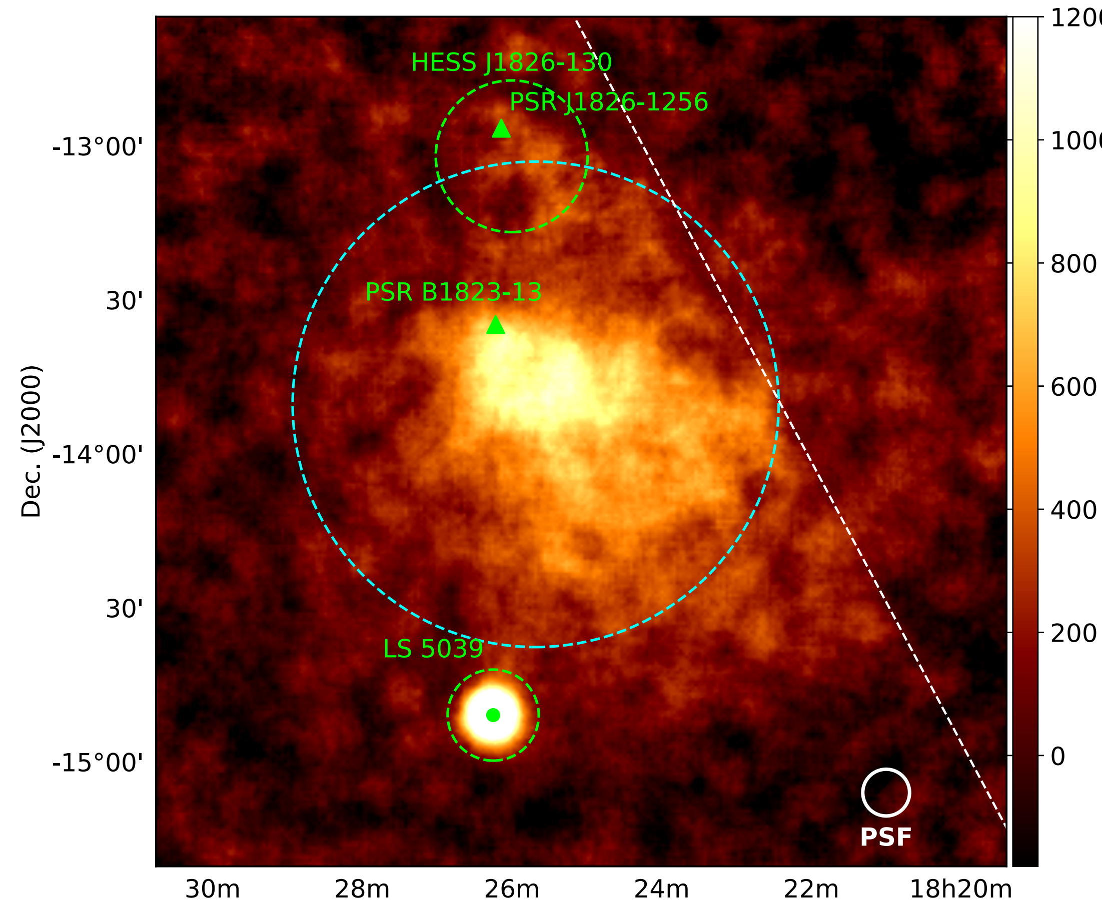

HESS coll. 2019

TeV halos

MILAGRO: detection of extended emission (~3 degree, or > 20 times the size of the PWN as seen in X-rays) from Geminga
Abdo+ (2007)

Measurement later confirmed/improved by the HAWC Collaboration
Abeysekara+ (2017)

Abdo et al. (2007)

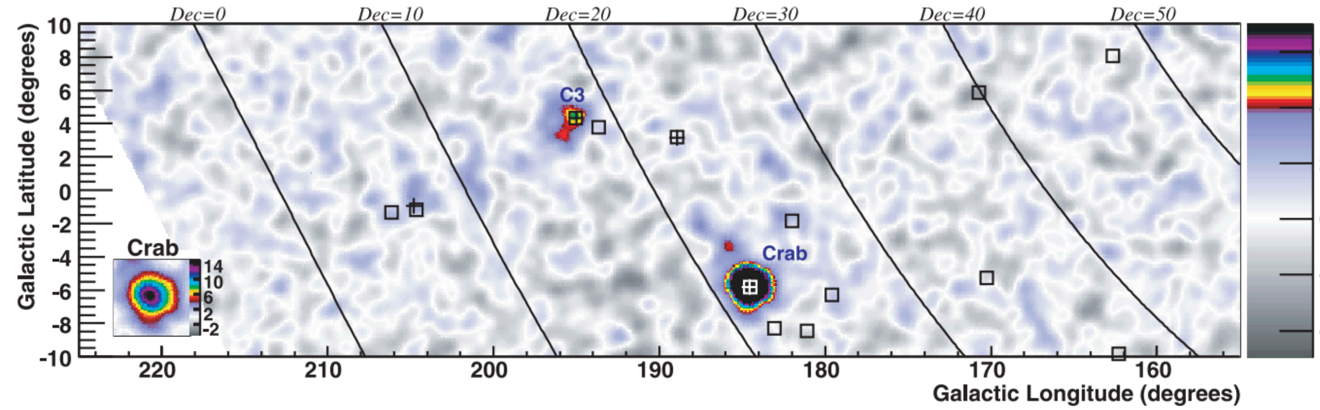

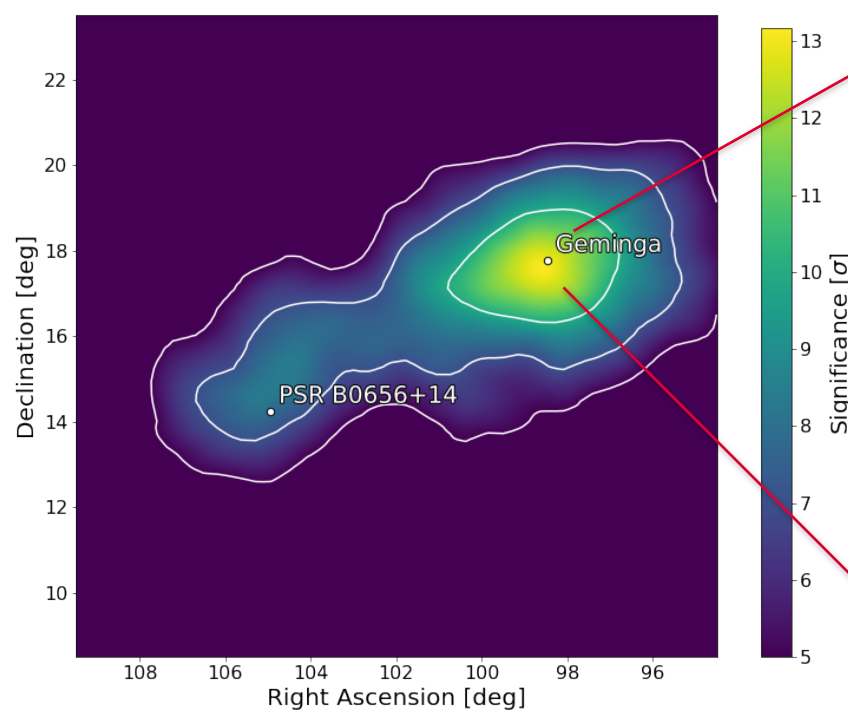

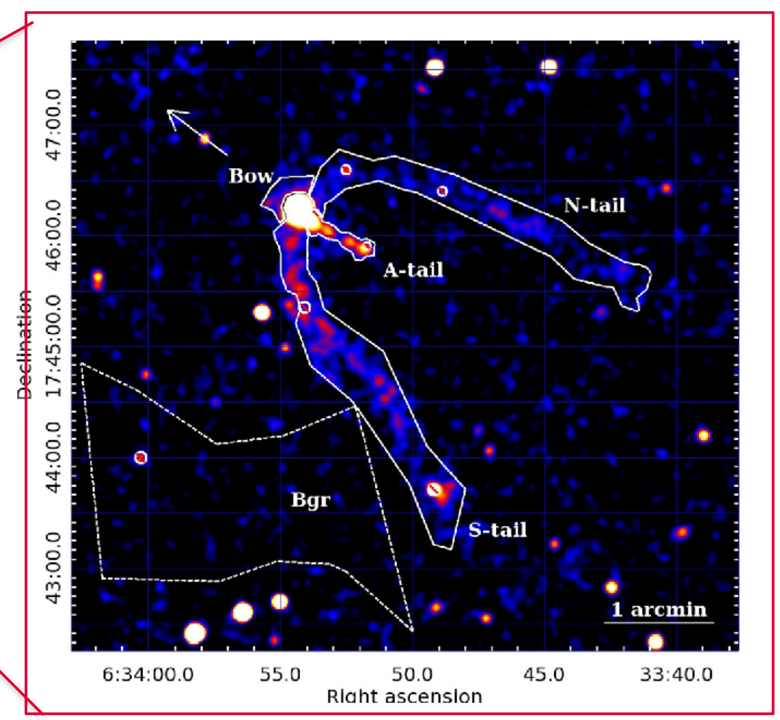

Abeysekara et al. (2017)

Posselt et al. (2017)

TeV halos

Geminga also detected recently by LHAASO (KM2A, 25-63 TeV) and for the first time with IACTs (H.E.S.S.) at energies 0.5 - 40 TeV

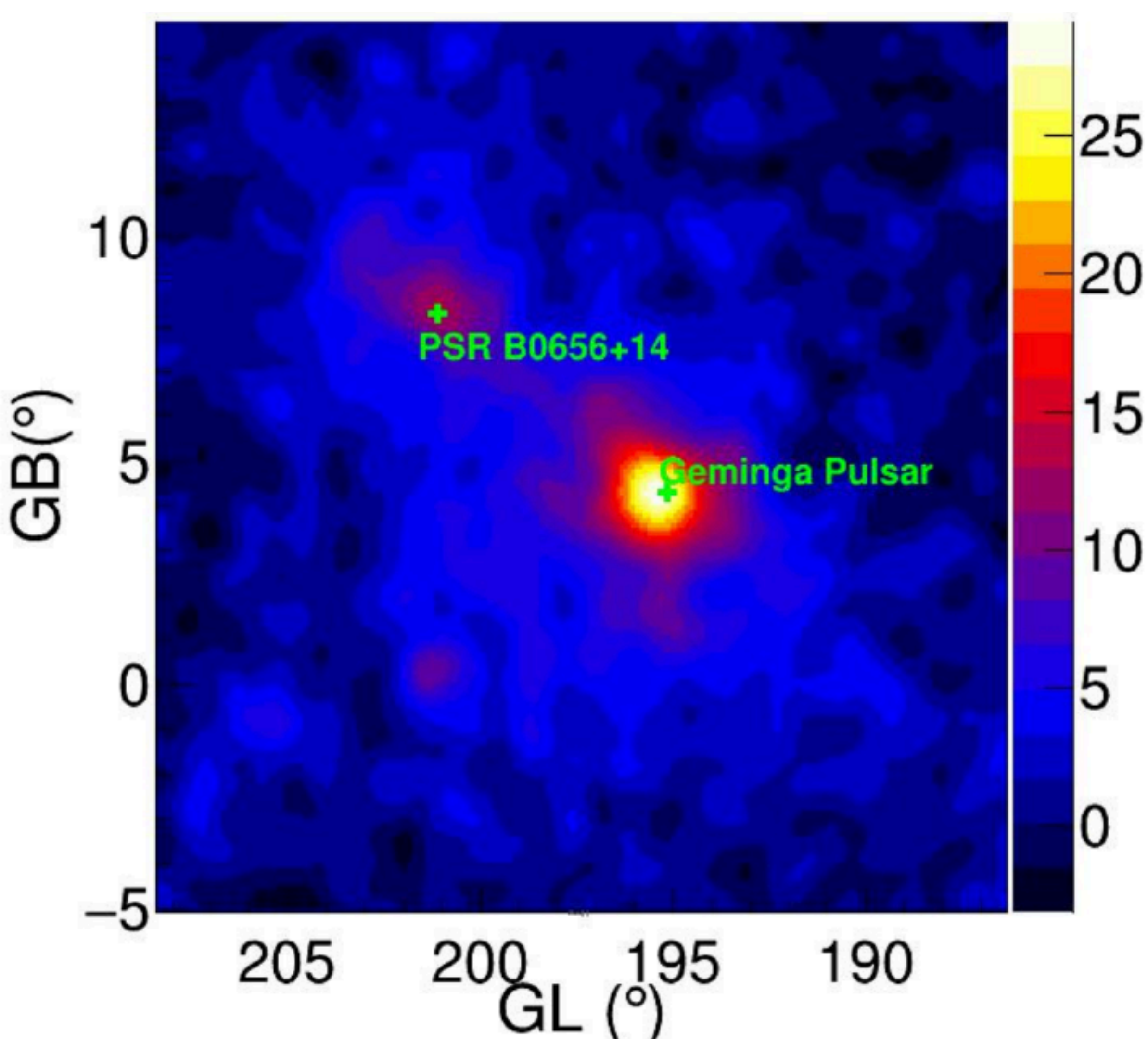

Chen et al. (2023)

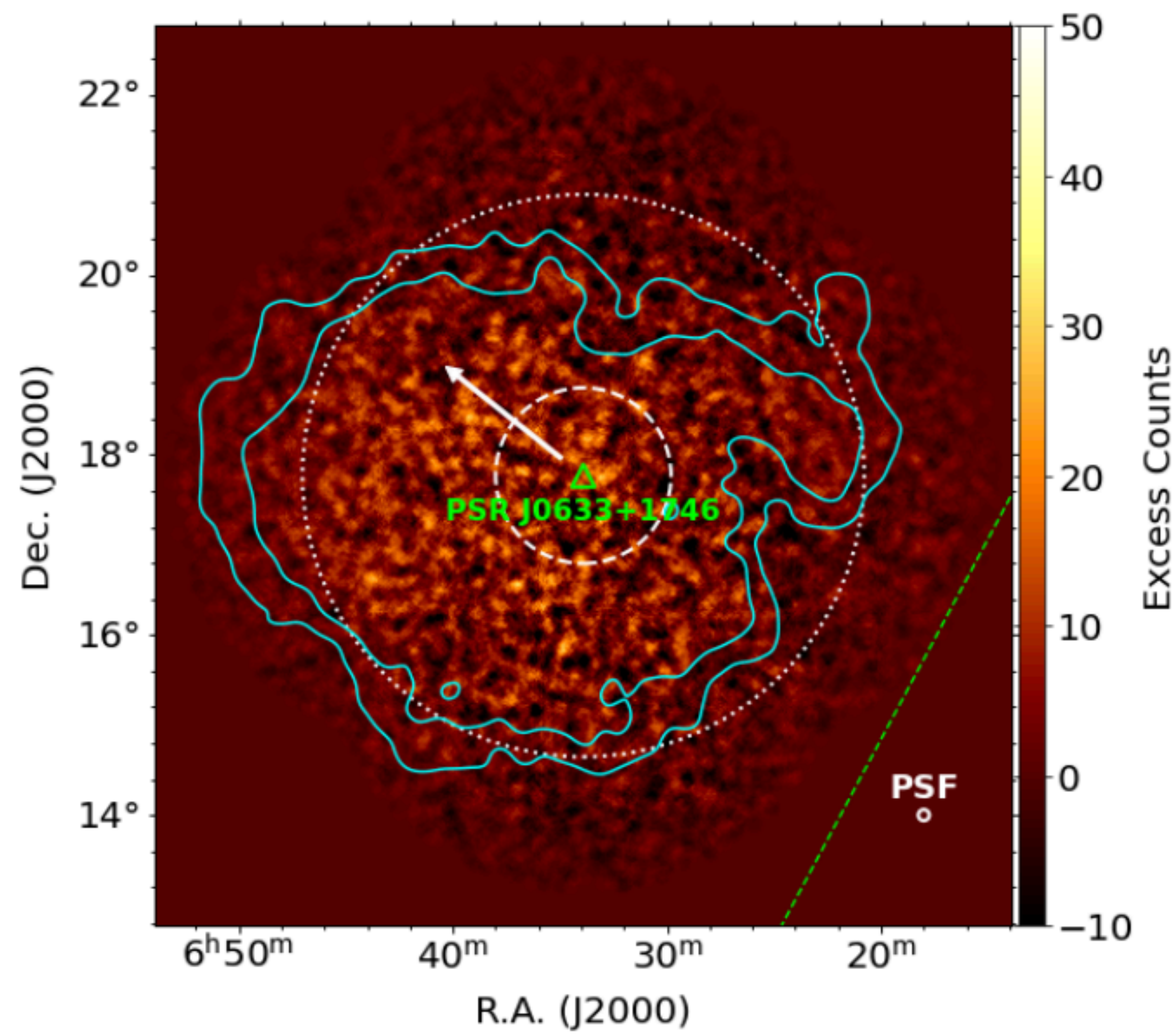

H.E.S.S. Coll. (2023)

TeV halos

Proposed associations with TeV halos

2HWC Name	ATNF Name	Distance (kpc)	Angular Separation	Projected Separation	Expected Flux ($\times 10^{-15}$)	Actual Flux ($\times 10^{-15}$)	Flux Ratio	Expected Extension	Actual Extension	Age (kyr)	Chance Overlap
J0700+143	B0656+14	0.29	0.18°	0.91 pc	43.0	23.0	1.87	2.0°	1.73°	111	0.0
J0631+169	J0633+1746	0.25	0.89°	3.88 pc	48.7	48.7	1.0	2.0°	2.0°	342	0.0
J1912+099	J1913+1011	4.61	0.34°	27.36 pc	13.0	36.6	0.36	0.11°	0.7°	169	0.30
J2031+415	J2032+4127	1.70	0.11°	3.26 pc	5.59	61.6	0.091	0.29°	0.7°	181	0.002
J1831-098	J1831-0952	3.68	0.04°	2.57 pc	7.70	95.8	0.080	0.14°	0.9°	128	0.006

2HWC Name	ATNF Name	Distance (kpc)	Angular Separation	Projected Separation	Expected Flux ($\times 10^{-15}$)	Actual Flux ($\times 10^{-15}$)	Flux Ratio	Expected Extension	Actual Extension	Age (kyr)	Chance Overlap
J1930+188	J1930+1852	7.0	0.03°	3.67 pc	23.2	9.8	2.37	0.07°	0.0°	2.89	0.002
J1814-173	J1813-1749	4.7	0.54°	44.30 pc	243	152	1.60	0.11°	1.0°	5.6	0.61
J2019+367	J2021+3651	1.8	0.27°	8.48 pc	99.8	58.2	1.71	0.28°	0.7°	17.2	0.04
J1928+177	J1928+1746	4.34	0.03°	2.27 pc	8.08	10.0	0.81	0.11°	0.0°	82.6	0.002
J1908+063	J1907+0602	2.58	0.36°	16.21 pc	40.0	85.0	0.47	0.2°	0.8°	19.5	0.26
J2020+403	J2021+4026	2.15	0.18°	6.75 pc	2.48	18.5	0.134	0.23°	0.0°	77	0.01
J1857+027	J1856+0245	6.32	0.12°	13.24 pc	11.0	97.0	0.11	0.08°	0.9°	20.6	0.06
J1825-134	J1826-1334	3.61	0.20°	12.66 pc	20.5	249	0.082	0.14°	0.9°	21.4	0.14
J1837-065	J1838-0655	6.60	0.38°	43.77 pc	12.0	341	0.035	0.08°	2.0°	22.7	0.48
J1837-065	J1837-0604	4.78	0.50°	41.71 pc	8.3	341	0.024	0.10°	2.0°	33.8	0.68
J2006+341	J2004+3429	10.8	0.42°	80.07 pc	0.48	24.5	0.019	0.04°	0.9°	18.5	0.08

Linden+ (2017)

Table 3. 1LHAASO sources associated pulsars

Source name	PSR name	Sep.(°)	d (kpc)	τ_c (kyr)	$\dot{E}$ (erg s^{-1})	P_c	Identified type in TeVCat
1LHAASO J0007+7303u	PSR J0007+7303	0.05	1.40	14	4.5e+35	7.3e-05	PWN
1LHAASO J0216+4237u	PSR J0218+4232	0.33	3.15	476000	2.4e+35	3.6e-03	
1LHAASO J0249+6022	PSR J0248+6021	0.16	2.00	62	2.1e+35	1.5e-03	
1LHAASO J0359+5406	PSR J0359+5414	0.15	-	75	1.3e+36	7.2e-04	
1LHAASO J0534+2200u	PSR J0534+2200	0.01	2.00	1	4.5e+38	3.2e-06	PWN
1LHAASO J0542+2311u	PSR J0543+2329	0.30	1.56	253	4.1e+34	8.3e-03	
1LHAASO J0622+3754	PSR J0622+3749	0.09	-	208	2.7e+34	2.5e-04	PWN/TeV Halo
1LHAASO J0631+1040	PSR J0631+1037	0.11	2.10	44	1.7e+35	3.5e-04	PWN
1LHAASO J0634+1741u	PSR J0633+1746	0.12	0.19	342	3.3e+34	1.3e-03	PWN/TeV Halo
1LHAASO J0635+0619	PSR J0633+0632	0.39	1.35	59	1.2e+35	9.4e-03	
1LHAASO J1740+0948u	PSR J1740+1000	0.21	1.23	114	2.3e+35	1.4e-03	
1LHAASO J1809-1918u	PSR J1809-1917	0.05	3.27	51	1.8e+36	6.2e-04	
1LHAASO J1813-1245	PSR J1813-1245	0.01	2.63	43	6.2e+36	6.3e-06	
1LHAASO J1825-1256u	PSR J1826-1256	0.09	1.55	14	3.6e+36	1.6e-03	
1LHAASO J1825-1337u	PSR J1826-1334	0.11	3.61	21	2.8e+36	2.8e-03	PWN/TeV Halo
1LHAASO J1837-0654u	PSR J1838-0655	0.12	6.60	23	5.6e+36	2.2e-03	PWN
1LHAASO J1839-0548u	PSR J1838-0537	0.20	-	5	6.0e+36	6.1e-03	
1LHAASO J1848-0001u	PSR J1849-0001	0.06	-	43	9.8e+36	1.2e-04	PWN
1LHAASO J1857+0245	PSR J1856+0245	0.16	6.32	21	4.6e+36	3.1e-03	PWN
1LHAASO J1906+0712	PSR J1906+0722	0.19	-	49	1.0e+36	5.9e-03	
1LHAASO J1908+0615u	PSR J1907+0602	0.23	2.37	20	2.8e+36	6.8e-03	
1LHAASO J1912+1014u	PSR J1913+1011	0.13	4.61	169	2.9e+36	1.5e-03	
1LHAASO J1914+1150u	PSR J1915+1150	0.09	14.01	116	5.4e+35	1.8e-03	
1LHAASO J1928+1746u	PSR J1928+1746	0.04	4.34	83	1.6e+36	1.6e-04	

LHAASO Coll. (2023)

HAWC detection of TeV emission near PSR B0540+23

ATel #10941; *Colas Riviere (University of Maryland), Henrike Fleisch*
Technological University), Andres Sandoval (Universidad Nacional Auto
behalf of the HAWC collaboration
on 9 Nov 2017; 23:11 UT
Credential Certification: Colas Riviere (riviere@umd.ed

HAWC detection of TeV source HAWC J0635+070

ATel #12013; *Chad Brisbois (Michigan Technological University), Colas Riviere (University of Maryland), Henrike Fleischhack (Michigan Technological University), Andrew Smith (University of Maryland) on behalf of the HAWC collaboration*
ere@umd.edu)

Extended Very-High-Energy Gamma-Ray Emission Surrounding PSR **J0622 + 3749** Observed by LHAASO-KM2A

F. Aharonian *et al.* (LHAASO Collaboration)
Phys. Rev. Lett. **126**, 241103 – Published 16 June 2021

TeV halos

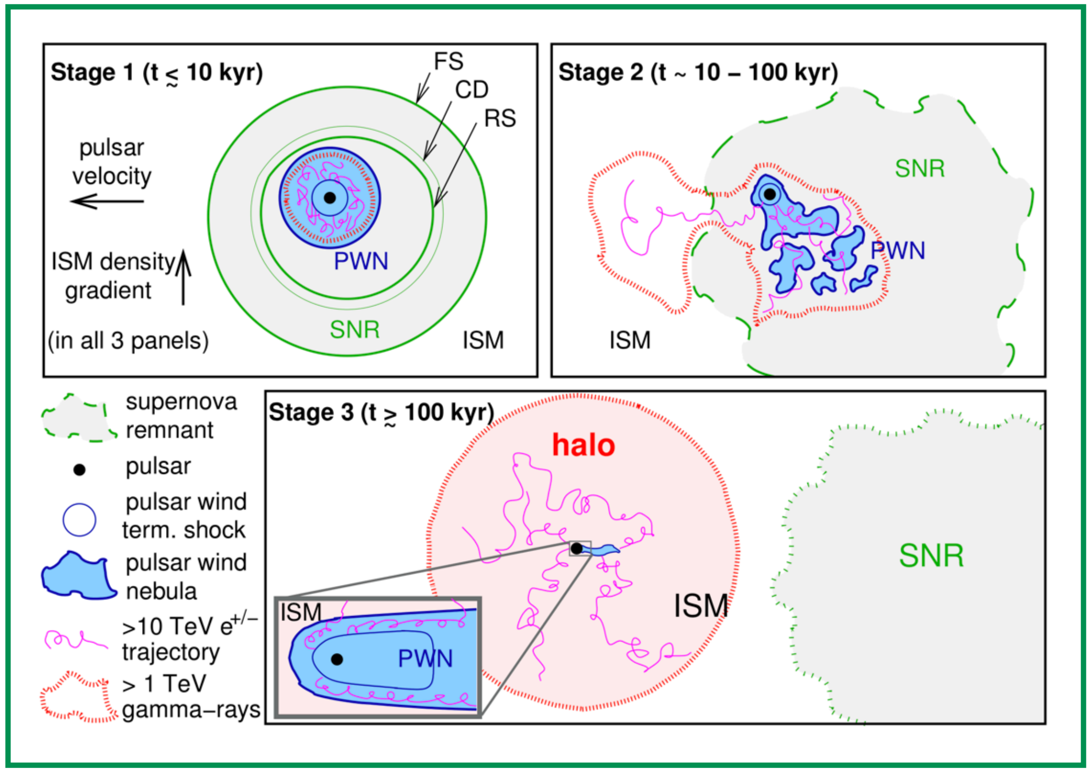

Giacinti et al. (2020)

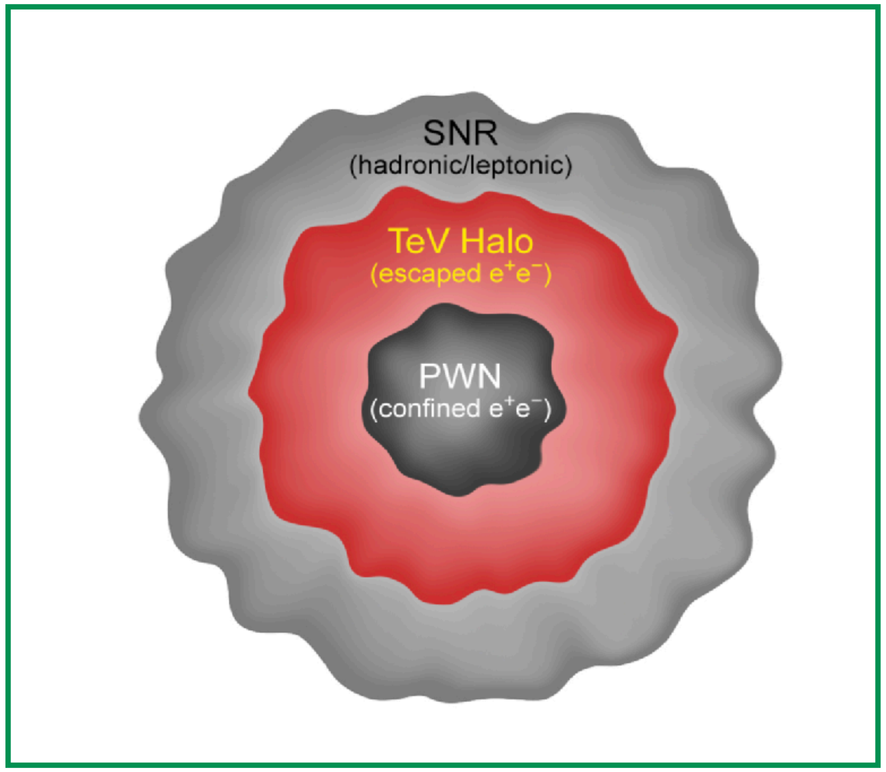

Sudoh et al. 2019

- Different definitions for “TeV halos”, depending on source age, whether or not the PWN is still inside the parent SNR, and on whether escaped $e^{-/+}$ from the (BS)PWN shall dominate the surrounding ISM dynamics

TeV halo definition not discussed here. Restrict to observational evidences for particle escape from BSPWN beyond the PWN limits (as observed in X-rays)

TeV halos

unveil new PSRs

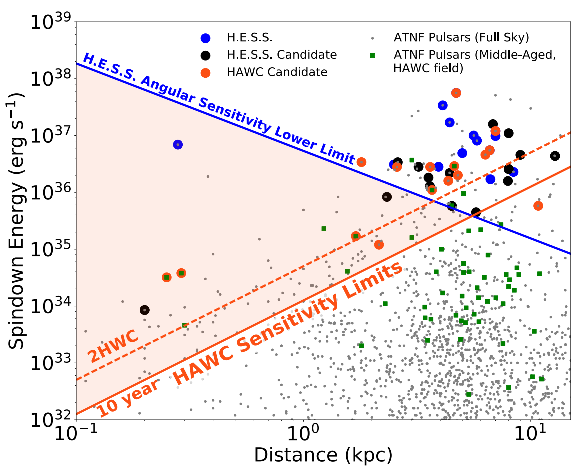

Linden+ (2017)

positron excess

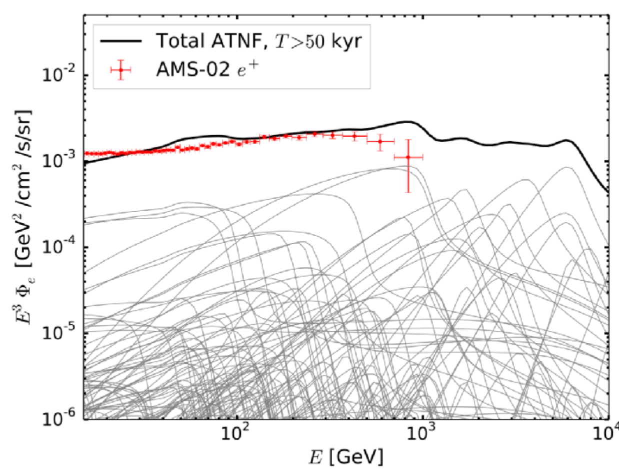

Manconi+ (2020)

Milagro and LHAASO diffuse emission

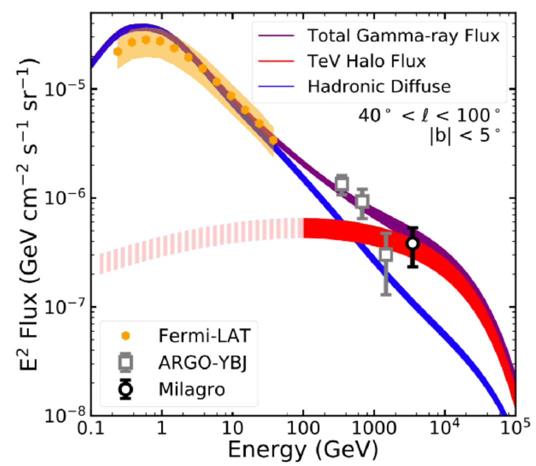

Linden+ (2018)

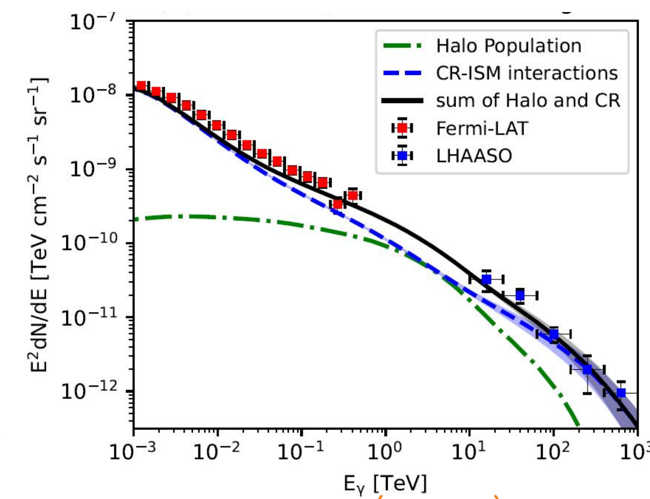

Yan+ (2023)

- PWN halos are ideal probes for CR propagation in localized regions of the Galaxy: e^- can IC-scatter off background photons to produce the gamma-ray halos, so the observed morphologies unambiguously trace the propagation of these particles.
- The most intriguing result is that the inferred electron diffusion coefficient is several hundred times smaller than the average CR diffusion coefficient in the Galaxy (see e.g. Aharonian et al. 2021, López-Coto et al. 2022)
- This finding has in turn significant impact on some key issues of CRs, such as the origin of the positron excess and the diffuse TeV gamma-ray excess.

TeV halos

- TeV halos → X-ray halos? high-energy $e^{-/+}$ through IC off the surrounding photon fields. For a given B-field in the region, X-ray emission from the same $e^{-/+}$ population should give rise to morphologically similar X-ray halos (see e.g. Linden et al. 2017).

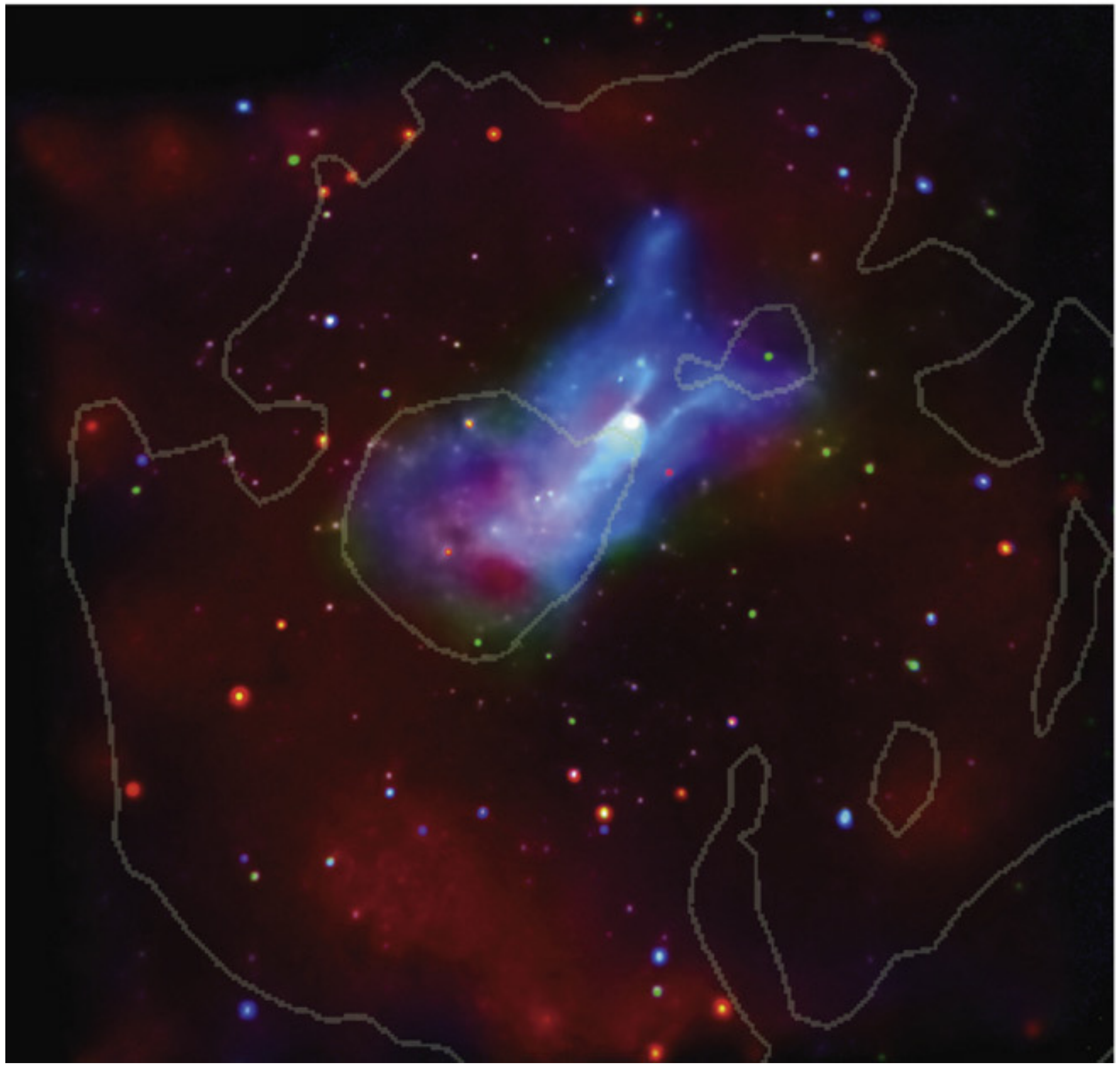

Temim et al. 2015

- PWN in the SNR G327.1-1.1
  - d = 9kpc (Sun+ 1999, Temim+2009)
  - L_{sd}~ 3.1e36 erg/s (Temim+ 2015)
  - Age ~ 17kyr => recently crushed by the SNR reverse shock (Eagle+ 2022)

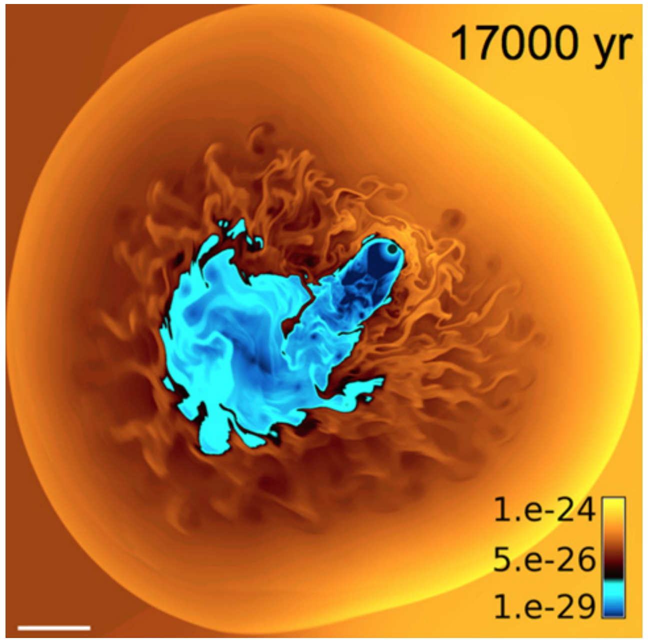

TeV halos

- TeV halos → high-energy $e^{-/+}$ through IC off the surrounding photon fields. For a given B-field in the region, X-ray emission from the same $e^{-/+}$ population should give rise to morphologically similar X-ray halos (see e.g. Linden et al. 2017).

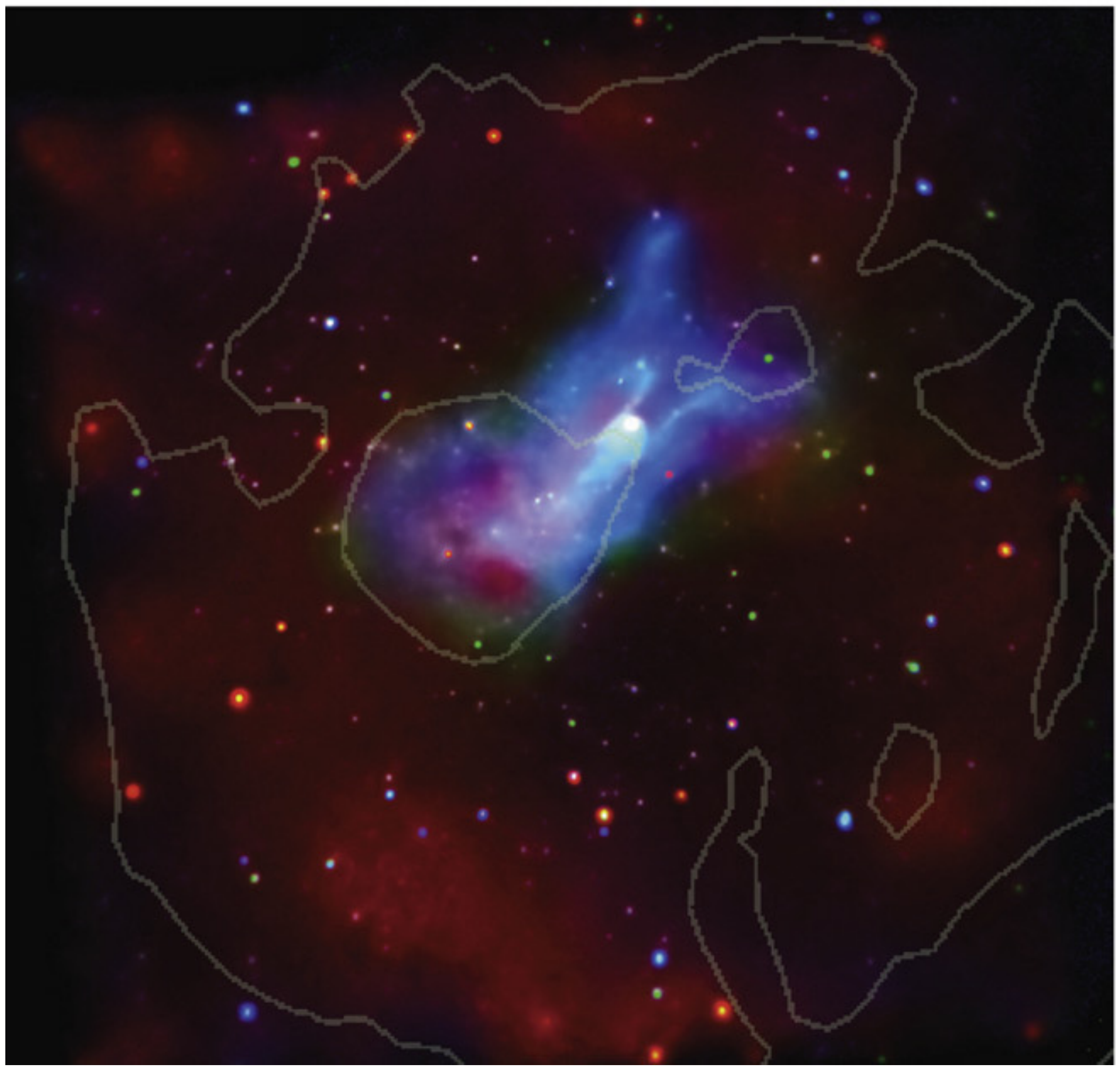

Temim et al. 2015

- PWN in the SNR G327.1-1.1

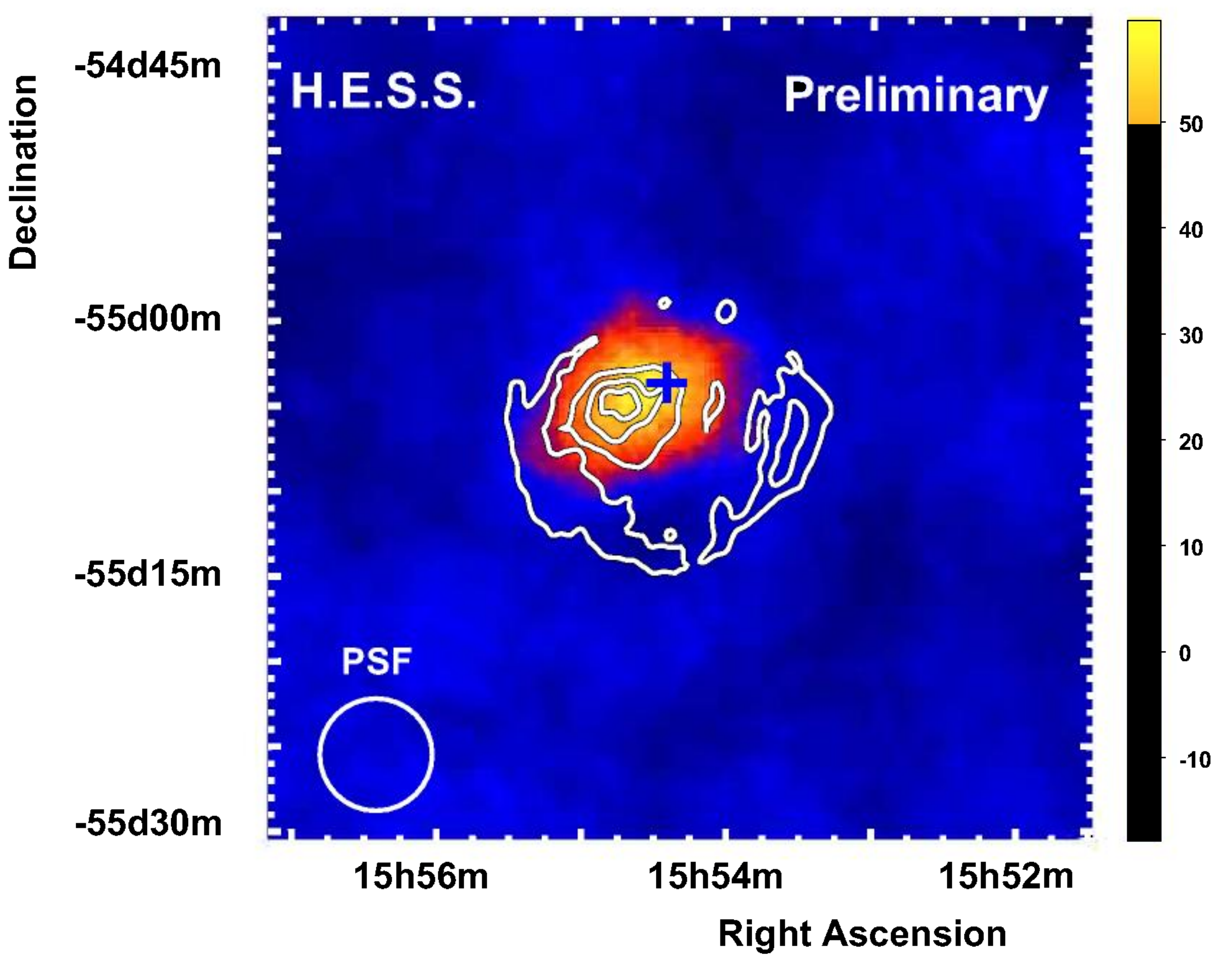

Acero et al. 2011

Binary systems

GREBs: Gamma-ray emitting binaries

γBs	PSR B1259–63 [1], LS 5039 [2], LS I +61 303 [3], HESS J0632+057 [4], 1FGL J1018.6–5856 [5], LMC–P3 [6], PSR J2032+4127 [7], HESS J1832–093 [8] 4FGL J1405.1-6119 [9], HESS J1828-099* [10]
μQs	Cyg X-3 [11], Cyg X-1 [12], SS433 [13], V4641 Sgr [?] V404 Gyg* [14], AGL J2241+4454* [15]
CWBs	Eta Carinae [16], γ^2Velorum [17], HD 93129A* [18]
Novae	V407 Cyg 2010 [19], V1324 Sco 2012 [20], V959 Mon 2012 [21], V339 Del 2013 [22], V1369 Cen 2013 [23], V5668 Sgr 2015 [24], V5855 Sgr [25], V5856 Sgr [26], V549 Vel [27], V357 Mus [28], V906 Car [29], V392 Per [30], V3890 Sgr [31], V1707 Sco [32], YZ Ret [33], V1674 Her [34], RS Oph [35]

updated from Paredes & Bordas (2019)

1. Aharonian et al. (2005), 2. Aharonian et al. (2005b), 3. Albert et al. (2006), 4. Aharonian et al. (2007), 5. Corbet et al. (2011), 6. Corbet et al. (2016), 7. Lyne et al. (2015), 8. HESS Collaboration (2015), 9. Corbet et al. (2019), 10. De Sarkar et al. (2022), 11. Tavani et al. (2009), 12. Albert et al. (2007), 13. Bordas et al. (2015), 14. Loh et al. (2016), 15. Lucarelli et al. (2010), 16. Tavani et al. (2009), 17. Mart-Devesa et al. (2020), 18. Chernyakova et al. (2019), 19. Abdo et al. (2010), 20. Cheung et al. (2012), 21. Cheung et al. (2012b), 22. Hays et al. (2013), 23. Cheung et al. (2013), 24. Cheung, et al. (2015), 25. Li, et al. (2016), 26. Li et al. (2016b), 27. Li et al. (2017), 28. Li et al. (2018), 29. Jean et al. (2018), 30. Li et al. (2018), 31. Buson et al. (2019), 32. Li et al. (2019), 33. Li et al. (2020), 34. Munari et al. (2021), 35. Cheung et al. (2021)

GeV/TeV emitting XRBs: ACCRETION vs. NON ACCRETION

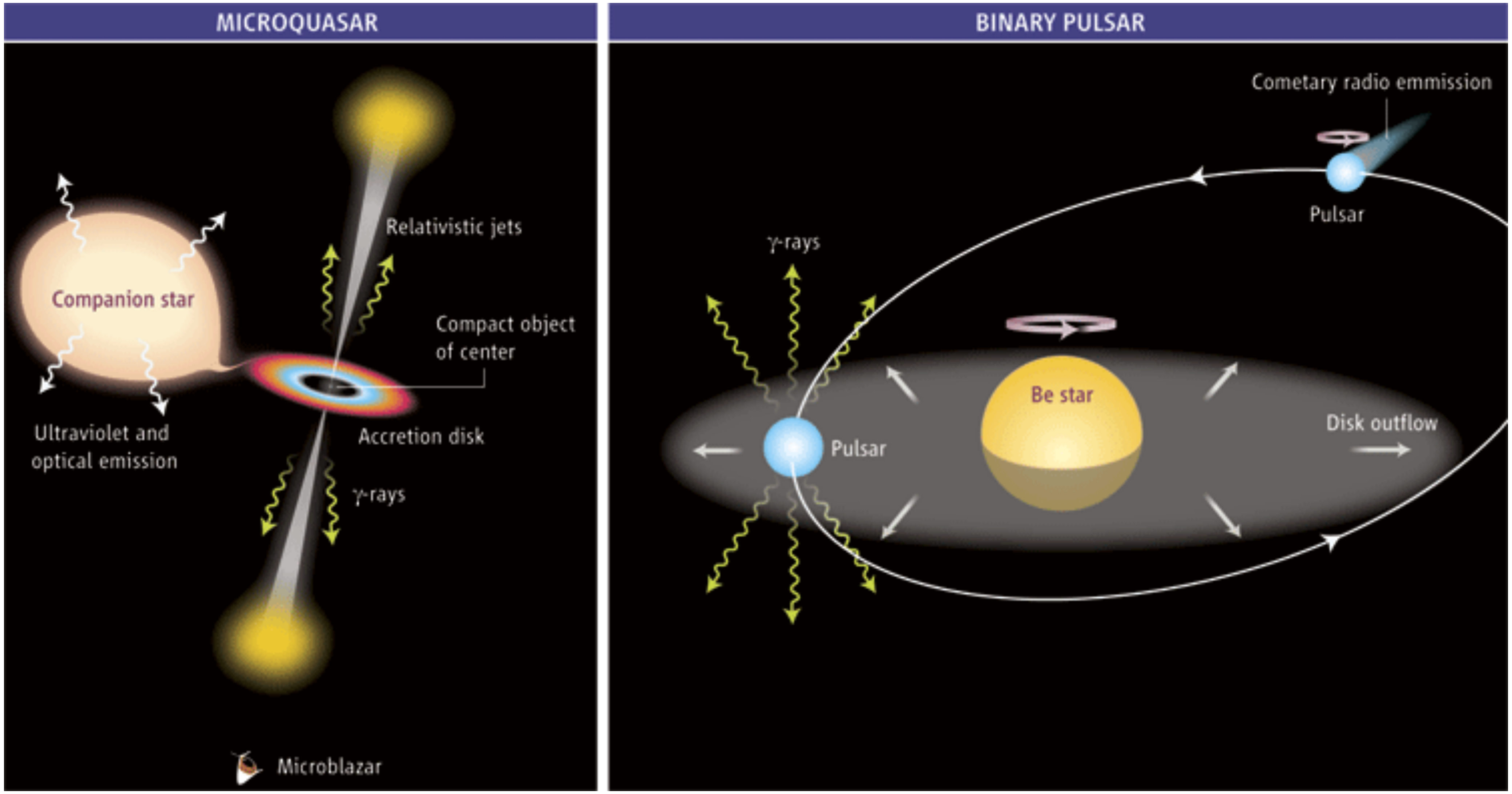

Gamma-ray binaries (γBs)

PSR B1259-63

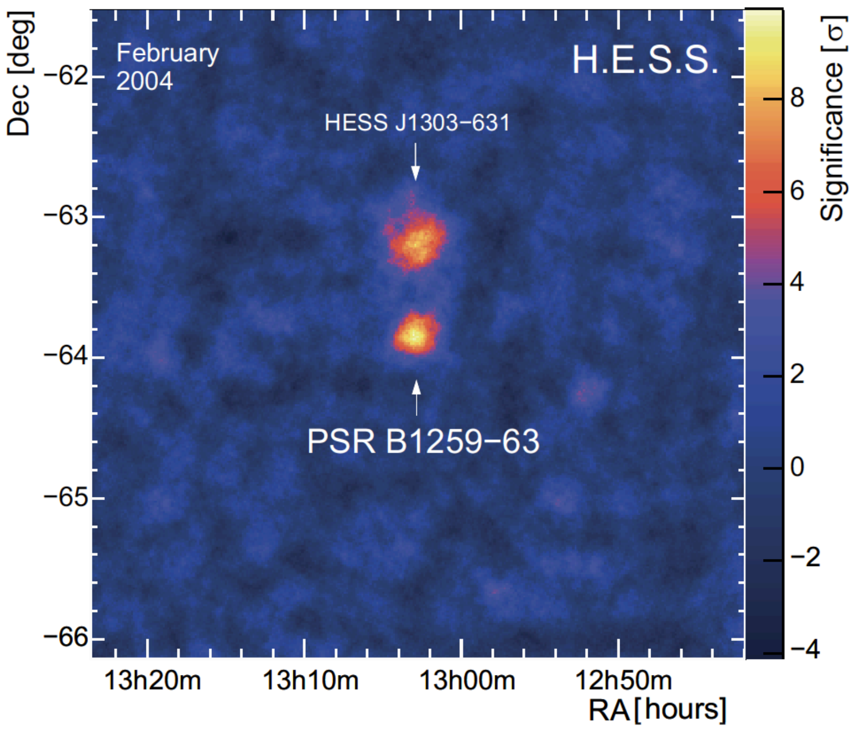

Aharonian et al. (2006a)

Johnston et al.(1992)

Tavani & Arons (1997)

LS 5039

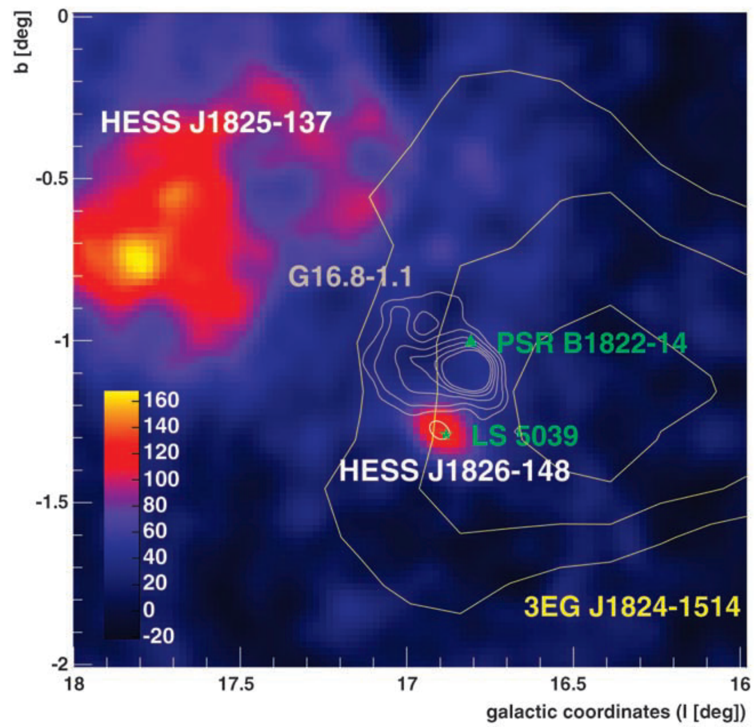

Aharonian et al. (2006b)

Motch et al. (1997)

Paredes et al. (2000)

LS I +61 303

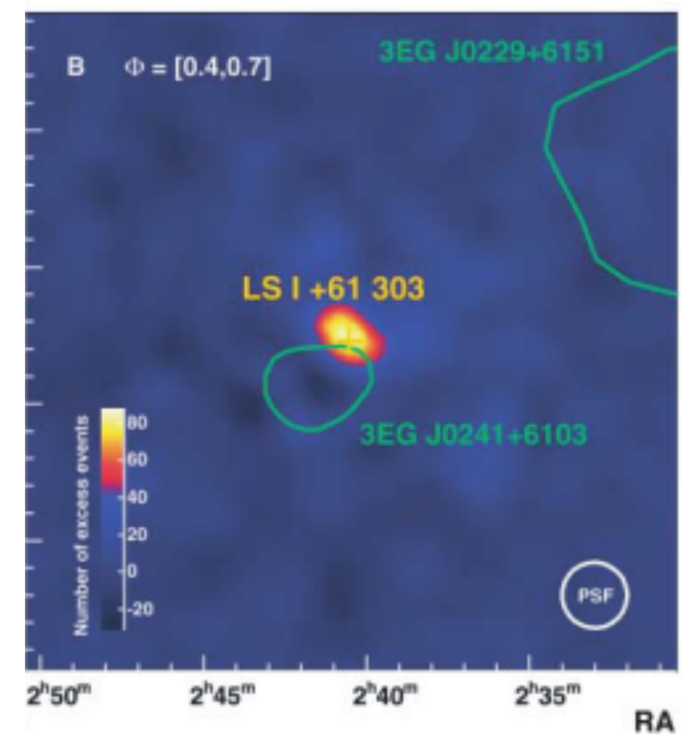

Albert et al. (2006)

Hermsen et al. (1977)

Gregory & Taylor (1978)

Gamma-ray binaries (γBs)

HESS J0632+057

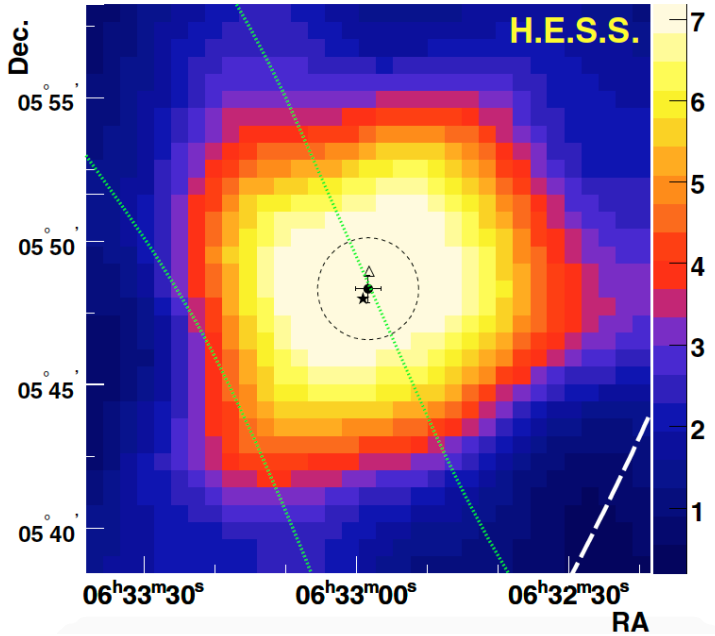

H.E.S.S. Col. (2007)

HESS J1832-093

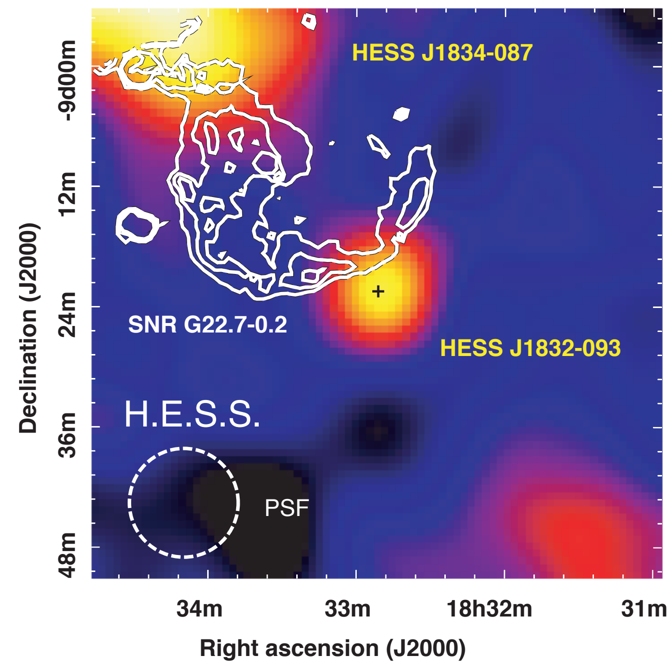

H.E.S.S. Col. (2014)

1FGL J1018.6−5856

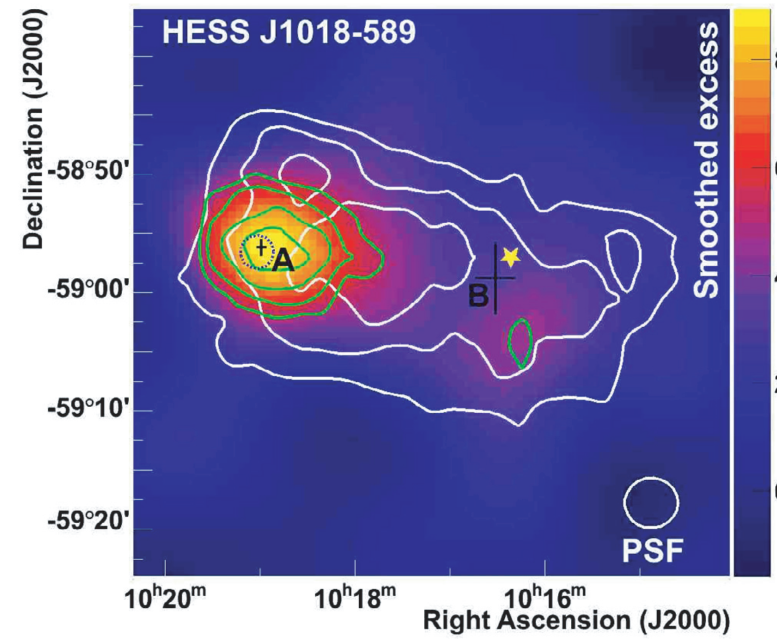

H.E.S.S. Col. (2012)

LMC P3

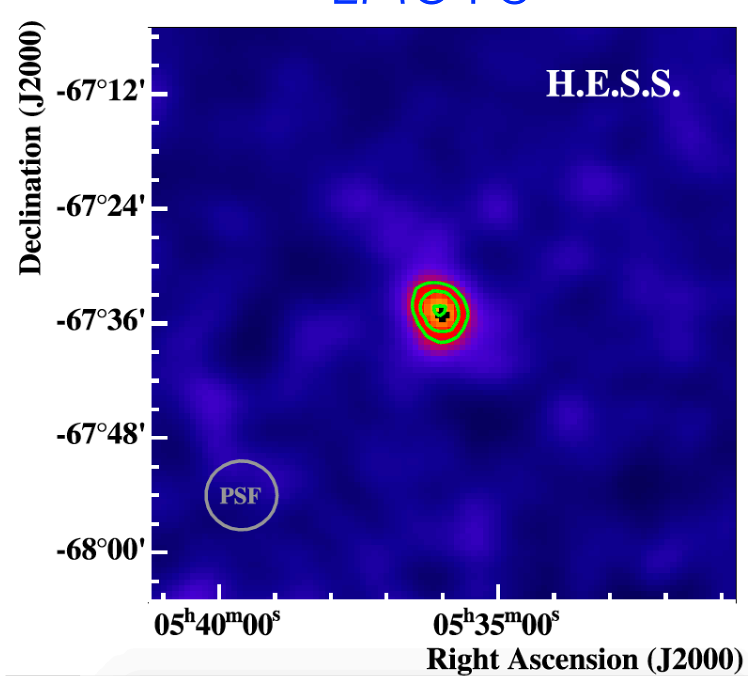

H.E.S.S. Col. (2018)

PSR J2032+4127

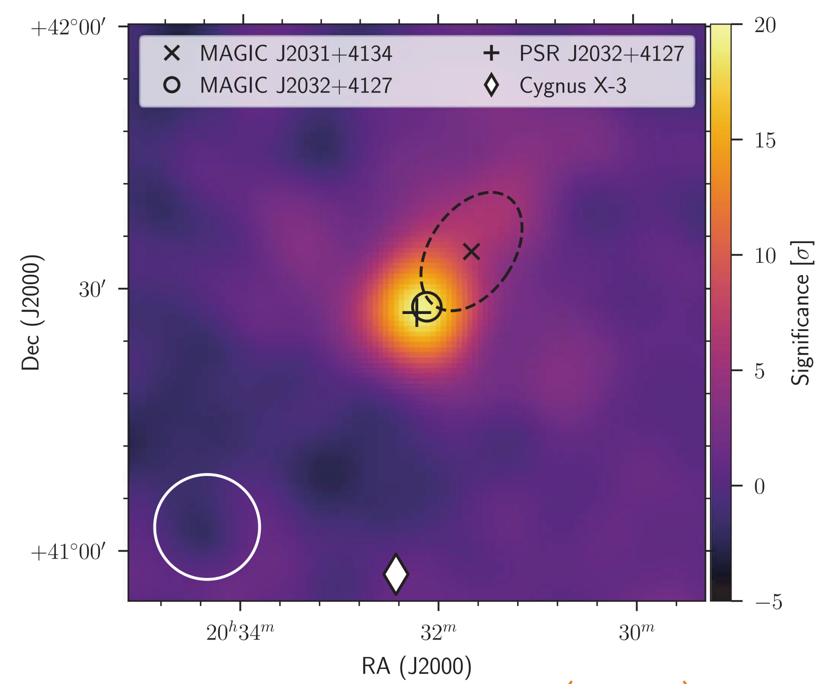

Abeysekara et al. (2018)

4FGL J1405.1-6119

Corbet et al. (2019)

Gamma-ray binaries (γBs)

	HE	VHE	Class	Components	P_{orbit}
PSR B1259-63	yes	yes	PSR binary	Oe + NS	~3.4 yrs
LS I +61 303	yes	yes	**PSR binary**	B0 Ve + NS	26.5 d
HESS J0632+057	**yes**	yes	?	B0 pe + ?	**317.3 d**
PSR J2032+4127	**~yes**	**yes**	**PSR binary**	**B0 Ve + PSR**	**~50 yrs**
HESS J1832-093	**yes**	**yes**	**?**	**B8V - B1.5V + ?**	**86.3 d**
LS 5039	yes	yes	**PSR binary (?)**	ON6.5V + **PSR?**	3.9 d
1FGL J1018.6–5856	yes	yes	?	O6V + ?	16.5 d
LMC P3	yes	yes	?	O5III + ?	10.3 d
4FGL J1405.1-6119	**yes**	no	**?**	**O6.5 III + ?**	**13.7 d**

Gamma-ray binaries (γBs)

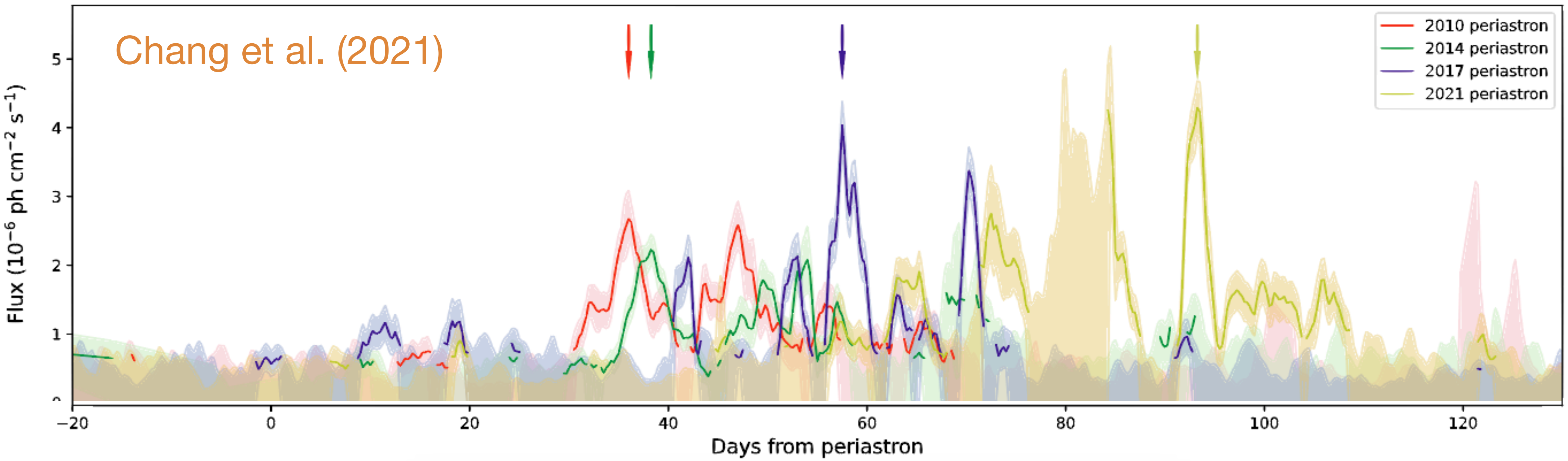

- L_γ > pulsar spin-down power (if isotropic) => **Doppler-boosting**, e.g. Kong et al. 2012, may not be however efficient enough (see Khangulyan et al. 2014); see also numerical MHD simulations in Bogovalov et al. 2012, 2019 in which **both for low and high magnetisation winds** collimation seems rather difficult to attain.

- Other models do not rely on Doppler boosting, e.g. **Comptonization of a cold pulsar wind** (Khangulyan et al. 2012), **GeV-emitting pairs with a Maxwellian distribution** injected in shock at high pulsar latitudes (Dubus & Cerutti 2013), **IC of soft photons from an accretion disk** formed around the PSR (Yi & Cheng 2017), or a combination of **bremsstrahlung +IC emission** from unshocked and weakly-shocked electrons of the pulsar wind (Chernyakova et al. 2020)

Gamma-ray binaries (γBs)

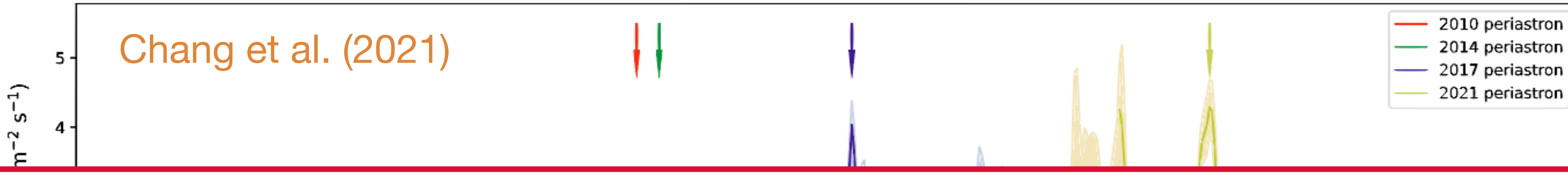

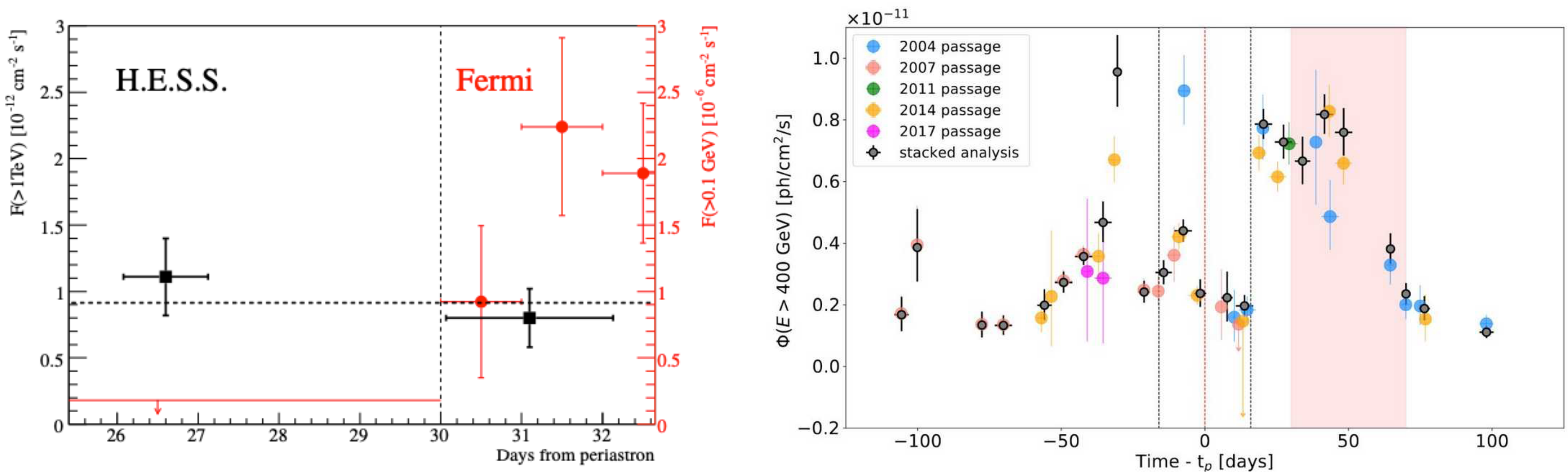

H.E.S.S. Col. (2020)

injected in shock at high pulsar latitudes (Dubus & Cerutti 2013), **IC of soft photons from an accretion disk** formed around the PSR (Yi & Cheng 2017), or a combination of **bremsstrahlung +IC emission** from unshocked and weakly-shocked electrons of the pulsar wind (Chernyakova et al. 2020)

SS433

- **Binary system**
  - d ~ 5.5 kpc, τ_{SS433} ~ 3 × 10^4 yrs
  - likely BH (M~10-20 $M_\odot$) + A-supergiant (Fabrika 2004)
  - supper-critical accretion rate, dM/dt ~ 10^{-4} $M_\odot$/yr
  - 13d (162d) orbital (precession) period (Gies+ 2002)
- **jets**
  - mildly relativistic vjets= 0.26 c, i = 78°, θ_{prec} = 21°
  - extremely powerful, $L_{jet} \gtrsim 10^{39}$ erg/s
  - evidence of baryons (Marshall+ 2002, Migliari+ 2002)
  - detected in radio, IR, optical, X-rays

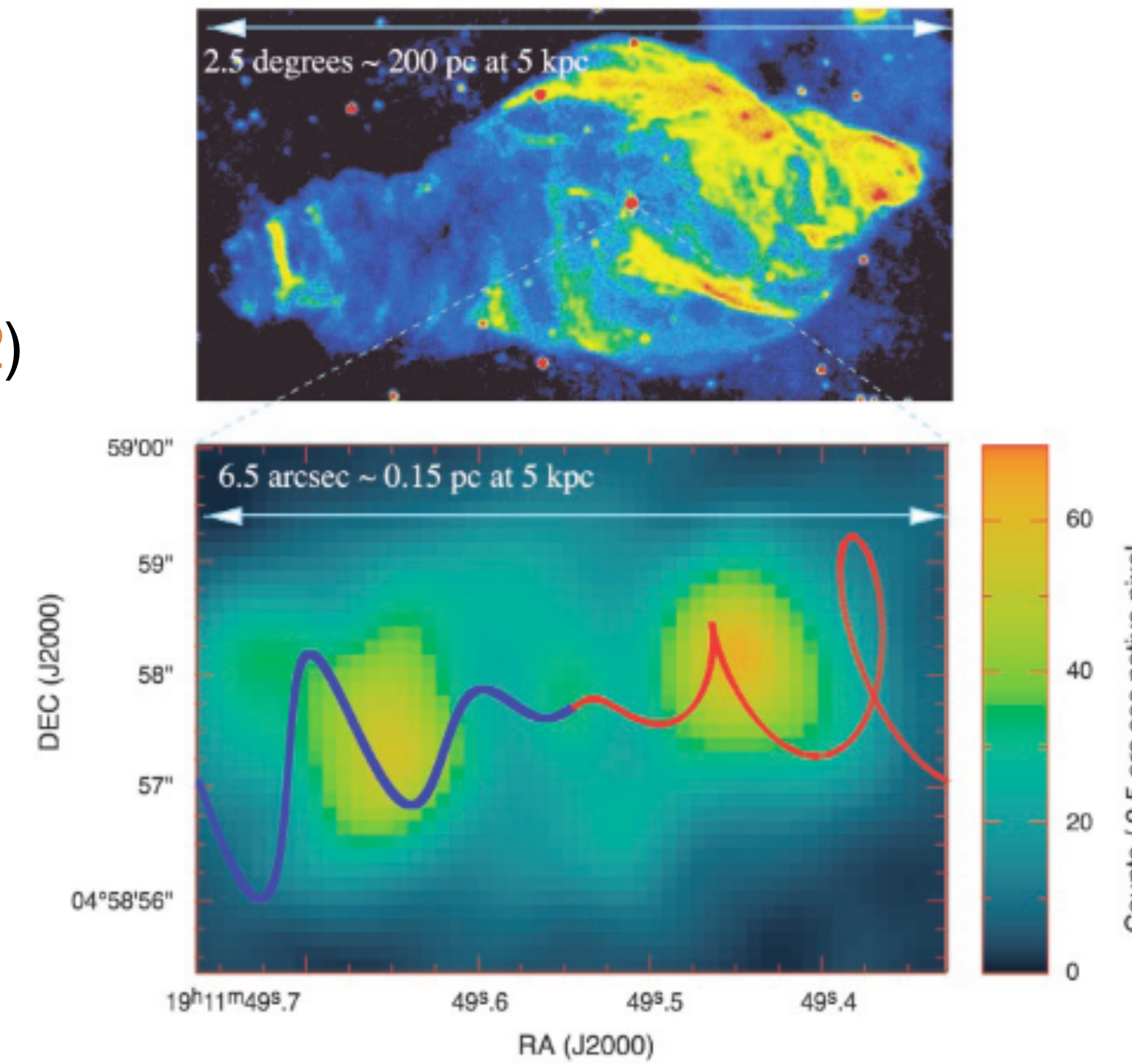

(Dubner et al 1998, Migliari et al. 2002)

SS433

Abeysekara et al. (2018)

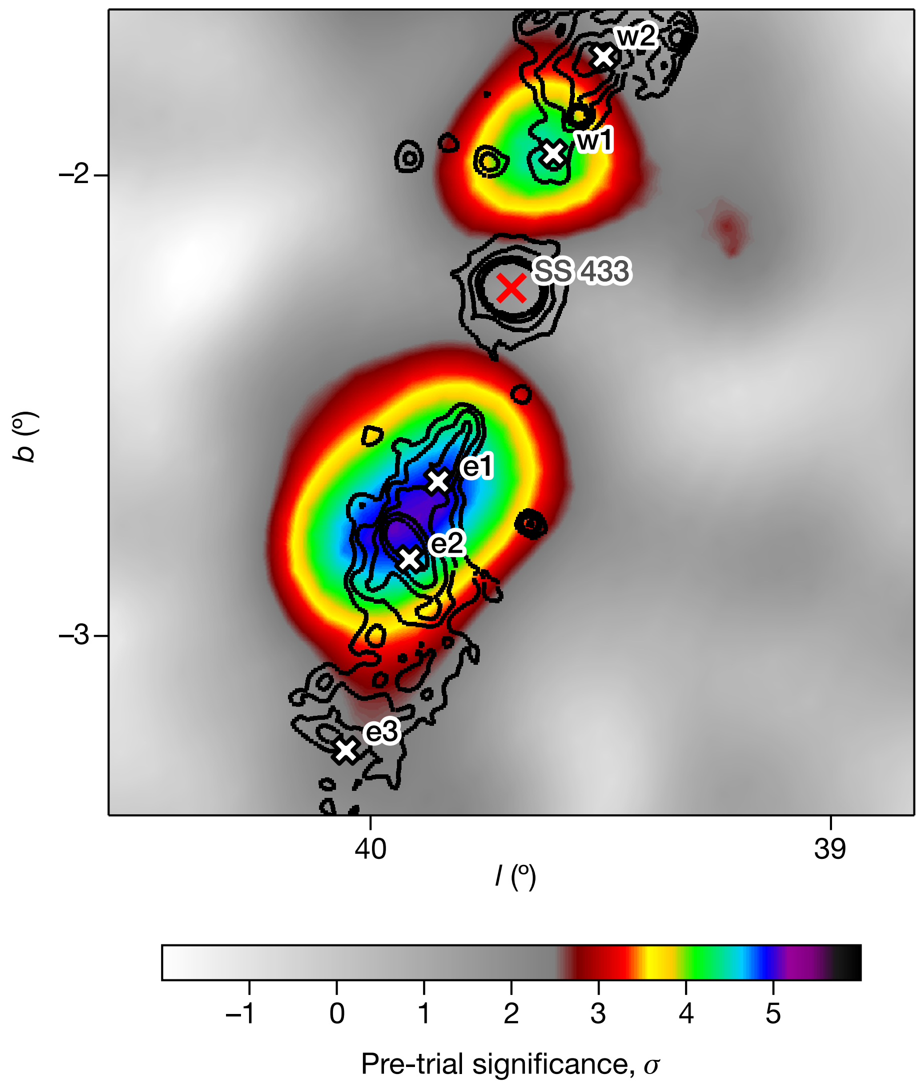

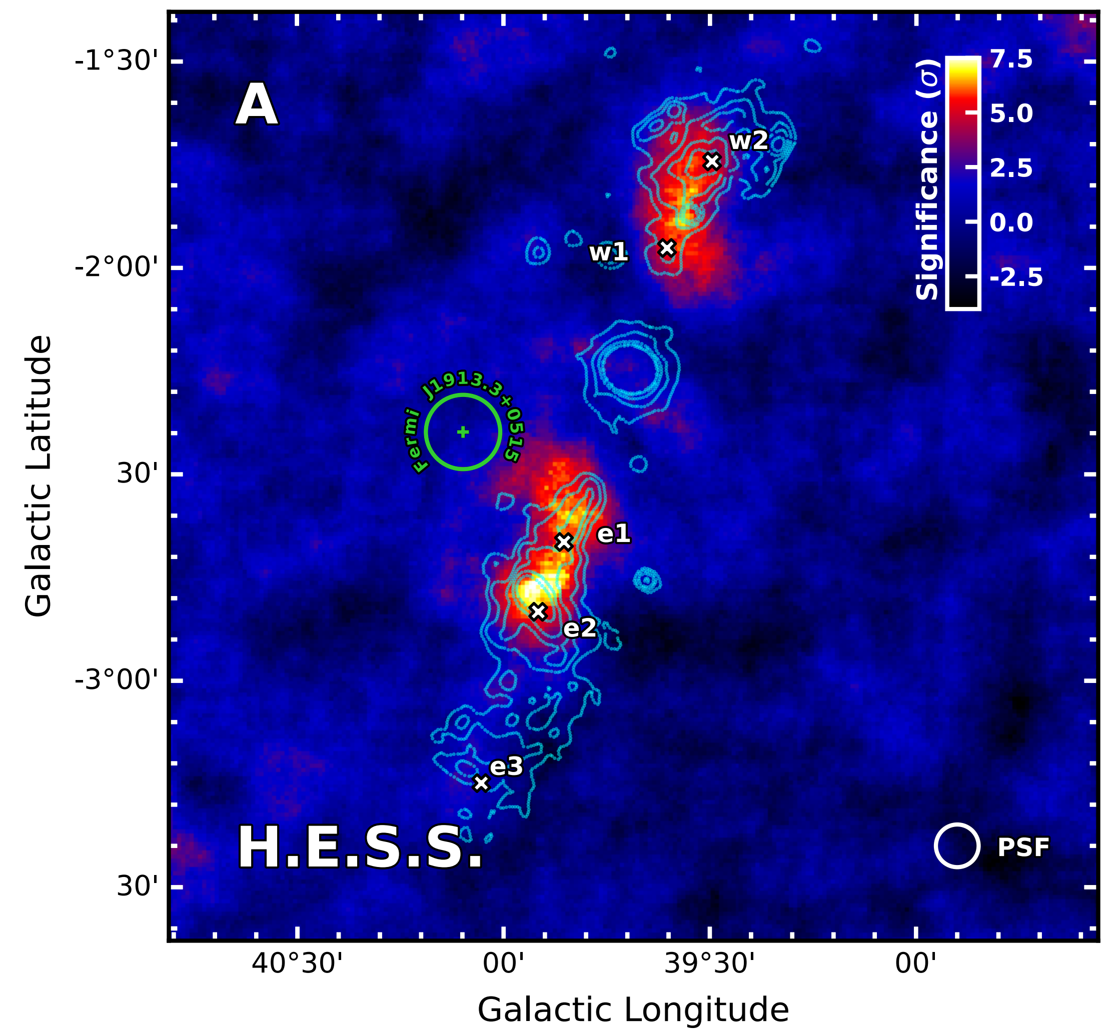

Abeysekara et al. 2018

- ~3 years of HAWC data: e1 + w1: ~ 5.4σ
- E> 20 TeV, SS433: $\Phi < 5.3 \times 10^{-17}$ TeV^{-1} cm^{-2} s^{-1}

H.E.S.S. coll. 2024

- 200h of observations with H.E.S.S.
- E-dependent morphology
- leptonic models favored

SS433

Abeysekara et al. (2018)

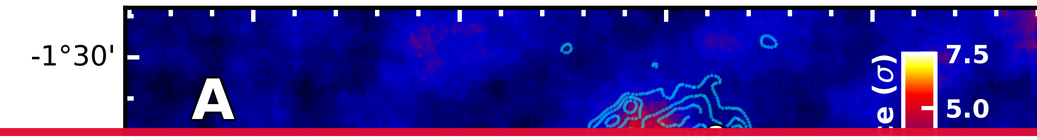

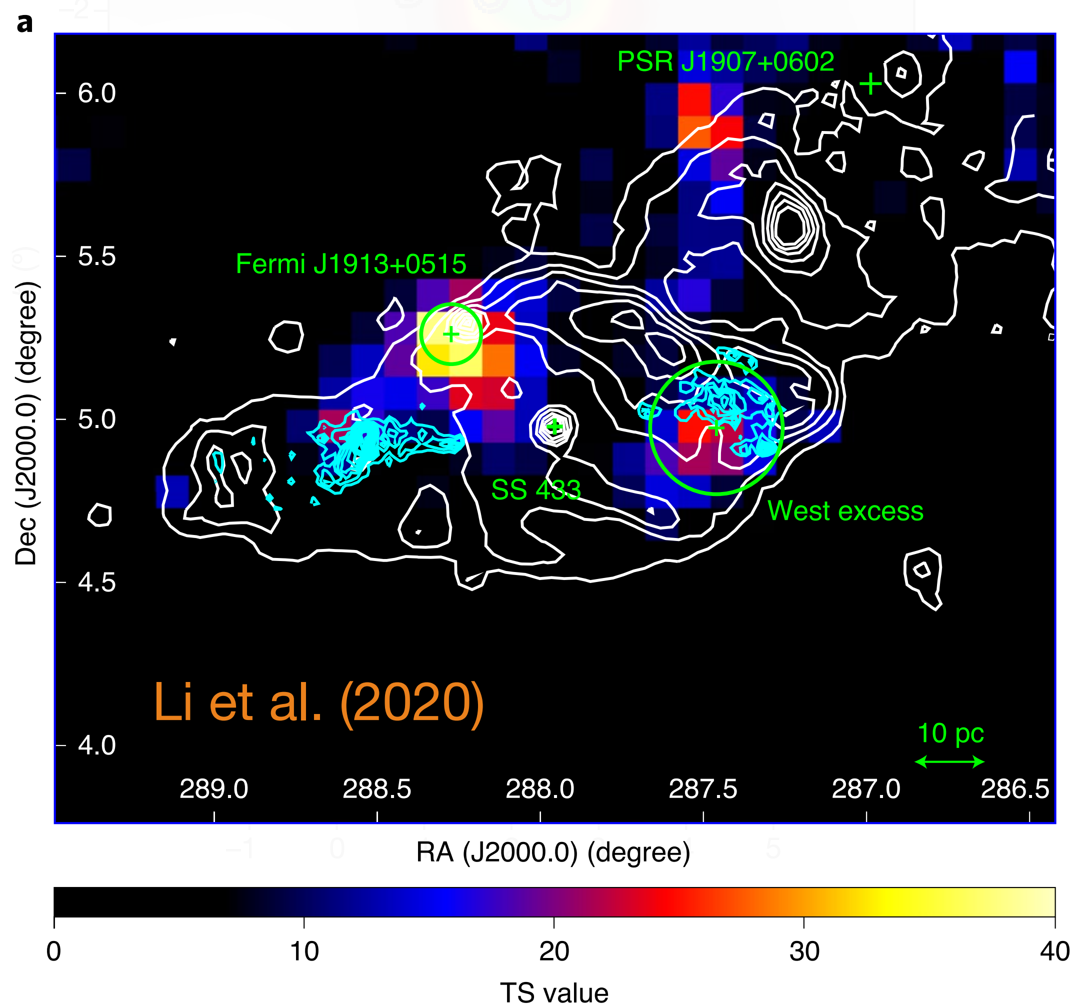

Li et al. 2020

- ~ 10.5 years of LAT data
- **Fermi J1913+0515**: TS = 39 (6.5σ)
- west int. region: TS = 15 (3.5σ)

- ~3 years of HAWC data: e1 + w1: ~ 5.4σ
- E> 20 TeV, SS433: $\Phi < 5.3 \times 10^{-17}$ TeV^{-1} cm^{-2} s^{-1}

- 200h of observations with H.E.S.S.
- E-dependent morphology
- leptonic models favored

Novae at VHEs

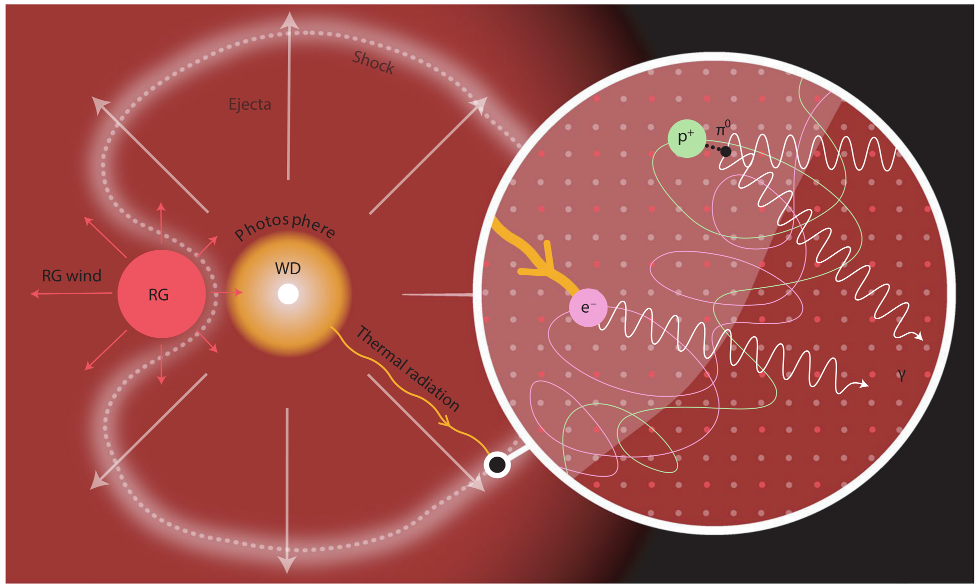

from Acciari et al. (2022)

- Novae are produced by the **thermonuclear fusion** of hydrogen on the surface layers of a WD when accreting the mass from its companion star in a binary system.
- In classical nova the companion star is a MS star, and the WD is “smoothly" fed by the wind from the companion through Roche-lobe overflow.
- Symbiotic recurrent novae are instead composed of a ~massive WD (> 1.1 M_{sun}) and a red giant companion, and the WD accretes from the massive star wind.

Novae at VHEs

RS Ophiuchi

- **Detection (13.2σ) of the recurrent nova RS Ophiuchi** with MAGIC at energies 60-250 GeV.
- MAGIC flux ~cte in the first 4 days, while LAT flux decreases => **migration of the γ-ray emission towards higher E <=> increase of particle's E_{max}**
- The *Fermi*-LAT and MAGIC measurement **can be well described with a proton-only model, with a PL + expCut with Γ ≈ 2, with E_{cutoff} increasing with t**
- Un-cooled accelerated protons will eventually escape, and contribute (dominate) to the galactic CR see in the immediate surroundings (~0.5 pc)

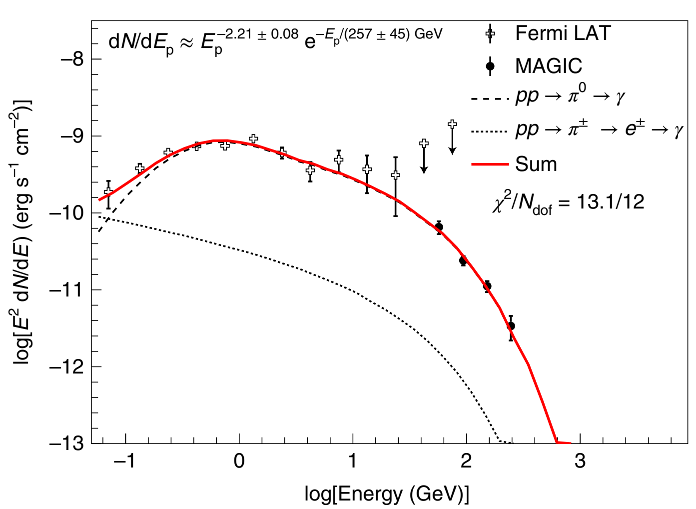

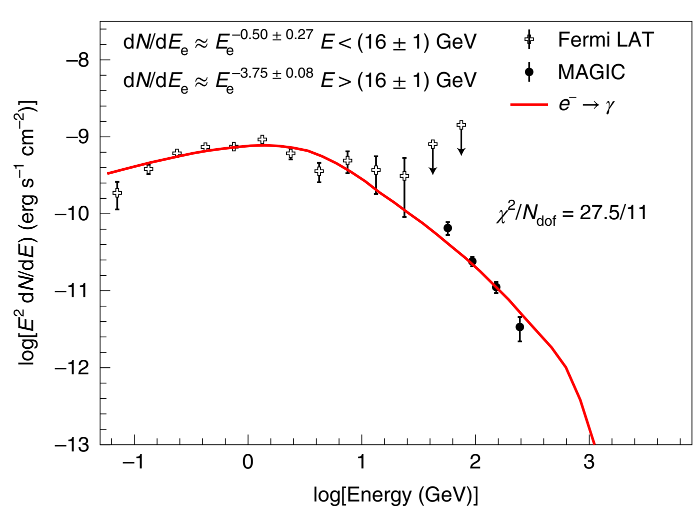

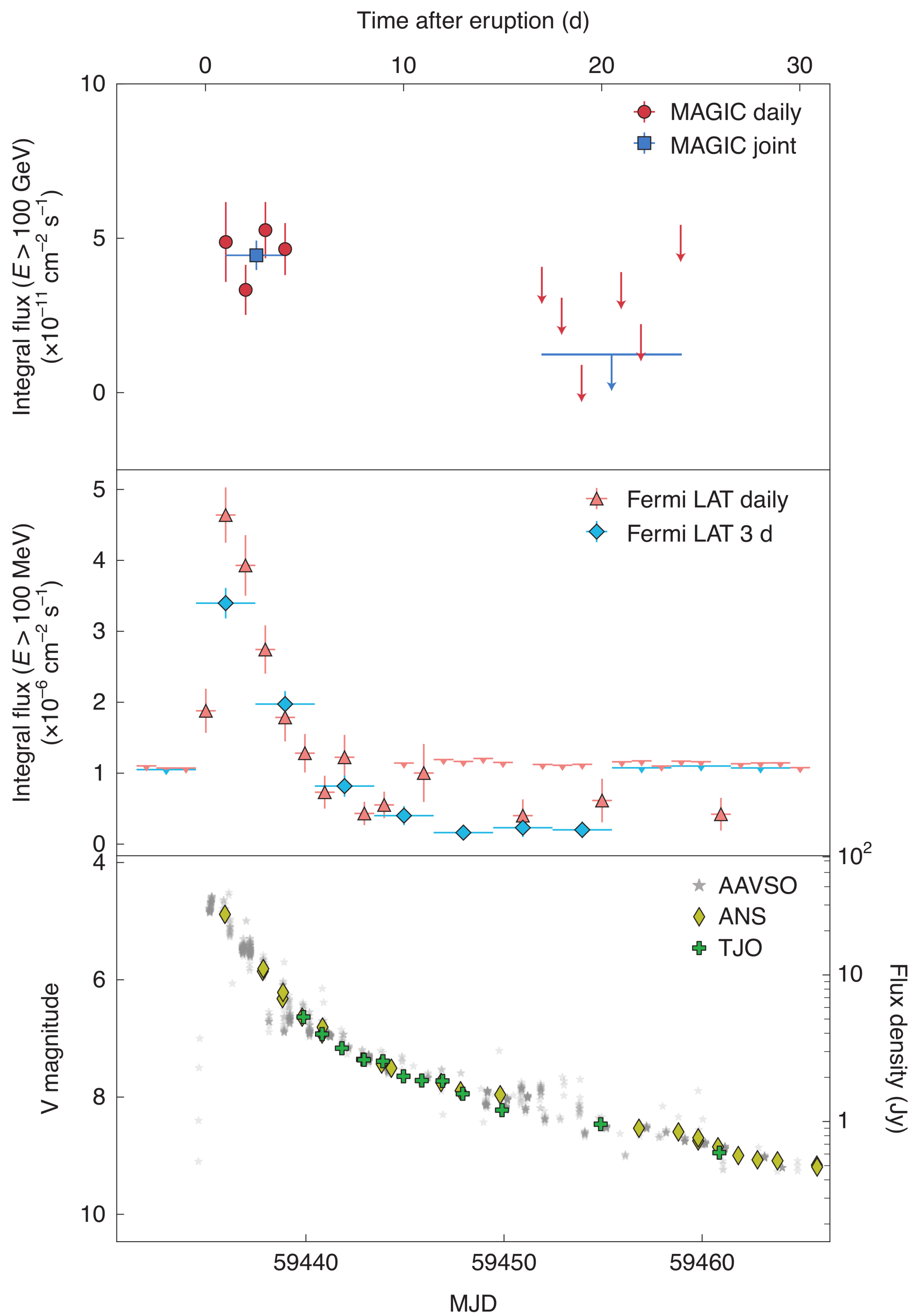

Acciari et al. (2022)

Highlights: detection of Novae at VHEs

RS Ophiuchi

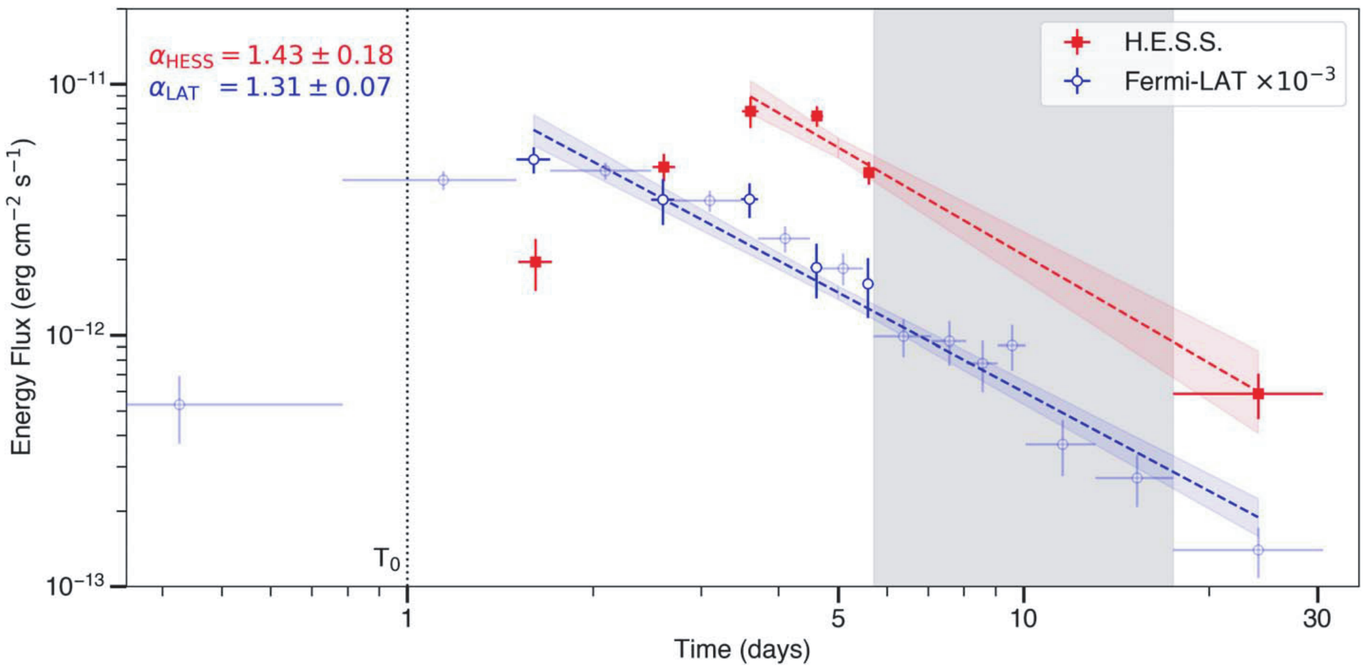

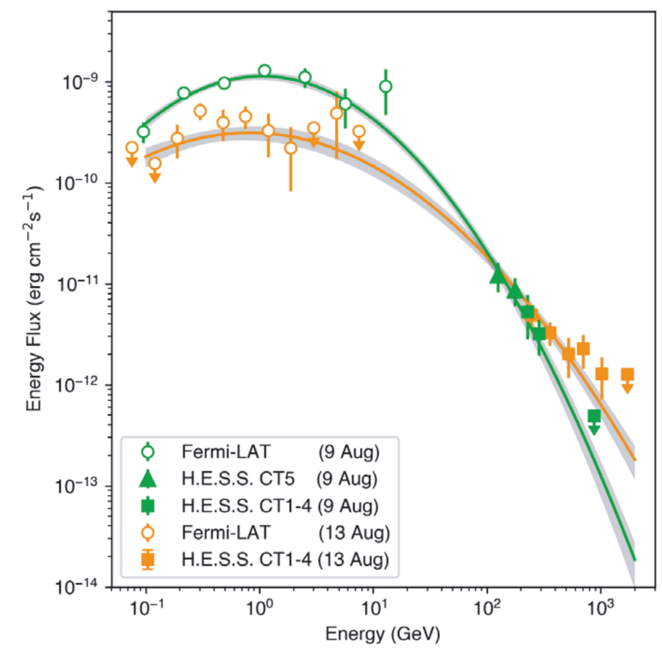

H.E.S.S. Col (2022)

- H.E.S.S. detected RS Oph **up to ~1 month after the 2021 outburst** with a **daily significances ~6σ** for the first 5 nights. **The VHE flux profile closely follows that at HEs** with a shift/delay of ~2 days.
- RS Oph spectrum **consistent with a log-parabola model, with N_0 decreasing and the parabola widening over time,** also similar to the LAT spectrum.
- An hadronic scenario is favoured over a leptonic model, with proton **E_{max} increasing with time** up to ~10 TeV, and a **conversion efficiency > 10%**.
- The **contribution to the local CR density** can be significant within ~1pc^3 volume. If a similar accel. efficiency operates in SNe, **these could sustain the galactic CR flux at PeV energies**.

Summary => CTAO perspectives

- **Surveys of the Galactic Plane** have demonstrated to be extremely useful for the discovery of new sources, as well as for source population studies. In the CTAO era, a number of configurations of the different arrays are being considered to maximize the scientific return of a deep GPS (e.g. diverging pointing)
- The Galactic center is the **richest region of our Galaxy** for the study of a variety of sources and physical phenomena. In the next years, further discoveries may be granted to CTAO, including a final conclusion on the PeVatron nature of Sgr A*
- **SNRs are the best candidates to sustain the Galactic CR population** from energetic grounds. It is still to be solved whether they can also be (some of) the source accelerators up to the knee. CTAO, with a much improved angular resolution and sensitivity should be able to resolve a number of physical mechanisms taking place in SNRs, as well as on its interaction with nearby MCs
- For PSRs, the **recent detection of multi-TeV gamma-rays from the Crab and particularly for the Vela PSR** makes CTAO perspectives bright for the detection of new PSRs at TeV energies.
- CTAO will also be able to resolve the **physics related to PWN** in much greater detail. Tdiscovery of a number of new sources at lower flux levels may reveal/confirm also the presence of a number of new TeV halos surrounding PWNe
- For gamma-ray binaries, several new systems are expected to be discovered from the CTAO galactic scan. Further insights into their variable emission, as well as possible flares, are assured.

BACKUP

Open clusters

Galactic open clusters.

HESS J1646–458 is found to be coincident with the young stellar cluster **Westerlund 1**, but also with the magnetar CXOU J164710.2−455216, the X-ray binary 4U 1642–45 and the pulsar PSR J1648–4611 **(Abramowski et al. 2012)**. **In a single-source scenario, Wd 1 is favoured as site of VHE particle acceleration**. Here, a hadronic parent population would be accelerated within the stellar cluster. Beside this, **there is evidence for a multi-source origin**, where a scenario involving PSR J1648–4611 could be viable to explain parts of the VHE γ-ray emission of HESS J1646–458.

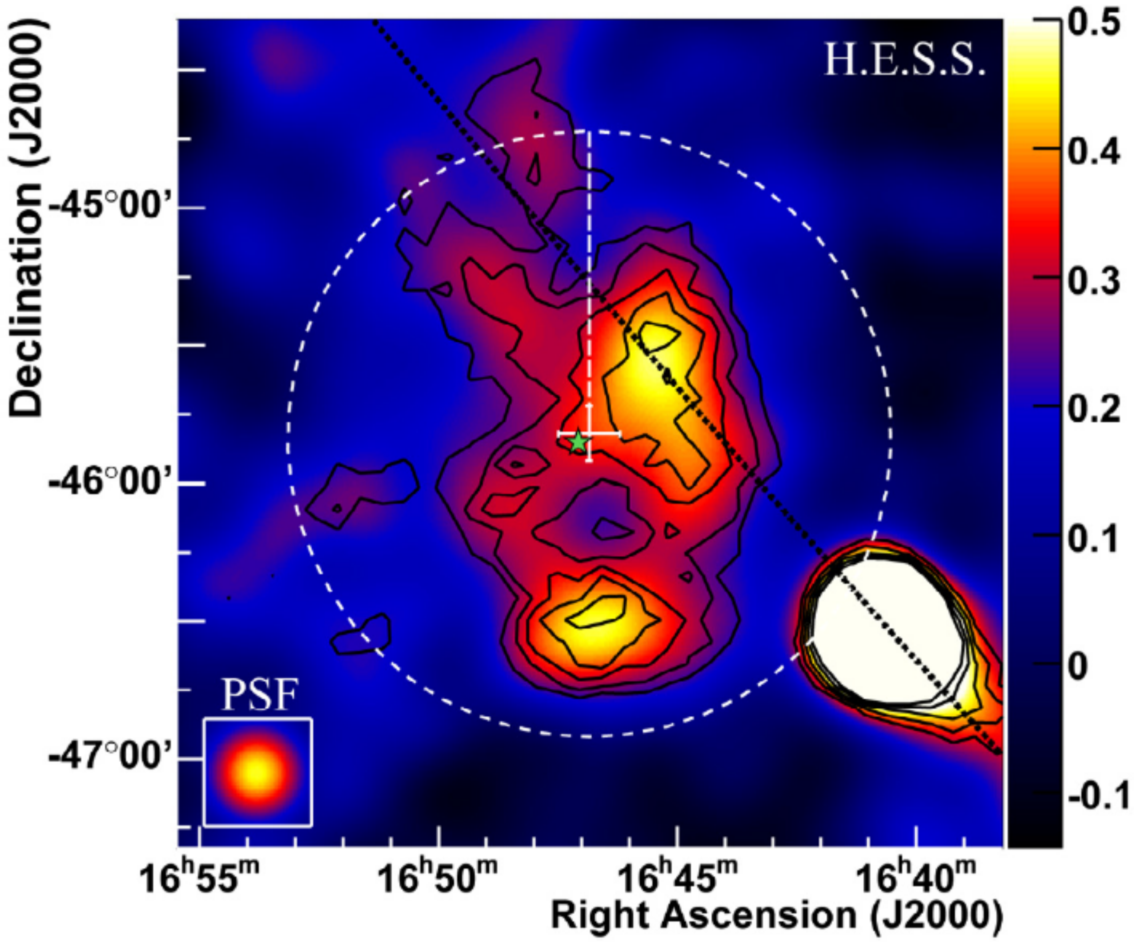

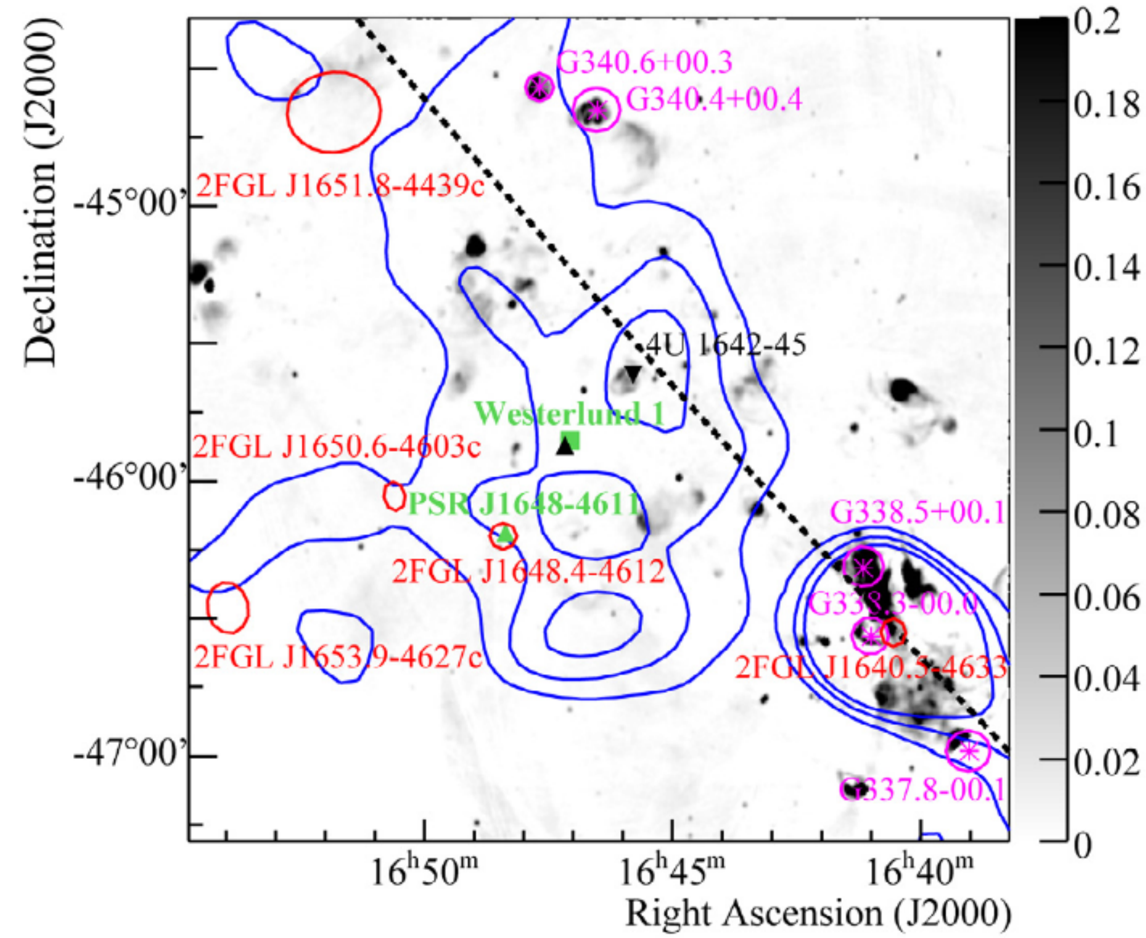

Galactic open clusters.

HESS J1023–575 is found to be coincident with the young stellar cluster **Westerlund 2** in the well-known HII complex RCW49 **(Aharonian et al. 2007)**. **Considered emission scenarios** include emission from the colliding wind zone of WR 20a, collective stellar winds, diffusive shock acceleration in the wind-blown bubble itself, and supersonic winds breaking out into the interstellar medium (ISM).

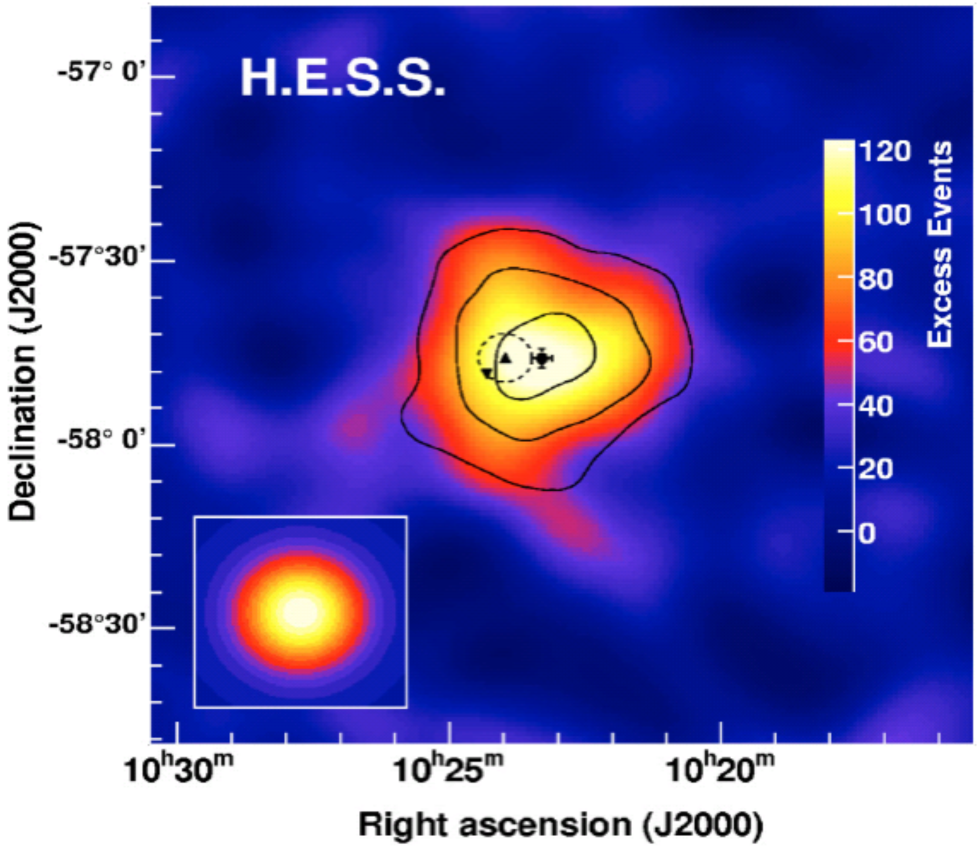

Globular clusters

Globular clusters.

GeV emitting globular clusters as seen by ***Fermi*/LAT (Abdo et al. 2010)**:

➢ 8 globular clusters detected.
➢ 5 of them show **hard spectral power indices** ($0.7 < \Gamma < 1.4$) and clear evidence for an **exponential cut-off** in the range 1.0−2.6 GeV, which is the **characteristic signature of magnetospheric emission from MSPs**.

Name	d (kpc)	L_γ (10^{34} erg s^{-1})	$N_{\rm MSP}$
47 Tucanae	4.0 ± 0.4 (1)	$4.8^{+1.1}_{-1.1}$	33^{+15}_{-15}
Omega Cen	4.8 ± 0.3 (2)	$2.8^{+0.7}_{-0.7}$	19^{+9}_{-9}
M 62	6.6 ± 0.5 (3)	$10.9^{+3.5}_{-2.3}$	76^{+38}_{-34}
NGC 6388	11.6 ± 2.0 (4)	$25.8^{+14.0}_{-10.6}$	180^{+120}_{-100}
Terzan 5	5.5 ± 0.9 (5)	$25.7^{+9.4}_{-8.8}$	180^{+100}_{-90}
NGC 6440	8.5 ± 0.4 (6)	$19.0^{+13.1}_{-5.0}$	130^{+100}_{-60}
M 28	5.1 ± 0.5 (7)	$6.2^{+2.6}_{-1.8}$	43^{+24}_{-21}
NGC 6652	9.0 ± 0.9 (8)	$7.8^{+2.5}_{-2.1}$	54^{+27}_{-25}
NGC 6541	6.9 ± 0.7 (9)	<4.7	<47
NGC 6752	4.4 ± 0.1 (10)	<1.1	<11
M 15	10.3 ± 0.4 (11)	<5.8	<56

➢ 3 of them have no known radio or X-ray MSPs yet still exhibit MSP spectral properties.
➢ From the observed gamma-ray luminosities, **the total number of MSPs** that is expected to be present in these globular clusters **can be estimated**.
➢ **2600−4700 MSPs in Galactic GCs**, commensurate with previous estimates.

See also **Tam et al. (2011)** and **Hui et al. (2011)** for updates, or **de Menezes et al. (2018)** for a more recent update with 23 GCs detected by *Fermi*/LAT.

Globular clusters.

HESS J1747-248, overlapping with Terzan 5, detected at TeV energies by HESS (Abramowski et al. 2011).

Terzan 5 has the **largest population of identified millisecond pulsars**, a very high core stellar density and the **brightest GeV range flux** as measured by *Fermi*/ LAT.

Name	d (kpc)	L_γ (10^{34} erg s^{-1})	N_{MSP}
47 Tucanae	4.0 ± 0.4 [(1)]	$4.8^{+1.1}_{-1.1}$	33^{+15}_{-15}
Omega Cen	4.8 ± 0.3 [(2)]	$2.8^{+0.7}_{-0.7}$	19^{+9}_{-9}
M 62	6.6 ± 0.5 [(3)]	$10.9^{+3.5}_{-2.3}$	76^{+38}_{-34}
NGC 6388	11.6 ± 2.0 [(4)]	$25.8^{+14.0}_{-10.6}$	180^{+120}_{-100}
Terzan 5	5.5 ± 0.9 [(5)]	$25.7^{+9.4}_{-8.8}$	180^{+100}_{-90}
NGC 6440	8.5 ± 0.4 [(6)]	$19.0^{+13.1}_{-5.0}$	130^{+100}_{-60}
M 28	5.1 ± 0.5 [(7)]	$6.2^{+2.6}_{-1.8}$	43^{+24}_{-21}
NGC 6652	9.0 ± 0.9 [(8)]	$7.8^{+2.5}_{-2.1}$	54^{+27}_{-25}
NGC 6541	6.9 ± 0.7 [(9)]	<4.7	<47
NGC 6752	4.4 ± 0.1 [(10)]	<1.1	<11
M 15	10.3 ± 0.4 [(11)]	<5.8	<56

The **nature** of HESS J1747-248 is **uncertain**, since no counterpart or model can fully explain the observed morphology. An **association with Terzan 5 is tantalizing**, but the available data do not firmly prove this scenario.

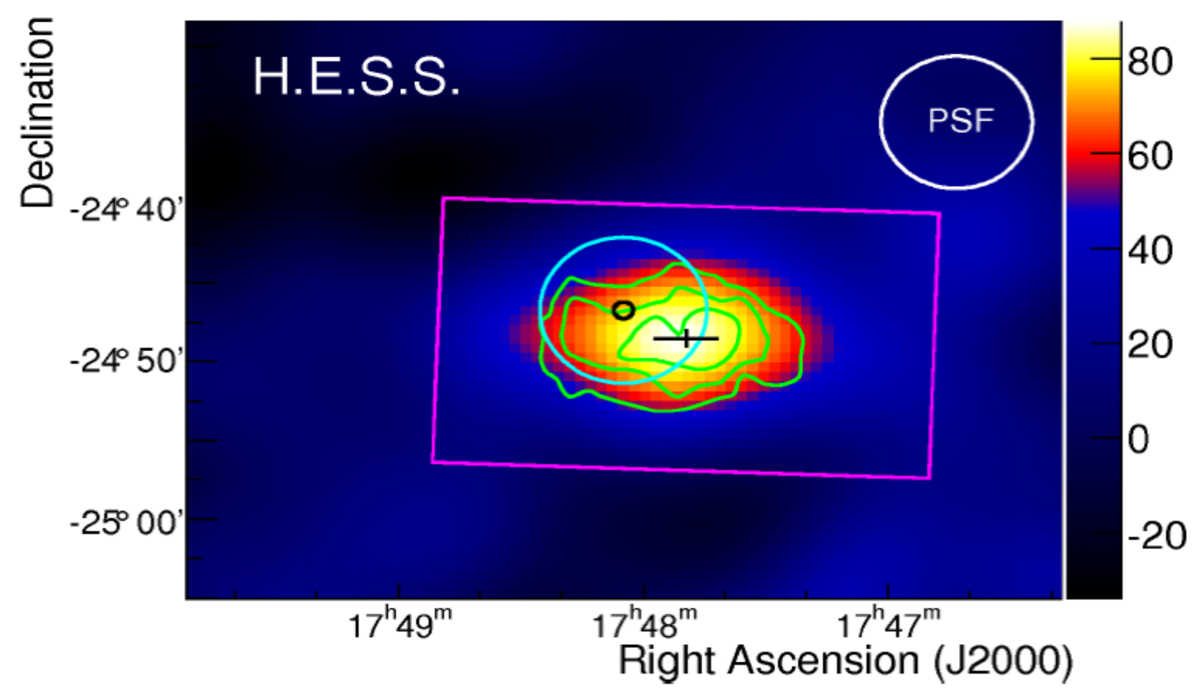

See also **Abramowski et al. (2013)**.

Colliding wind binaries

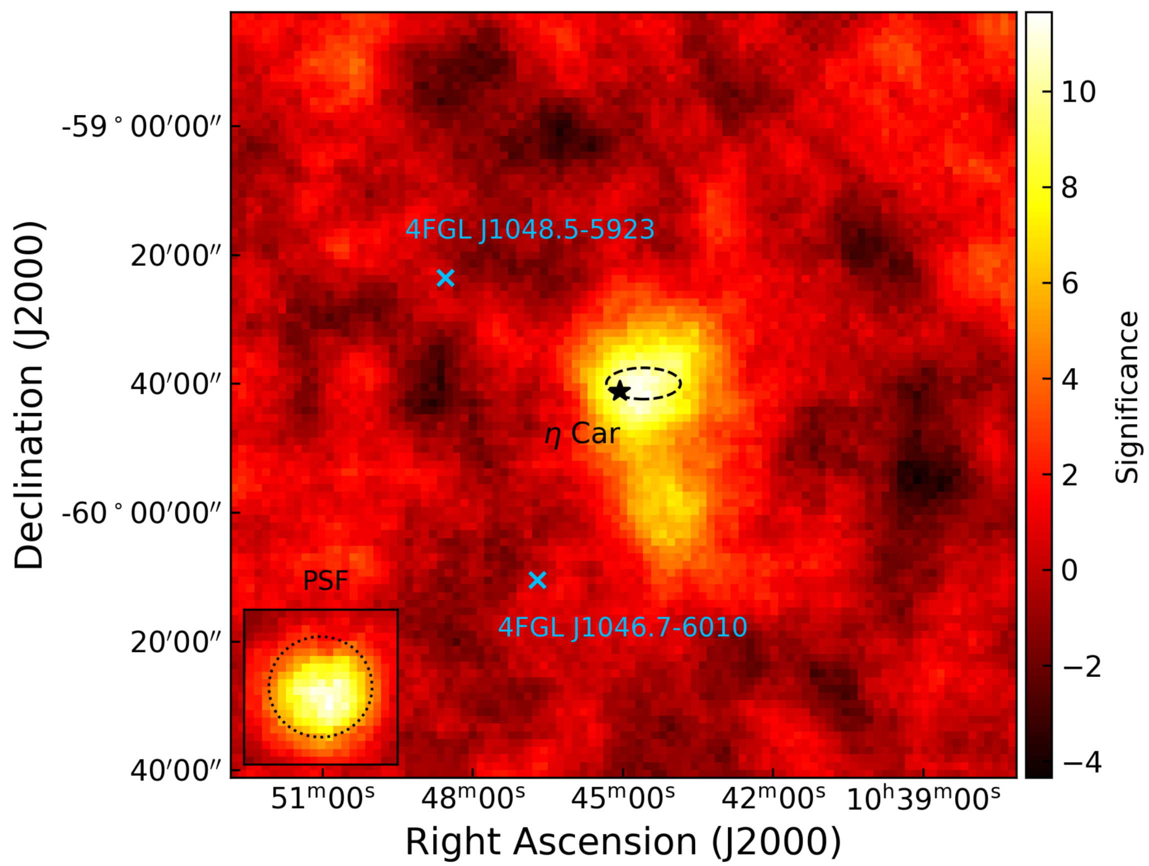

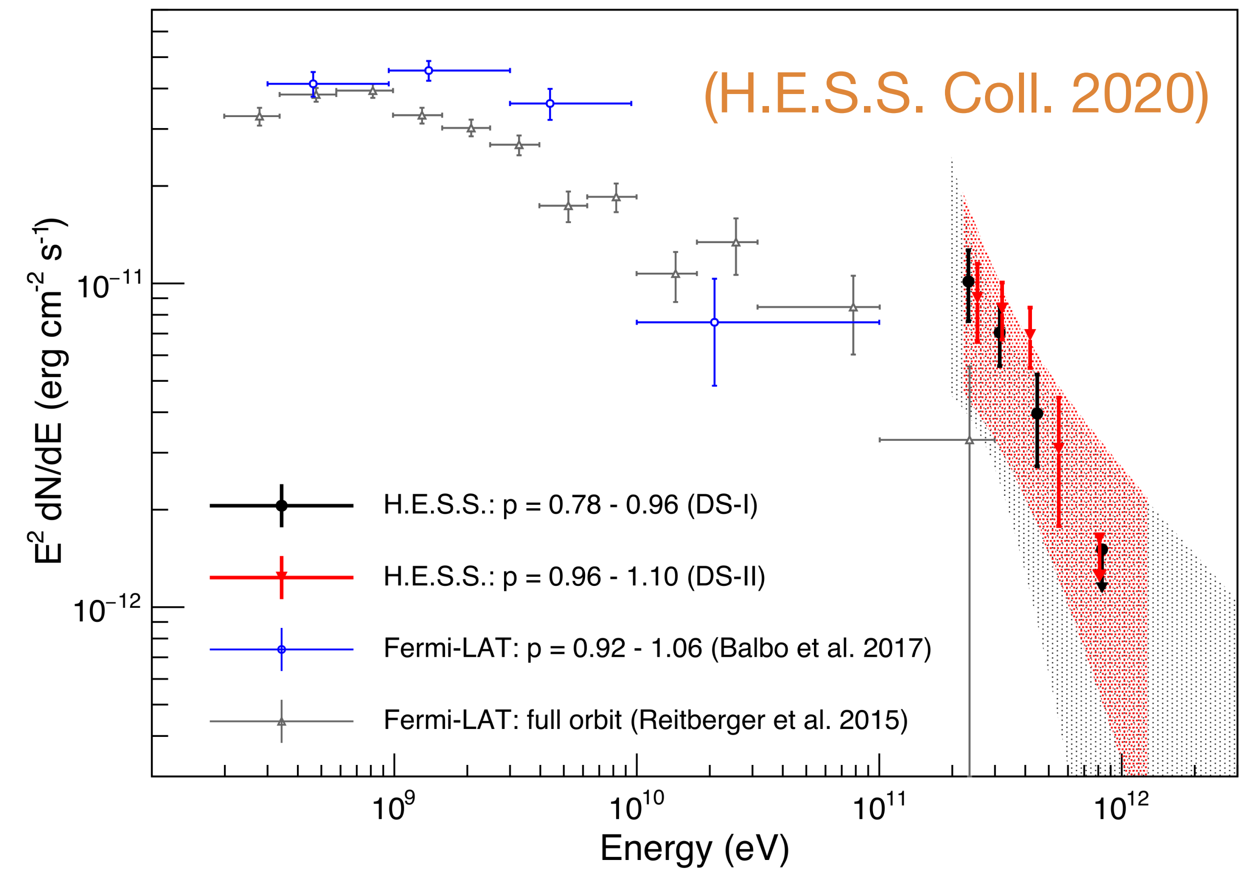

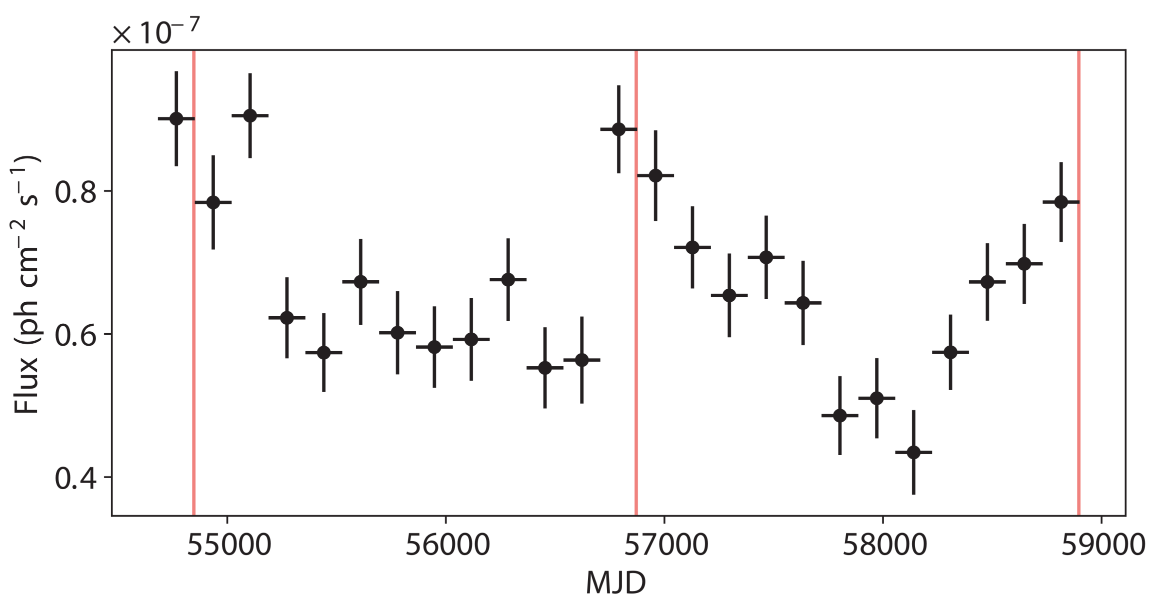

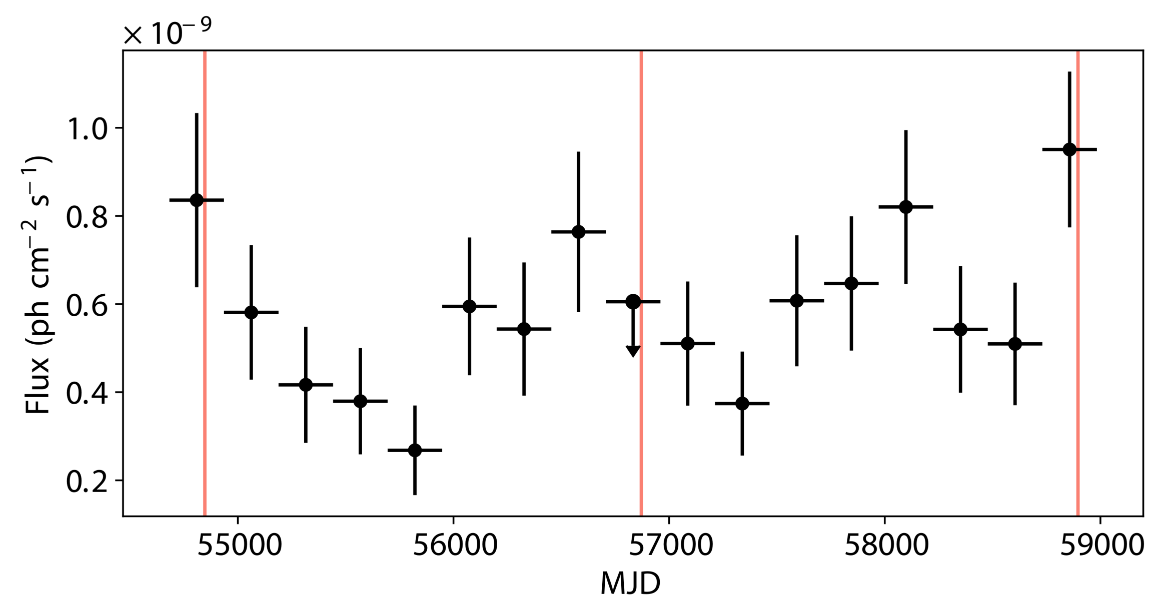

(Martí-Devesa et al. 2021)

Radio galaxies.

- FR I radio galaxy **M87** shows fast variability compatible with emitting region with size of the **Schwarschild radius** of the central black hole **(Acciari et al. 2009)**
- FR I radio galaxy **Centaurus A** detected (120 h) **(Aharonian et al. 2009)**.
- **TeV gamma rays are emitted by extragalactic sources other than blazars**, where jets are not relativistically beamed toward the observer.

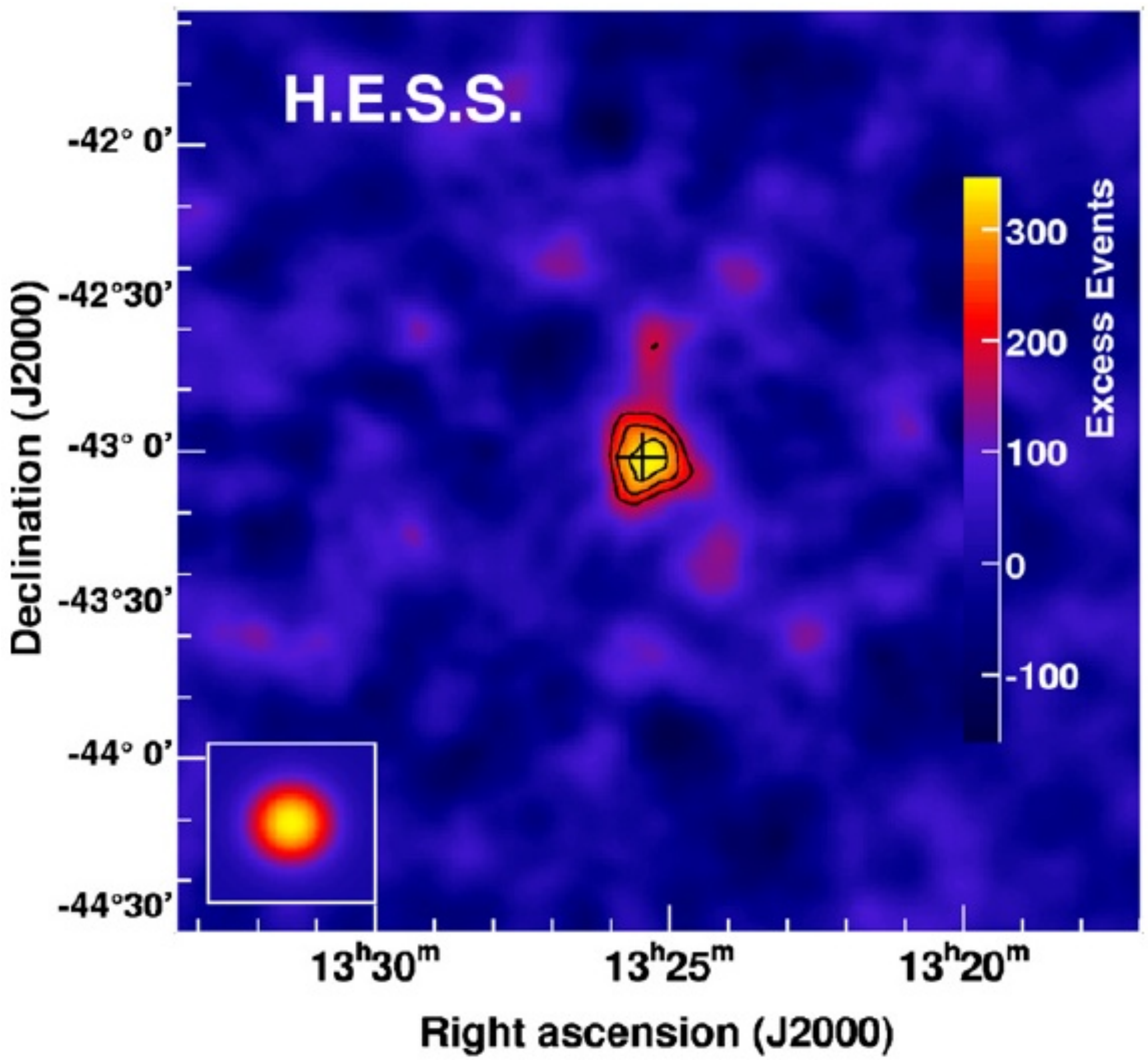

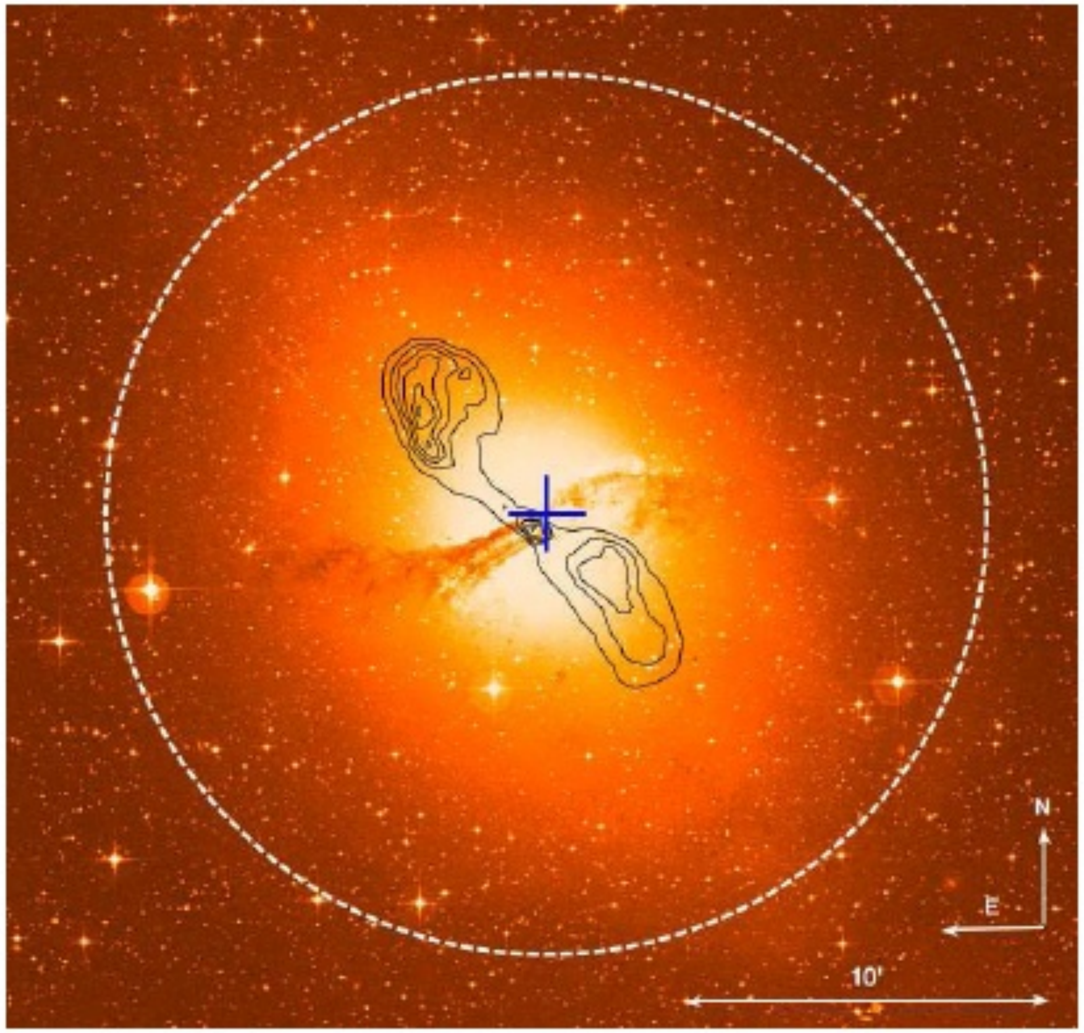

Starburst galaxies.

- **NGC 253** detected for the first time! **M82** soon afterwards!
- Starburst galaxies: **high-mass star-formation**, increased rate of **SNe**.
- They produce a lot of **cosmic rays** that interact with interstellar gas and radiation, producing diffuse TeV gamma-ray emission (neutral pion decay).
- In M82: cosmic-ray density about 500 times the average Galactic density.
- Cosmic-ray **acceleration tied** to **star formation** (SNe and stellar winds).

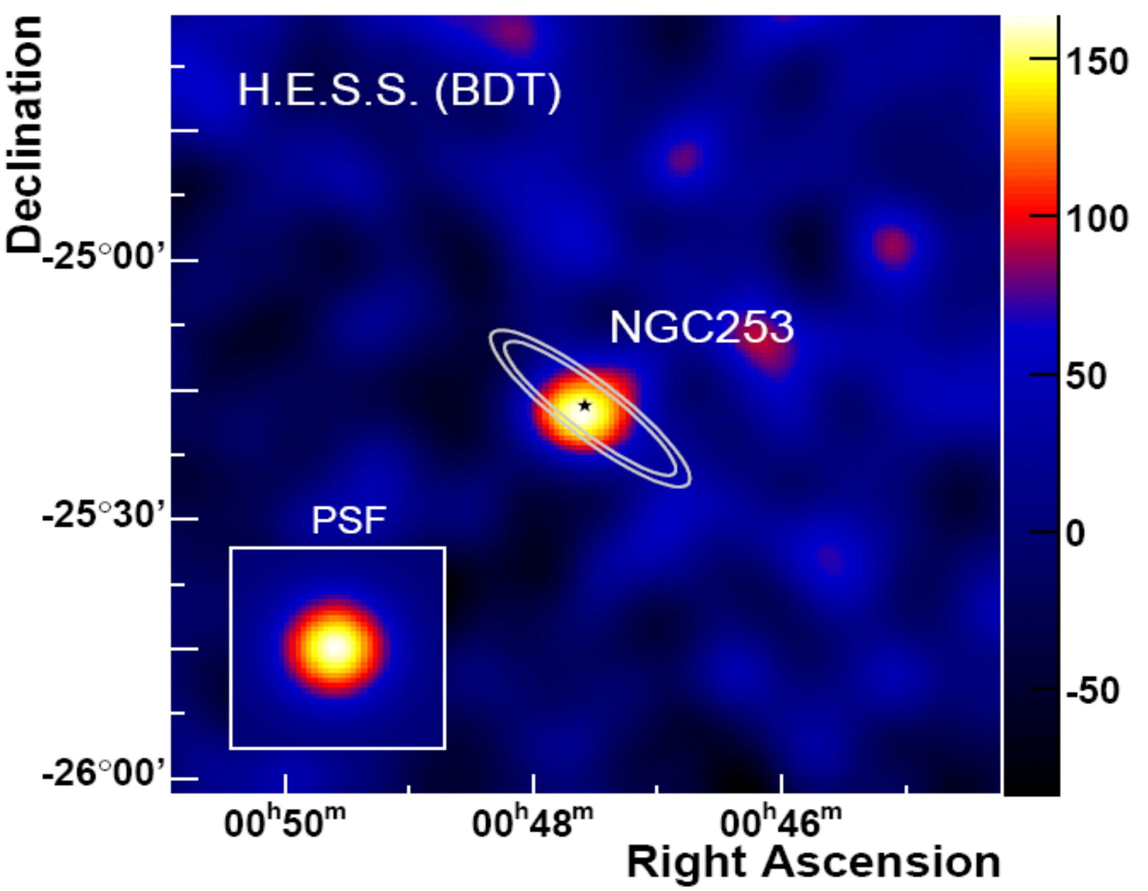

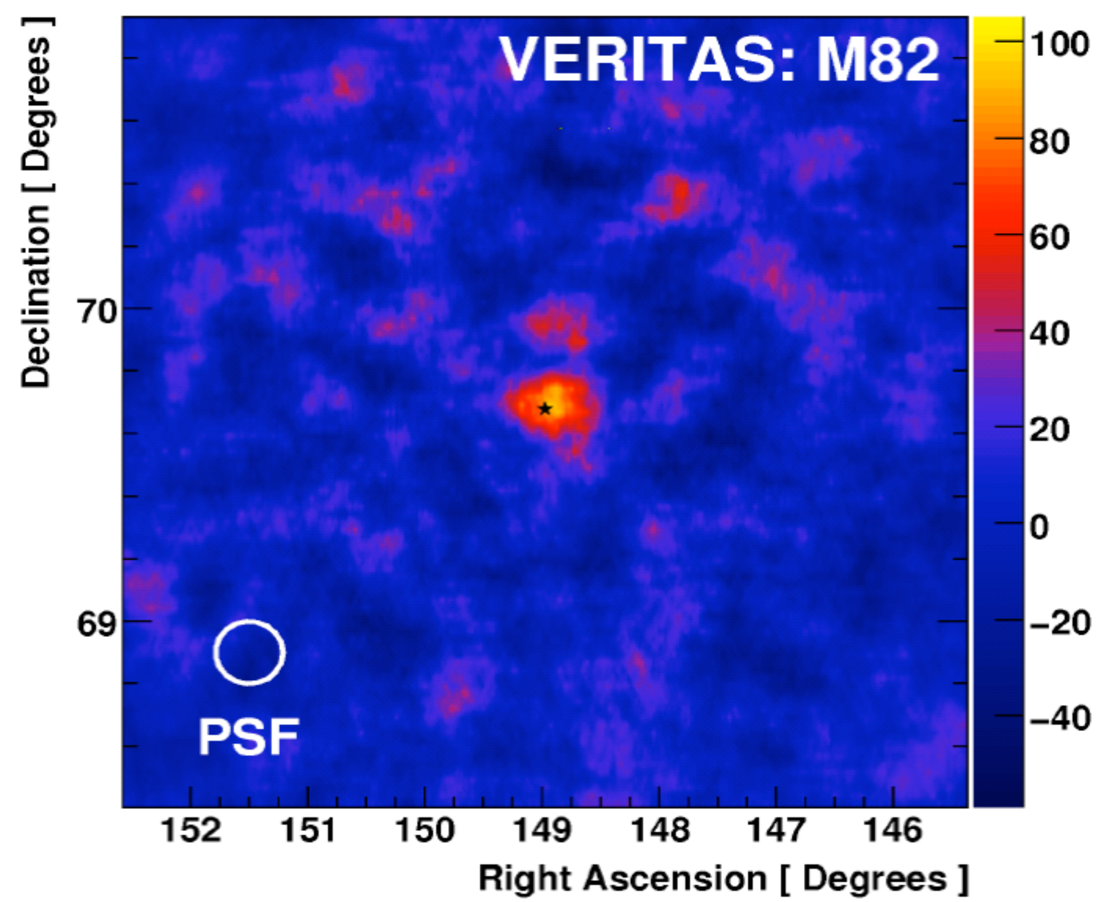

Starburst galaxies. **And also M82 (Acciari et al. 2009)**. The cosmic rays produced in the formation, life, and death of their massive stars are expected to eventually produce diffuse gamma-ray emission via their interactions with interstellar gas and radiation. The detection of >700 GeV gamma rays from M82 implies a cosmic-ray density of 250 eV cm^{-3} in the starburst core of M82, or about 500 times the average Galactic density. This result strongly supports that **cosmic-ray acceleration is tied to star formation activity, and that supernovae and massive star winds are the dominant accelerators**.

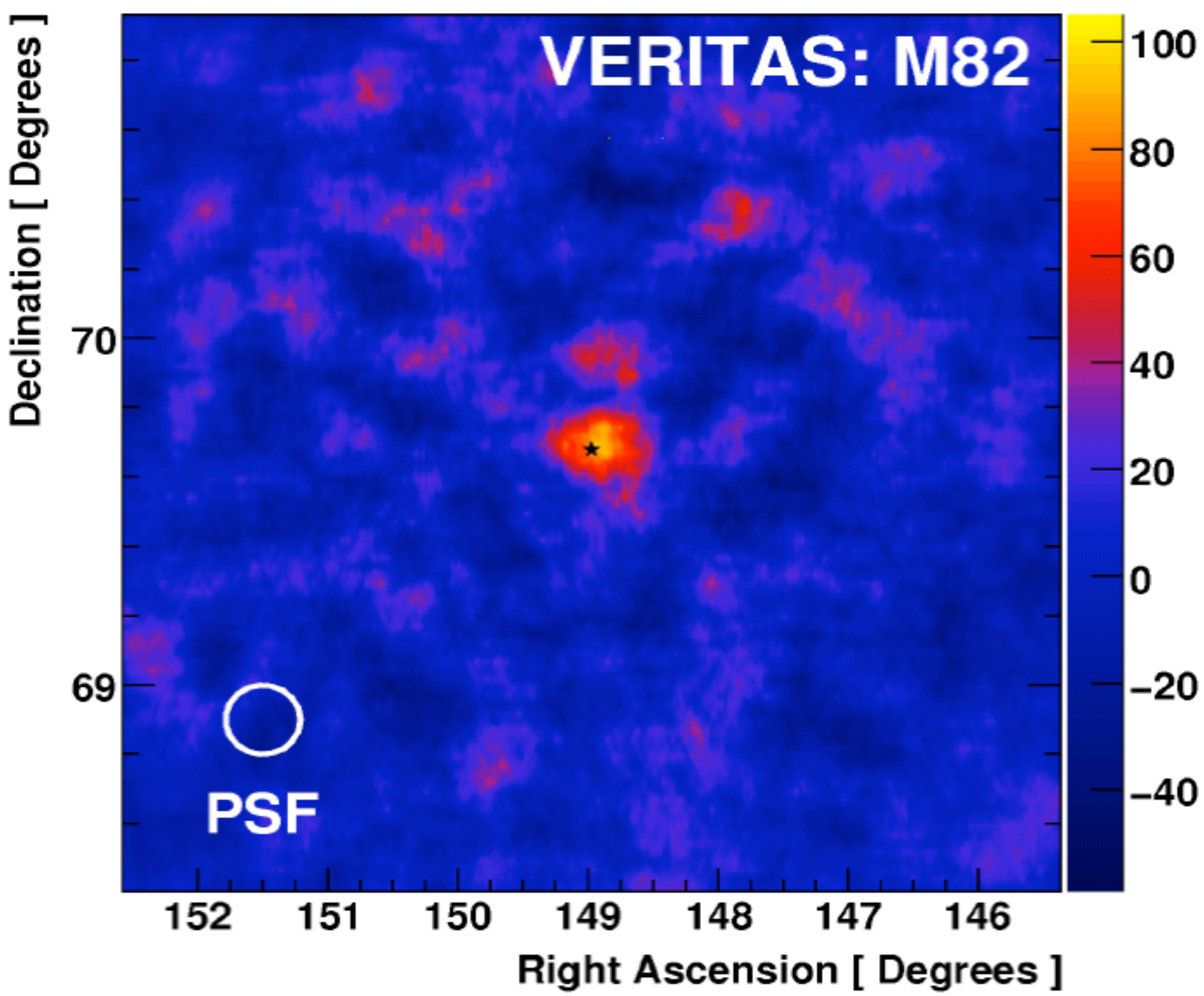

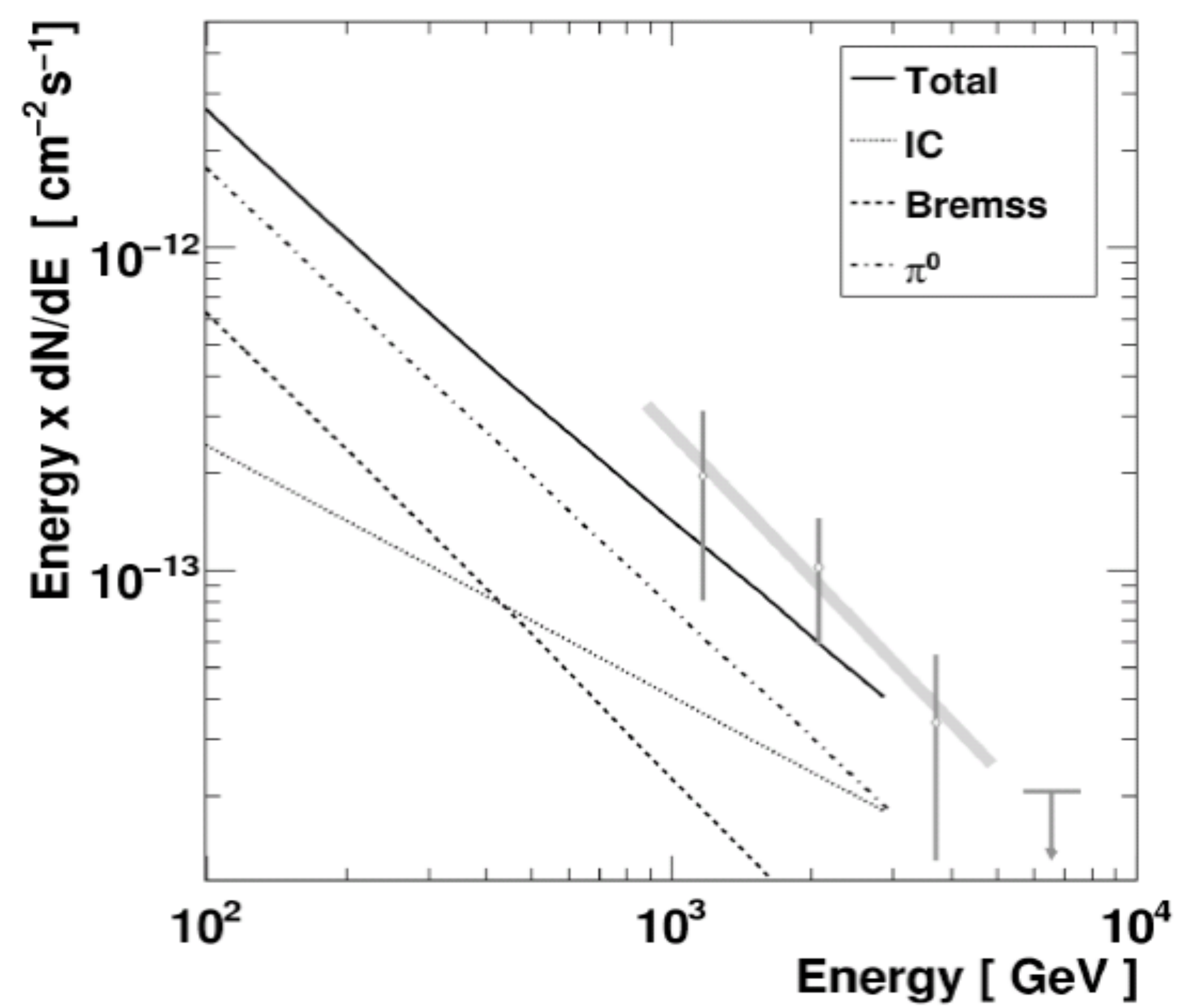

Clusters of galaxies.

- Expected to be **reservoirs of cosmic rays** (CRs).
- Should produce diffuse gamma-ray emission due to hadronic interactions with intra-cluster medium.
- Deep **250 h MAGIC** observations of the **Perseus cluster**.
- The central galaxy NGC 1275 is clearly detected at low energies, and the nearby head tail radiogalaxy IC 310 at all energies.
- **No diffuse gamma-ray emission is detected**.
- This constrains the average CR-to-thermal pressure ratio to be <1–2%. If CRs propagate out of the cluster core, this ratio is constrained to be <20% **(Ahnen et al. 2016)**.

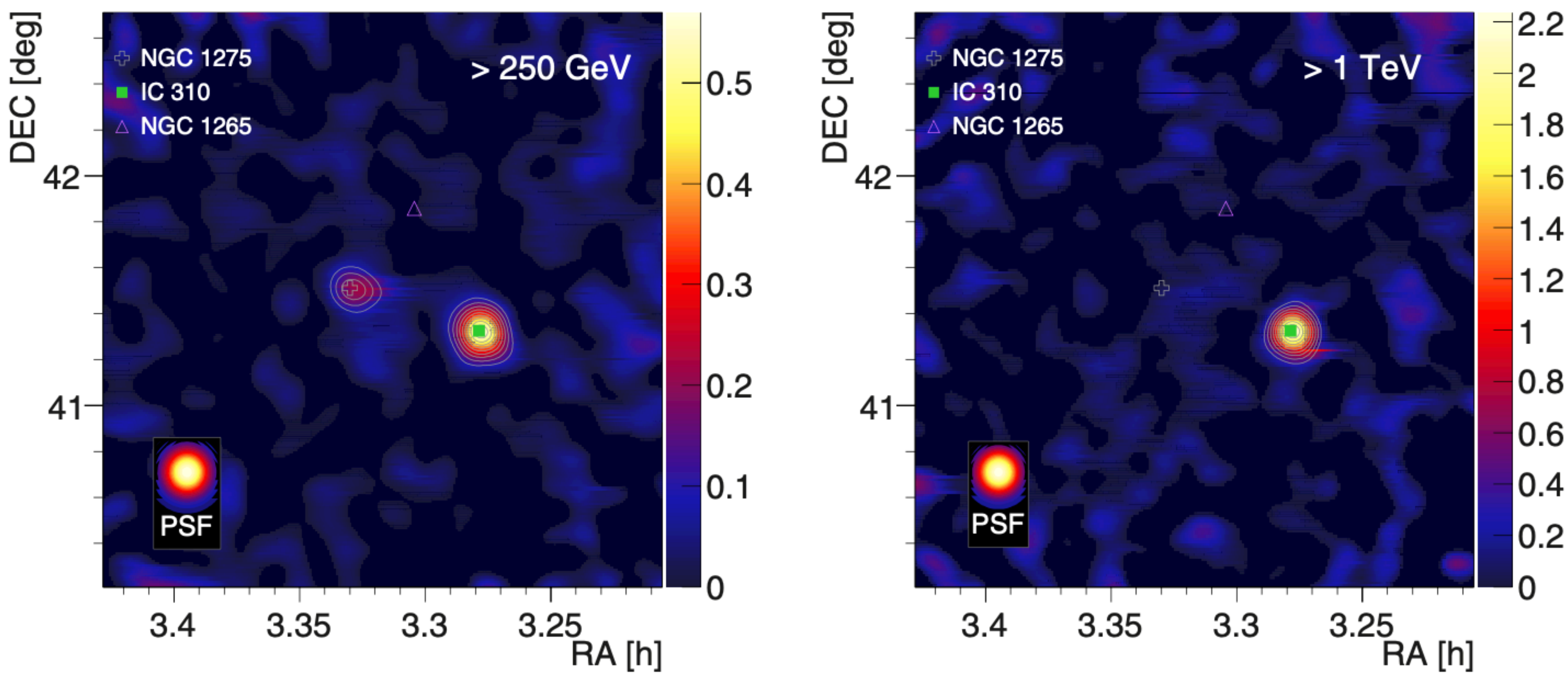

SNR cat

SNR_Name	Type	Other_Names	TeVCat	l	b	Distance	Age	MC_Mass	Flux100GeV	Flux1TeV
				°	°	kpc	yr	M_{sun}	$\mathrm{erg\,s^{-1}\,cm^{-2}}$	$\mathrm{erg\,s^{-1}\,cm^{-2}}$
G359.1-0.5	INT	HESSJ1745-303	TeV J1745-303	358.7	-0.65	7.6	10000.0	50000.0	4.177e-12	8.425e-13
HESSJ1731-347	SHELL	HESSJ1731-347	TeV J1732-347	353.54	-0.68	3.2	14500.0	0.0	1.6595e-11	6.615e-12
CTB37B	SHELL	HESSJ1713-381 G348.7+0.3	TeV J1713-382	348.63	0.38	13.2	5000.0	0.0	1.55e-13	4.436e-14
CTB37A	INT	G348.5+0.1	TeV J1714-385	348.38	0.1	9.0	16000.0	67000.0	3.886e-12	8.347e-13
RXJ1713.7-3946	SHELL	G347.3-0.5	TeV J1713-397	347.33	-0.48	1.0	1600.0	0.0	5.84869e-10	3.1538e-10
SN1006(NE)	SHELL		TeV J1504-418	327.84	14.56	1.6	1010.0	0.0	3.3779e-11	2.2221e-11
SN1006(SW)	SHELL		TeV J1504-421	327.86	15.35	1.6	1010.0	0.0	2.0084e-11	9.8858e-12
G318.2+0.1	INT	HESSJ1457-593	TeV J1457-594	318.36	-0.44	9.2	8000.0	0.0	4.87e-13	8.7534e-14
RCW86	SHELL	G315.4-2.3 MSH14-63	TeV J1442-624	315.41	-2.31	2.5	1800.0	0.0	1.3462e-11	5.9342e-12
G298.6-0.0				298.6	0.0	5.0	1000.0	0.0	5.2442e-11	5.1438e-11
Vela Junior	SHELL	RXJ0852.0-4622	TeV J0852-463	266.28	-1.25	1.0	3000.0	0.0	0.0	3.1786e-10
Puppis A				260.4	-3.4	2.2	4450.0	0.0	5.305e-12	7.9818e-13
IC443	INT		TeV J0616+225	189.1	3.0	1.5	10000.0	10000.0	1.1617e-11	8.5012e-13
Tycho	SHELL		TeV J0025+641	120.1	1.4	4.5	400.0	0.0	0.0	9.4669e-14
Cas A	SHELL		TeV J2323+588	111.7	-2.1	3.4	330.0	0.0	3.726e-12	8.1634e-13
Gamma Cygni				78.2	2.1	1.5	6600.0	0.0	2.3169e-11	7.9406e-12
Cygnus Loop				74.0	-8.5	0.8	15000.0	0.0	1.8e-13	2.7842e-16
W51C	INT	G49.2-0.7 HESSJ1923+141	TeV J1923+141	49.2	-0.7	5.6	30000.0	190000.0	1.1725e-11	1.9496e-12
W49B	INT	G43.3-0.2 HESSJ1911+090	TeV J1911+090	43.3	-0.2	8.0	2000.0	1000000.0	5.477e-12	3.8876e-13
W44	INT	G34.7-0.4	none	34.7	-0.4	3.0	20000.0	500000.0	1.003e-12	2.8471e-14
W41	INT	G23.3-0.3 HESSJ1834-087	TeV J1834-087	23.24	-0.33	4.8	100000.0	88000.0	6.118e-12	1.5368e-12
W28north	INT	HESSJ1801-233 3EGJ1800-2338	TeV J1801-233	6.65	-0.27	1.9	35000.0	50000.0	9.776e-12	1.4924e-12
W28A	INT	HESSJ1800-240A	TeV J1800-240A	5.88	-0.39	1.9	35000.0	40000.0	6.153e-12	2.6322e-12
W28B	INT	HESSJ1800-240B	TeV J1800-240B	5.88	-0.39	1.9	35000.0	60000.0	7.626e-12	2.8944e-12
W28C	INT	HESSJ1800-240C	TeV J1800-240C	5.88	-0.39	1.9	35000.0	20000.0	4.376e-12	2.0365e-12
G349.7+0.2	INT			349.7	0.2	11.5	1800.0	5000.0	2.8e-14	4.4379e-15
HESSJ1912+101			TeV J1912+101	44.39	-0.07	4.1	100000.0	12000.0	2.6006e-11	1.0625e-11
HESSJ1534-571			TeV J1534-571	323.65	-0.92	3.5	10000.0	1000.0	2.0676e-11	8.4906e-12
MSH1739	INT			357.7	-0.1	11.8	-1.0	35000.0	6.1e-14	4.57884e-16
HB21	INT			89.0	4.7	1.7	15874.0	55000.0	6e-15	1.3092e-17
HESSJ1614-518	SHELL		TeV J1614-518	331.52	-0.58	1.5	30000.0	0.0	6.4802e-11	2.7512e-11
W30	INT			8.7	-0.1	4.6	20493.0	190000.0	4.4596e-11	1.1907e-11
3C 391		Kes 77		31.9	0.0	7.1	9000.0	0.0	1.8e-14	1.4426e-16
CTB109				109.1	1.0	3.2	14000.0	0.0	2.191e-12	8.8208e-13
G337.0-0.1		CTB 33		337.0	-0.1	11.0	5000.0	0.0	7e-15	2.67153e-17
S147				180.0	-1.7	1.39	30000.0	0.0	1.22117e-10	1.0661e-10
Kes17				304.6	0.1	9.7	14000.0	0.0	0.0	1.8863e-14

Catalog of γ-SNRs

SNRs @ VHE gamma-rays

Faint SNRs.

SN 1006 detected after 130 hours of observations **(Acero et al. 2010)**. The **HESS spots are coincident with the non-thermal X-ray filaments** seen by *Chandra* and *XMM-Newton* in the NE and SW part of the SNR shell, produced by synchrotron radiation of **electrons accelerated to ~100 TeV**. Because the VHE emission appears to form in a thin rim, particle acceleration in shock waves is likely to be the origin of the gamma-ray signal. **Leptonic and mixed scenarios are compatible with TeV emission** provided *B*>30 microGauss.

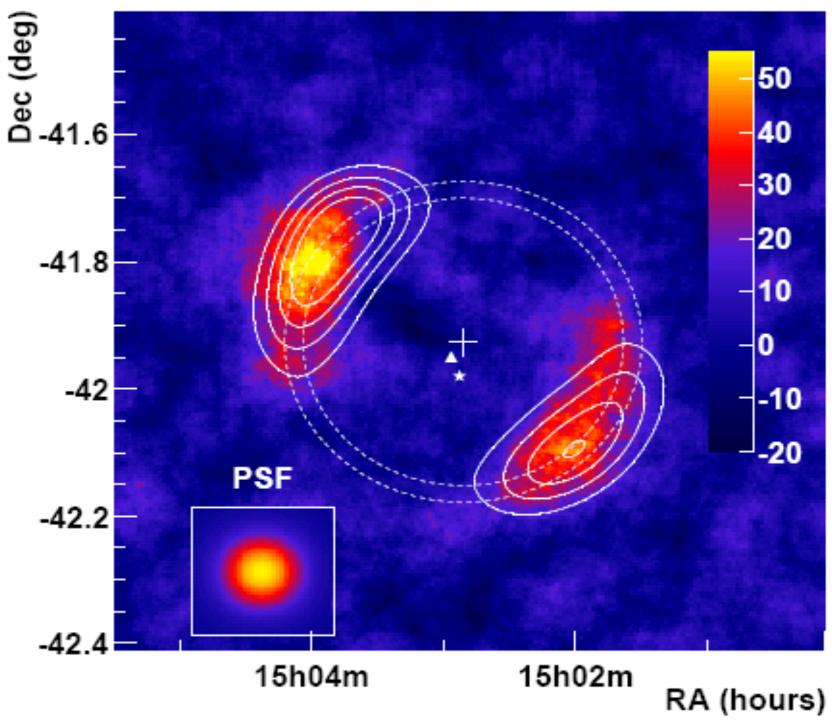

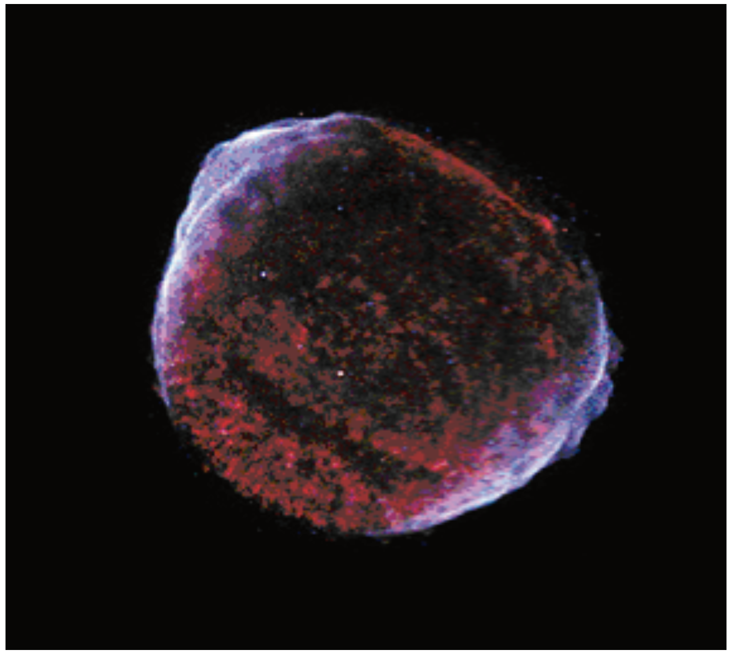

SNRs @ VHE gamma-rays

Faint SNRs.

Tycho SNR detected by VERITAS, after 68 hours. Integral flux above 1 TeV of just 0.9% of the Crab Nebula flux. Both **leptonic and mixed scenarios can explain the TeV emission** provided *B*>80 microGauss. Possible evidence for magnetic field amplification **(Acciari et al. 2011)**.

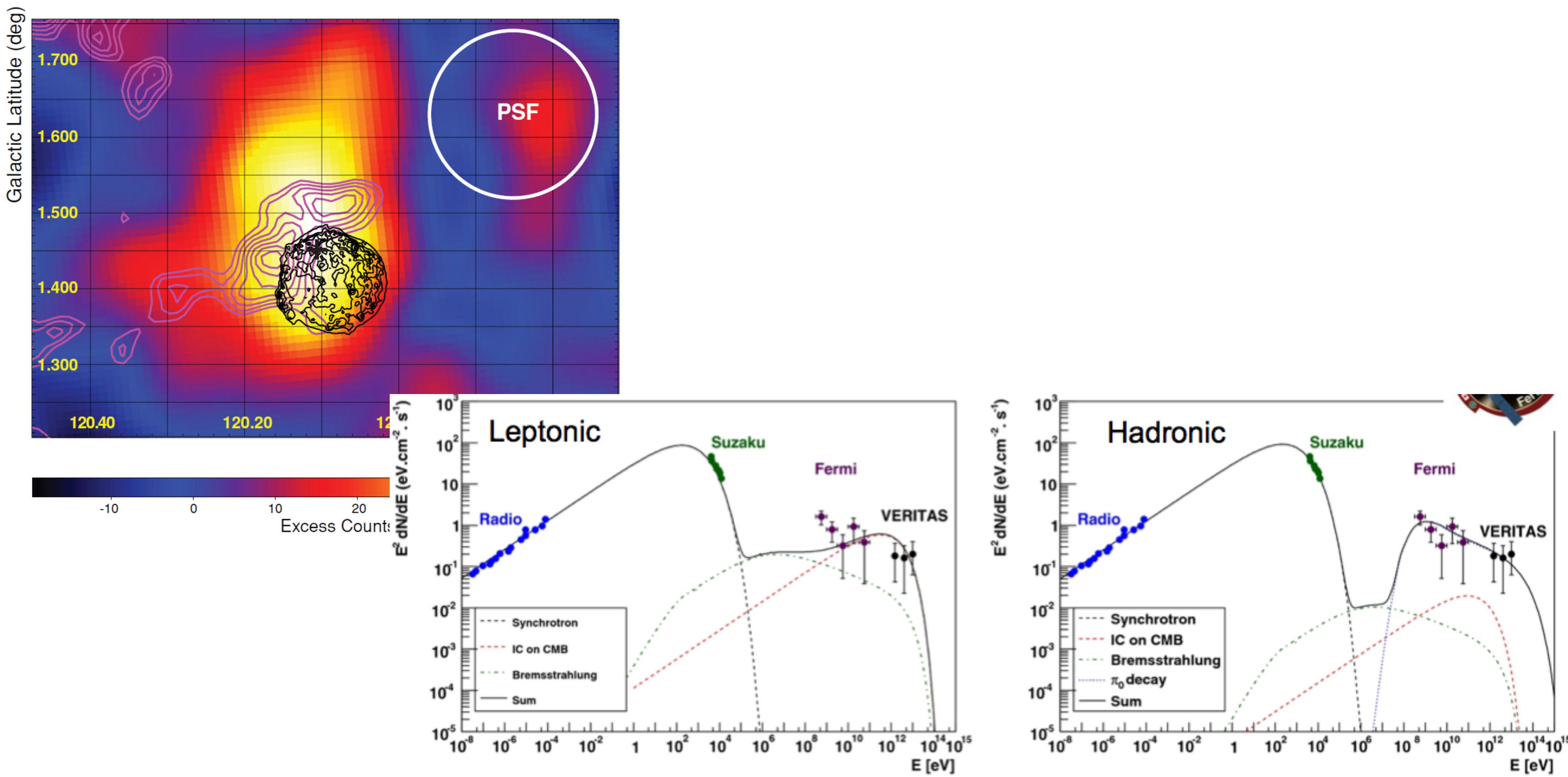

The ***Fermi* data support a hadronic** scenario **(Giordano et al. 2012)**.
The situation is **not so clear** after a recent update **(Archambault et al. 2017)**.

SNRs @ VHE gamma-rays

Evolved SNR close to molecular clouds.
MAGIC W51 complex. SNR W51C interacts with molecular clouds in W51B **(Aleksic et al. 2011)**.
The TeV emission coincides with the **shocked cloud region**.

^{13}**CO** **21 cm continuum**

0.3-1 TeV

***Fermi* above 1 GeV**

>1 TeV

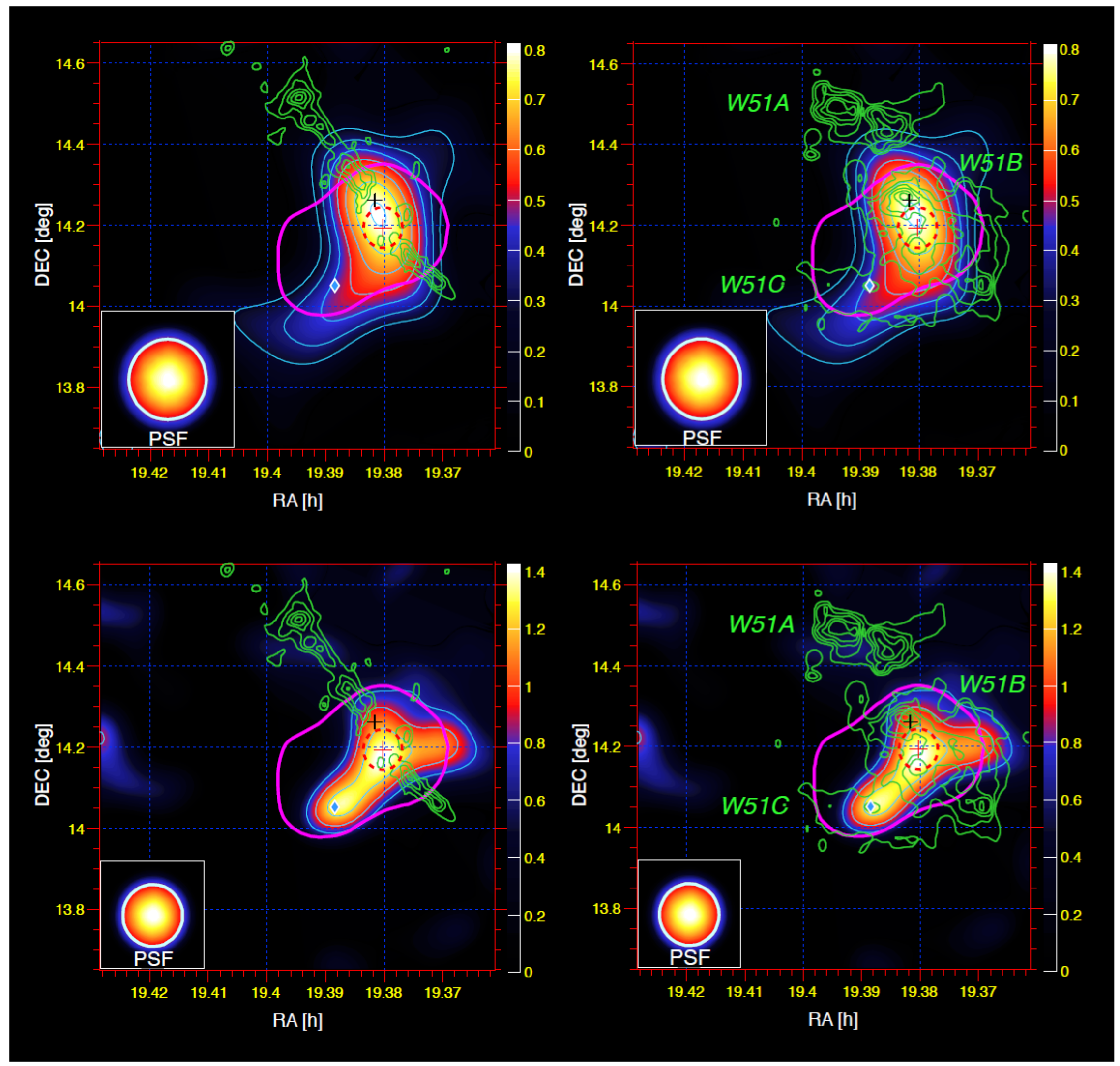

The broad band spectral energy distribution can be explained *only* with a **hadronic model** that implies proton acceleration above 100 TeV. This result, together with the morphology of the source, tentatively suggests that we observe **ongoing acceleration of ions** in the interaction zone between the supernova remnant and the cloud.